BTO 2015.012 | February 2015

BTO report

Drinking water temperature in future urban areas

KWR Watercycle Research Institute

BTO

Drinking water temperature in future urban areas

BTO 2015.012| February 2015

Project number
400554/046/002

Project manager
Edu Dorland

Client
BTO - TG Klimaat bestendige watersector

Quality Assurance
Jan Vreeburg

Author(s)
Claudia Agudelo-Vera, Mirjam Blokker, Paul van der Wielen and Bernard Raterman.

Sent to
This report is distributed to BTO-participants.
A year after publication it is public.

Year of publishing
2015

More information

T (030 60 69) 587
E claudia.agudelo-vera@kwrwater.nl

PO Box 1072
3430 BB Nieuwegein
The Netherlands

T +31 (0)30 60 69 511
F +31 (0)30 60 61 165
E info@kwrwater.nl
I www.kwrwater.nl

Keywords
soil temperature, urban heat island

KWR Watercycle Research Institute

Summary

Relevance

The temperature of the water at the customer's tap is strongly influenced by the soil temperature around the drinking water distribution pipes. Earlier research has shown that the water in the pipes reaches the soil temperature. Soil temperature is influenced by the weather (air temperature, solar radiation, etc.), the environment (rural vs. urban), soil type (sand vs. clay) and the level of urbanization due to the urban heat island effect. The term "heat island" describes built up areas that are hotter than nearby rural areas due to limited evapotranspiration, heat storage in buildings and urban surfaces, and due to anthropogenic heat sources. Sources of anthropogenic heat include cooling and heating buildings, manufacturing, transportation, lighting, etc.

Water temperature can be used as an indicator of water quality. In the Netherlands drinking water is distributed without additional residual disinfectant. Therefore the maximum acceptable temperature, temperature threshold, of drinking water at the customers' tap is 25ºC. During a warm year (2006), 0.1% of the routine water quality samples exceeded this value. With increasing extreme weather events due to climate change and with more local variations due to the urban heat island effect, more samples may be expected to exceed this temperature threshold in the future. Quantifying the effect of climate change on drinking water temperature in cities is crucial to evaluate and select measures which guarantee that the drinking water temperature at the customer tap does not exceed the temperature threshold.

Our hypothesis is that the drinking water temperature at the customers tap is higher in summer in urban areas compared to the temperature at the peri-urban area. In this study we investigate *i*) how often will the drinking water temperature exceed 25°C in the future, in urban areas (most of the Netherlands)? *ii*) What is the effect of these temperatures on the water quality? *iii*) Which measures are feasible to reduce the risk of exceeding the drinking water temperature threshold?

Approach

Although there are techniques to measure soil temperatures, in-situ measurements of soil temperature at various depths are spatially and temporally limited. Therefore, modelling is a flexible approach to better understand dynamics of energy partitioning in urban areas and the influence of different parameters, such as soil moisture. The objective of this study was to extend the soil temperature model described by Blokker and Pieterse-Quirijns (2013). The model was extended by including the urban evapotranspiration, anthropogenic heat emissions and the heat storage capacities of the buildings. Sandy soils were assumed for urban areas. A sensitivity analysis of the variation of the thermal properties of the soil as a function of its water content was performed.

For the validation of the model, different parameters were identified. Figure S.1 shows the different variables used in the model. It is important to emphasize that there are static and dynamic characteristics for a specific location. In this study, the objective was to validate the model for summer conditions. For the summer condition, some input variables were

assumed static based on values reported in the literature, see Figure S.1. A recently developed classification of urban areas, the Local Climate Zones – (LCZ), was used to determine some of the parameters related to the urban typology.

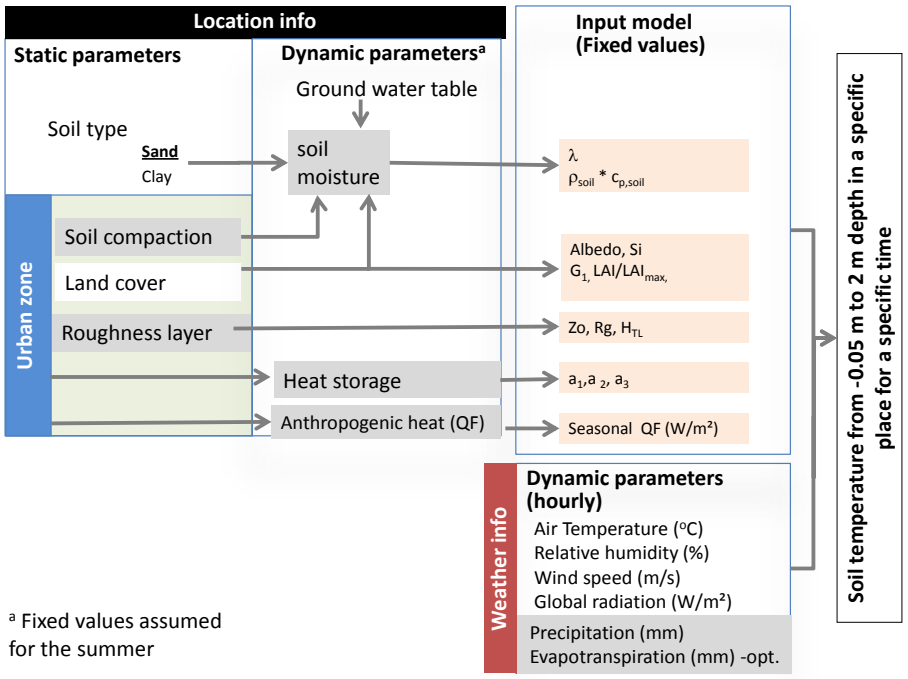

Figure S.1Overview of variables included in this study.

The model was validated for a peri-urban area and for an urban area. For the urban area, the city of Rotterdam was used as a case study. For the peri-urban area historic KNMI soil temperature records of the Bilt were used. For urban areas, two different datasets of measurements were used to validate the extended model: *i*) soil temperature measurements in two locations in Rotterdam and *ii*) Water temperature from samples at customers' tap reported by Evides.

Once the model was validated for the current situation, future scenarios were analyzed. The KNMI transformation tool for 2030 and 2050 was used to simulate the temperature and the precipitation for the G and W+ scenarios. Based on the predicted temperatures, the risk of pathogen regrowth in the distribution network was analyzed for 2030 and 2050.

Results

In this report we present an extended version of the existing model to predict soil temperature. The extended model met the expectations by better estimating soil temperature in peri-urban and urban areas by including evapotranspiration, heat storage and anthropogenic heat. A good correlation between the simulated peri-urban and urban soil temperatures and the measured soil temperature was found. This study demonstrates that it is possible to use meteorological information to predict urban soil temperature and therefore to estimate water temperature in the drinking water distribution network in peri-urban and urban areas.

In Peri-urban areas, the simulated temperature shows a better fit when introducing evapotranspiration and heat storage. In peri-urban areas, soil thermal properties have a

large influence on the model calibration. In urban areas, simulated soil temperature, using literature values, showed a good fit with the measured temperature at the customer's tap. Differences in temperature in different areas were also visible. This can be explained by differences in the urban type. The variation range can be simulated by defining three urban types: average urban for Rotterdam, peri-urban neighbourhoods and hot-spot areas. This suggests that the urban heat island effect can be also found in the water temperature in the distribution network. Our findings also suggest that anthropogenic sources are as important as soils thermal properties in the calibration of the model.

The analysis proves our hypothesis that drinking water temperature at the customers tap is in the summer higher in urban areas compared to the temperature at the peri-urban areas, our analysis showed that the influence of the water temperature at the pumping station has a limited effect.

The analysis of the drinking water temperature in future urban areas showed that areas in the peri-urban area do not have a risk to exceed the 25°C temperature threshold now or in the future. Considering the most extreme KNMI scenario, an average city may have 7 days above 25°C in the W+ scenario. Hot-spots are areas of concern: currently in a warm summer 9 days the temperature threshold is exceeded, this number is expected to increase to 55 days in 2030 and up to 83 days in 2050. In 2050 temperatures above 28°C could be frequently reached, Under these conditions, there is an increased risk for growth of *L. pneumophila* in the drinking water distribution system.

Different measures can contribute to reducing the urban heat island effect. Green roofs, or other measures such as placing the pipes deeper can reduce the temperature, but these benefits are limited. Therefore, different measures should be taken simultaneously to have a noticeable reduction on the soil temperature. However, in the average city and in the hot-spots, controlling anthropogenic sources would be the most efficient measure. Further, further research is needed to identify and rate anthropogenic heat sources.

Implementation

The model can be used for different purposes: *i*) to calculate the effect of measures, *ii*) to evaluate the effect of different anthropogenic sources and it can support the identification of hot-spots and *iii*) to predict future temperature as an early warning system (early research, Agudelo-Vera et al., 2014) and also long term analysis (e.g. drinking water temperature in 2050).

It is important to highlight that the objective of the model is not to exactly predict the soil temperature at one specific point. The model is instead a tool to estimate the temperature of a given area, within determined ranges of uncertainty. With this model sensitive parameters can be identified. Higher precision would require more detailed information per location, which is currently not available.

The model can be used for different urban locations by using literature values. Ranges in urban areas can be determined. For instance by using the different LCZ, different areas in the city can be identified. With the available data from the temperature at the customers' tap, the model can be validated for urban areas. The soil temperature model can be used to analyse the risk of exceeding the temperature threshold, particularly during warm summers and in highly urbanized areas, by using future climate information available at the KNMI.

Contents

1 Introduction

1.1 Background

The temperature of the water at the customer's tap is influenced by the soil temperature around the distribution pipes. Specifically for drinking water distribution systems (DWDS) at ca. 1 meter depth, it has been found that the water temperature in the DWDS approaches the surrounding soil temperature (Blokker and Pieterse-Quirijns 2013 and Müller, Kuttler et al. 2014). Water temperature is an important determinant of water quality, since it influences physical and chemical processes, such as absorption of chemicals, and chlorine decay. In the Netherlands drinking water is distributed without residual disinfectant. The maximum acceptable temperature, temperature threshold, of drinking water at the customers' tap is 25ºC (Drink Water Directive 2011). During a warm year, 2006, 0.1% of the routine water quality samples exceeded this value (Versteegh and Dik 2007). With increasing extreme weather events due to climate change and with more local variations due to the urban heat island effect, more samples may be expected to exceed this threshold. Quantifying the effect of climate change on drinking water temperature in cities is crucial to evaluate and select measures which guarantee that the drinking water temperature at the customer tap does not exceed the temperature threshold.

Various factors influence the temperature of the urban soil around the drinking water distribution network. Soil temperature fluctuations depend on meteorological conditions, soil properties and land cover (van der Molen 2002). In urban areas, the level of urbanization (urban heat island effect) may also influence soil temperature. Although there are techniques to measure soil temperatures, in-situ measurements of soil temperature at the surface and various depths are spatially and temporally limited (Mihalakakou 2002). Moreover, soil heat flux measurements in urban areas are inherently difficult because the sensors need to be buried in the ground and the positioning of these instruments is limited by practical considerations (Gentine, Entekhabi et al. 2012). Therefore, modelling is a more flexible approach to complement and validate on-site measurements. Moreover, modelling allows a better understanding of the dynamics of energy partitioning in urban areas and the influence of various parameters, such as soil moisture.

In the last decades, research on urban climate has gained a lot of attention. It is clear that there is a relationship between subsurface temperatures and urban development (Grimmond, Blackett et al. 2010; Grimmond, Roth et al. 2010). However, the relation between soil temperature, moisture and surface processes is complex and not yet well understood. Determining soil temperature in urban areas is important for different aspects; for instance to predict infrastructure performance, e.g. pavement durability (Diefenderfer, Al-Qadi et al. 2006) or coupled heat pumps (Garcia Gonzalez, Verhoef et al. 2012), and to determine the drinking water temperature (Blokker and Pieterse-Quirijns 2013).

Blokker and Pieterse-Quirijns (2013) developed a micrometeorology model to predict the soil temperature at various depths as a function of weather and environmental conditions. Blokker and Pieterse-Quirijns (2013) simulated an urban soil without vegetation. This means that evapotranspiration was neglected. Anthropogenic heat and heat storage in the buildings were also neglected. A recent German study reported a maximum of almost a 9°C subsurface heat island gradient on the hourly average at 70 cm below ground level (Müller, Kuttler et al. 2014). They also found differences of temperature between eight measurement

locations in the city. These differences could be explained by the different heat island effects in each of the locations. In urban areas, with concentrated population, multiple heterogeneous land cover and different urbanization levels, tools are needed to monitor and predict drinking water temperature in the network at small spatial scales to guarantee that the 25°C threshold is not exceeded, especially in hot summers.

1.2 Hypothesis and objectives

Our hypothesis is that the drinking water temperature at the customers tap is higher in summer in urban areas compared to the temperature at the peri-urban area due to:

- Drinking water temperature in the distribution network is determined by the soil temperature.
- Soil temperature in the urban areas is higher than peri-urban areas because sandy soil is used as 'soil improvement'.
- Soil temperature in urban areas is higher than in peri-urban areas due to the urban heat island effect, less evapotranspiration than in rural areas, heat storage in buildings and anthropogenic heat.

The objective of this study was to extend the soil temperature model developed by Blokker and Pieterse-Quirijns (2013). The model was extended by including the urban evapotranspiration, anthropogenic heat emissions and the heat storage capacities of the buildings. The effect of the moisture content in the sandy soil, typically used in urban areas, was also analysed. The specific research questions addressed in this study are:

- How often will the drinking water temperature exceed 25°C in the future, in urban areas (most of the Netherlands)?
- What is the effect of these temperatures on the water quality?
- Which measures are feasible to reduce the risk of exceeding the drinking water temperature limit?

1.3 Approach

The focus of this study is the urban area because the highest risks are expected there due to higher density and the urban heat island effect, possibly influencing the temperature of the water in the distribution system. The following steps are described in this report: Chapter 2 describes the analysis of the soil types in the Netherlands and the soil thermal properties and their relationship with soil moisture (with a focus on sand). Chapter 3 focuses on the soil temperature in the Netherlands. Chapter 4 focuses on urban climate and the energy balance in the city. Chapter 5 describes the extended model. Chapter 6 describes the validation of the model for a peri-urban area, using soil temperature measurements of the KNMI at meteorological stations. Chapter 7 describes the validation of the model for an urban area. The city of Rotterdam in the Netherlands was used as study area. Two different datasets of measurements were used to validate the extended model in urban areas: i) soil temperature measurements in two locations in Rotterdam performed by KWR and ii) water temperature at the customers' tap reported by Evides. Literature values and other data sets were used in the calibration and validation of the model.

Once the model was validated for the current situation, future scenarios were analyzed by using temperature and precipitation data sets generated with the KNMI transformation tool for 2030 and 2050 (Chapter 8). By doing this, it was quantified how often the temperature in the drinking water exceeds 25°C. In Chapter 9, the consequences for the water quality are described. Chapter 10 shows the discussion of the results and provides recommendation and Chapter 11 contains the conclusions.

2 Soil types and soil properties

2.1 Introduction

This chapter focuses on identifying the most common soil type(s) in the Netherlands, and the most common soil type in urban areas. An overview of the thermal properties of the soils is presented considering their relationship with the soil water content.

2.2 Soil types

Soils have many different properties, including texture, structure, water holding capacity, etc. In terms of soil texture, soil type usually refers to the different sizes of mineral particles in a particular sample. The ratio of these sizes determines soil type: clay, silt, etc. (Table 1). Soil may be mixed with larger aggregate, such as pebbles or gravel. There are many recognized soil classifications. Table 1 shows some parameters for the U.S., the maximum water content (θ_s) and the dry density (ρ_d) based on the U.S. geological survey for different soil types.

Table 1 Relevant soil parameters for U.S. Geological Survey (USGS) soil texture classifications (Yang and Koike 2005).

soil type	θ_s ($m^3\ m^{-3}$)	ρ_d ($g\ cm^{-3}$)
sand	0.373	1.66
loamy sand	0.386	1.63
sandy loam	0.419	1.54
loam	0.476	1.39
silt loam	0.471	1.40
silt	0.437	1.49
sandy clay loam	0.412	1.56
clay loam	0.478	1.38
silty clay loam	0.447	1.47
sandy clay	0.415	1.55
silty clay	0.478	1.38
clay	0.450	1.46

$\theta_s = V_{max,water}/V_{total}$, where $V_{max,water}$ is the maximum volume of water that can be contained in the soil, which is equal to the porosity. V_{total} is the total volume of the soil. ρ_d is the density of the soil when the saturation is zero.

2.2.1 Soil type in the Netherlands

The Netherlands has a number of distinct geographic soil regions. About half of the country is below sea level and would be inundated in the absence of dikes, dunes and pumping plants. It is also a wet country and more than 90% of the soils have groundwater within 140 cm of the soil surface during the winter. There is hardly soil derived from consolidated rock. Non-urban areas are dominated by sandy soils (43%), marine clays (24%), fluvial clays and loams (8%) and organic soils (14%) (Hartemink and Sonneveld 2013). Figure 1a shows the distribution of approx. 300 soil types and Figure 1b a generalized soil map (Alterra 2012).

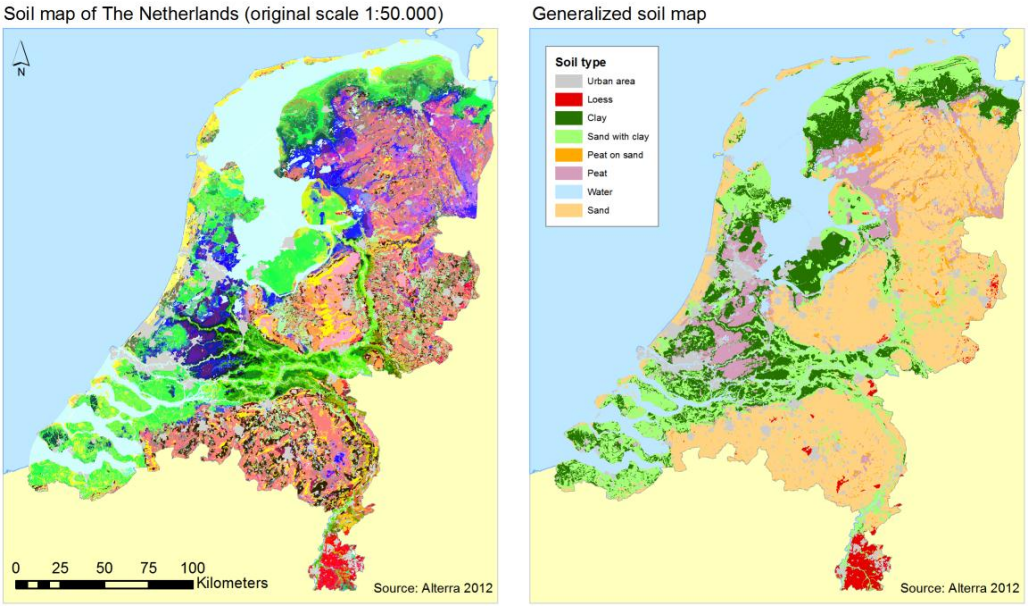

Figure 1 Soil map of the Netherlands left: differentiation of approx. 300 soil types and right: generalized map soil (Source: Alterra).

2.2.2 Soil improvement: Anthropogenic soil

Most soils in the city are intensively used and therefore heavily influenced by humans. Processes in these soils often differ greatly from those in rural soils. Modifications associated with urban infrastructure directly impact soil properties. In preparation for the urban infrastructure, topsoil is removed, leading to reductions in soil organic matter. Physical soil modification is necessary for infrastructure. Road engineering requires packing soils to high bulk densities for load-bearing. Soil compaction increases bulk density by reducing total pore volume and increasing the percentage of small pores. In particular, soil bulk density, microbial biomass and activity, and organic matter are impacted by anthropogenic activities. Scharenbroch, Lloyd et al. (2005) found soils from older urban landscapes (mean landscape age of 64 years) to be distinct from newer urban landscapes (mean landscape age of 9 years). Soil bulk densities were significantly greater in newer (1.73 g cm^{-3}) compared to older urban soils (1.41 g cm^{-3}), which is evidence of the spatial variability of soils in urban environments. Anthropogenic top soils are being mapped in the Netherlands, (Figure 2). Mapping of anthropogenic soils include not only their distribution, but also their thickness. Figure 2b shows a detail for Rotterdam, where the thickness of the anthropogenic soil in average is 1.5 m depth varying from 0.5 m to 5 m. Typically, in the Netherlands, sand is used to improve urban soils. This study focuses on urban areas and their heat urban effect. Therefore, in this study, sandy soils are assumed for Rotterdam.

2.3 Moisture content

2.3.1 The groundwater table

Moisture content influences the soil properties. The groundwater table, that expresses the groundwater level, has a large influence on the moisture content of the soil. For the Netherlands the average ground water table, with respect to the surface level, is shown in Figure 3 (right), which varies from 0.1m to 80m below surface level. The topographic map of the Netherlands is shown in Figure 3 (left), approximately 27 % of The Netherlands lies below sea level.

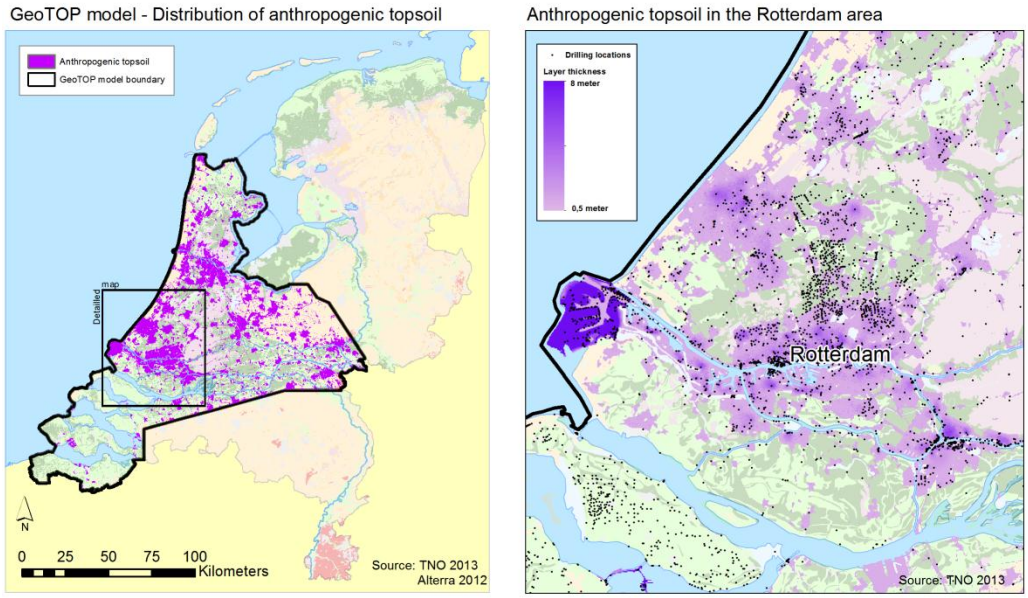

Figure 2 Anthropogenic topsoil (Source: Alterra/TNO). Left: distribution of anthropogenic soil in the Netherlands and right: depth of the anthropogenic soils in Rotterdam.

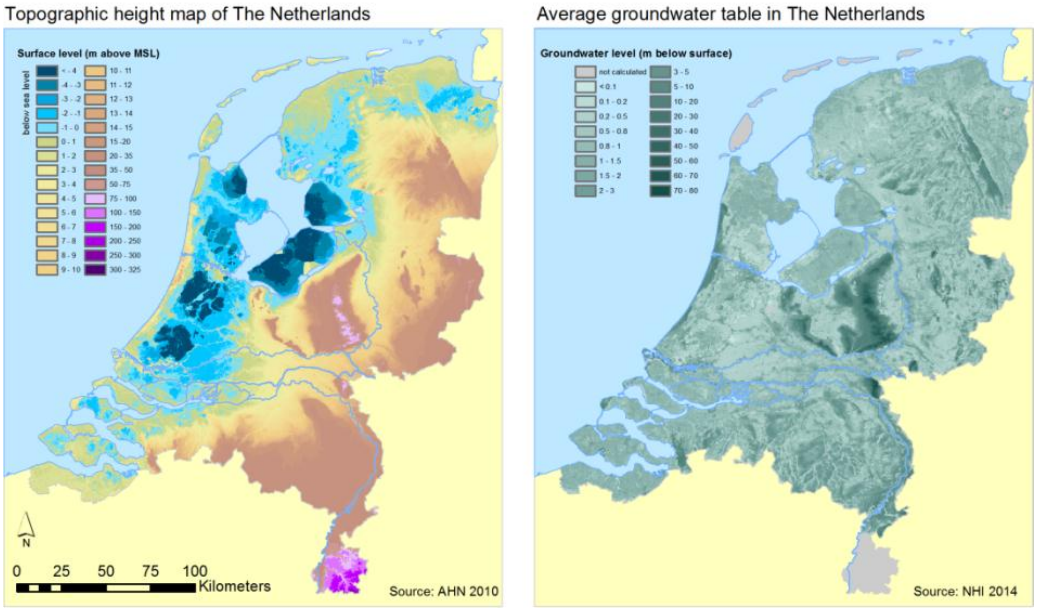

Figure 3 Left: Topographic height map of the Netherlands. Right: average groundwater table in the Netherlands.

2.3.2 Modelling the moisture content based on the groundwater table

Urban soils often have an impermeable cover, which disrupts the natural water balance by limiting infiltration and evapotranspiration (this is further addressed in §4.3.5). Then, the groundwater level has a large influence on the moisture content of the urban soil. Assuming a completely impermeable surface cover, the water content can be modelled at a given point

in time by neglecting precipitation and evapotranspiration, and assuming a static condition: a constant water level and no horizontal water flow.

In this study a model which generates the soil moisture profile was developed to gain insight into the variation of the water content around 1m depth. This moisture content represents the minimum moisture content, since it assumes an impermeable surface, which does not allow water from precipitation to enter the soil. This will be the case in sealed urban areas. The model accounts for a homogenous soil profile and horizontal fluxes are neglected. Figure 4 shows the variation of the simulated water content at -1m depth to surface level for different sandy soil types as function of the ground water level. The ground water level is expressed as the groundwater table depth varying from 1m up to 2.5m. The soil types are described in Table 2. The water content at -1m, when the groundwater is -1m, is the maximum water content of the soil type, saturated condition or soil wetness 100%, Appendix III. For the sandy soils, the maximum water content varies between 0.32 and 0.46, if the water table drops to 2m depth the water content varies from 0.12 to 0.35, which are a variation of 38% and 0.76% of the soil saturation respectively.

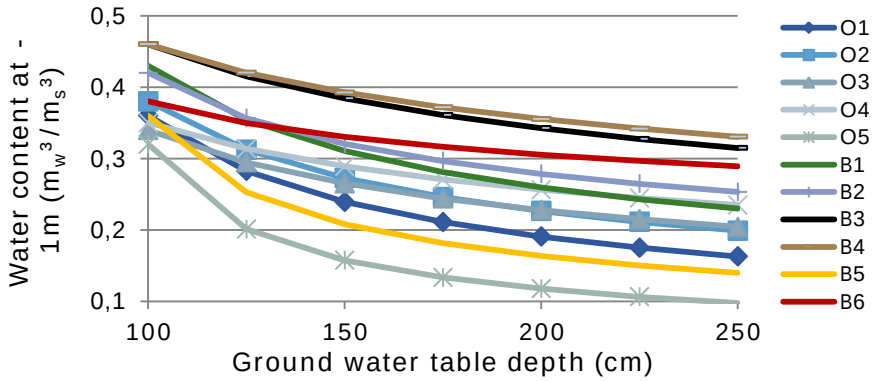

Figure 4 Modelled water content at 1m depth for different sandy soils types and different groundwater levels, B: topsoils, O: subsoils.

Table 2 Description of sandy soil types used in figure 4, B: topsoils, O: subsoils.

soil type	Description			
	% Loam	% OM	M50 (µm)	Density (g/cm3)
O1	1-10	0-3	105-205	1.4-1.8
O2	10-16	1-3	105-175	1.4-1.7
O3	20-32	0-2	114-172	1.4-1.8
O4	36-47	0-2	128-170	1.4-1.7
O5		0-2	220-400	1.5-1.7
B1	4-10	1-4	140-170	1.4-1.7
B2	11-18	1-10	125-175	1.2-1.6
B3	18-29	3-13	105-165	1.1-1.5
B4	37-50	2-5	118-165	1.1-1.5
B5	1-3		350-500	1.3-1.6
B6	5-39	1-8	150-400	1.1-1.6

m50 = median size of grains above 50 μm. Half of the weight is above this size, half below.
OM = Organic Matter

2.3.3 Spatial and temporal variations of the groundwater table

The groundwater table fluctuates at various time scales: days up to years. Moreover, spatial variations are observed within a few kilometres. Figure 5 shows the variation on the groundwater level in three locations in de Bilt reported by the Dinoloket (2014).

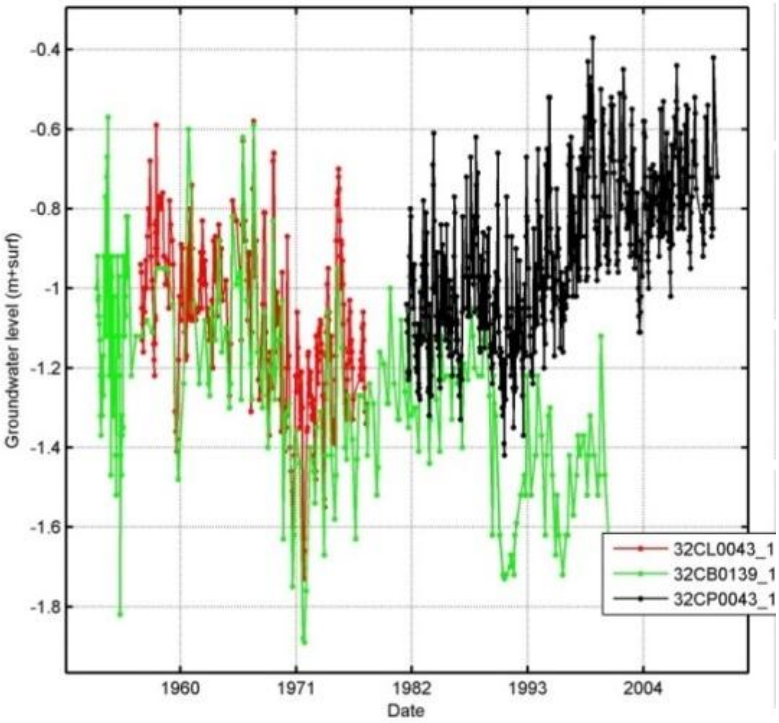

Figure 5 Inter annual variation of the groundwater table (Source: Dino loket) in three locations in the Bilt visualised with the Menyanthes software.

In § 2.3.2, it was shown that for a static condition the moisture can be modelled. In an urban area though not all the surface is completely impermeable and other factors can influence the water table level: leakages of drinking water or sewer systems, existence of underground levels, where water pumping modifies the water level. All these uncertainties make it difficult to determine the water table level and therefore the soil moisture content. In this study we focus on the summer condition, especially in hot summers. It is assumed for this condition that the soil water content can be assumed constant.

Rotterdam has several monitoring wells to measure the ground water level. However, these measurements are not registered on regular basis. For the case of Rotterdam, we use the surface level information, Figure 6, and the water table levels of the monitoring wells reported in August 2013. Using GIS we identify the location of the wells and interpolate the groundwater level for an area in Rotterdam (Figure 7). Figure 7 gives only an approximation of the real ground water level. In this case the ground water level reported and the surface level was considered in a simple interpolation, however different interpolation methods could be applied, providing a different distribution of the water table. However, the ranges can provide an indication of the variability in urban areas.

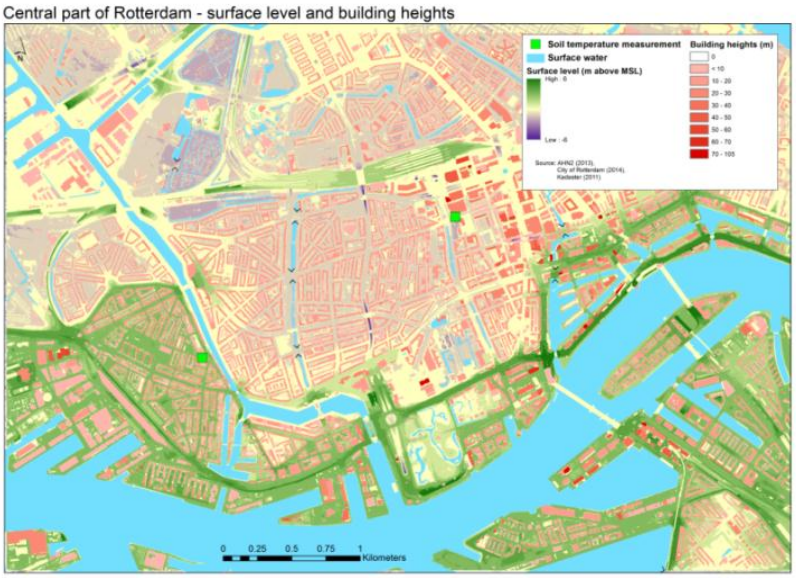

Figure 6 Surface level and building heights in the centre of Rotterdam.

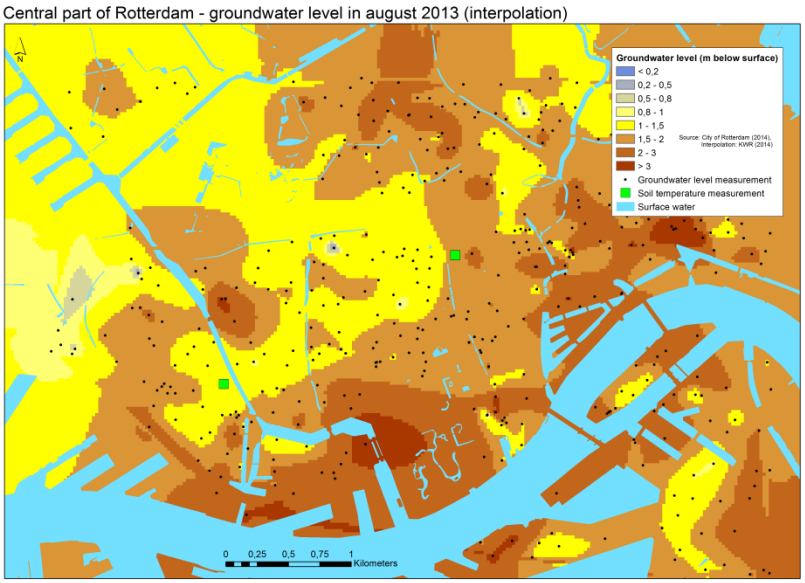

Figure 7 Interpolated groundwater table levels (with reference to the source level) for the month of August 2013 based on the water level of the monitoring wells, for the centre of Rotterdam. Groundwater table levels are in meters below surface level.

2.4 Thermal properties of soils

The thermal properties of soil are a component of soil physics. These properties influence how energy is partitioned in the soil profile. The main soil thermal properties are: Volumetric heat capacity [J m^{-3} K^{-1}], Thermal conductivity [W m^{-1} K^{-1}] and Thermal diffusivity [m^2 s^{-1}]. Factors that affect the effective thermal diffusivity in soil include grain size, mineral composition, and moisture content (Taylor and Stefan 2009).

It is well known that moisture affects the thermal properties of soil. Although theoretically thermal properties could be derived when the characteristics of the soil are known: composition, porosity and water content, reported empirical values for a limited number of locations show a large variability, which cannot be generalized. This is due to anisotropic characteristics of the soils (varying in the three dimensions). Additionally, these characteristics are dynamic (varying in time), due to their dependence on their surrounding environment, e.g. seasonal variations, precipitation, land use change, etc. Previous studies showed large uncertainty on estimating soil thermal properties, see Table 3. Yang and Koike (2005) used three different sets of empirical relations to calculate thermal conductivity and thermal diffusivity of different soil types with varying water content (θ) expressed as the volume of water in the soil (m^3/m^3), see Table 4 and Appendix I and Appendix II. This shows the large uncertainty in the thermal properties of soils.

Table 3 Comparison of thermal conductivity values W $m^{-1}K^{-1}$.

Saturation	Sand (η=0.4, q=0.95)	Clay (η=0.4, q=0.25)	Peat (η=0.8, q=0.0)
0	0.3[a]	0.25[a]	0.05[a]- 0.06[c]
0.25	1.05[c]	0.63[c]	0.13[a]
0.5	1.95[c] -1.76[b]	0.12[c]- 1.17[b]	0.22[a]- 0.29[c]
0.75	2.16[c]	0.33[c]	0.33[a]
1	2.2[c] - 2.18[b]	1.58[c]- 1.59[b]	0.5[a,b,c]

η: porosity, q: quartz content
[a] Farouki (1986), [b] de Vries (1963), [c] Pielke (1984).
Source: (Peters-Lidard, Blackburn et al. 1998).

Table 4 Thermal properties for sand and clay for different moisture content (Yang and Koike 2005).

Soil type	Condition	θ	Soil thermal properties[a] ρ [10^3 kg m^{-3}]	C_p [10^3 J Kg^{-1} K^{-1}]	ρ C_p [10^6 J m^{-3} K^{-1}]	λ (min - max) [W $m^{-1}K^{-1}$]	α [m^2 s^{-1}]
Sand	Dry	0.0	1.66	0.81	1.34	0.17 – 0.25	0.13 – 0.19
	50% saturation	0.5	1.83	1.11	2.03	0.7 – 5.0	0.94 – 2.46
	Saturated	1.0	2.0	1.37	2.74	2.6 - 14	0.95 – 5.11
Clay	Dry	0.0	1.47	0.82	1.21	0.17 – 0.30	0.14 – 0.25
	50% saturation	0.5	1.69	1.25	2.11	0.17 – 1.35	0.08 – 0.64
	Saturated	1.0	1.91	1.6	3.06	1.3 – 6.7	0.43 – 2.19

The soil heat capacity can be calculated as:

$$C_{p,soil}(\theta) = \rho_d c_d + \rho_w c_w \theta \quad (1)$$

Where $\rho_w c_w$ is the water heat capacity and $\rho_d c_d$ is the heat capacity of the dry soil. Here $\rho_w c_w$ = 4.18 x 10^6 J m^{-3} K^{-1} and $\rho_d c_d$ = (0.075+0.748 ρ_d) * 10^6 J m^{-3} K^{-1}; ρ_d is the bulk density of the dry soil (g cm^{-3}), dry condition in Table 4 (Yang and Koike 2005).

The soil thermal diffusivity is expressed as:

$$a = \frac{\lambda_{soil}}{\rho_{soil} C_{p,soil}} \qquad (2)$$

Although soils are anisotropic, often, energy balance models consider the soil as a continuous and homogeneous medium with a homogenous mixture of air, water and minerals. Thermal capacity and conductivity as well as the density parameters are considered constant in time and space. Therefore, the only factor that influences the direction of heat flow is the temperature gradient.

2.5 Conclusions

Determining thermal properties of soil remains a difficult task. Soil thermal properties are determined by the soil type, compaction and moisture content. Soil type and compaction vary over three dimensions. To describe the soil type of a specific area, several on-site measurements are required. Moisture varies not only spatially but also temporally (four dimensions).

The soil thermal properties, λ, ρ and $c_{p,}$ are not easy to measure, neither the moisture content. Moreover, the effect of moisture content in λ, ρ and $c_{p,}$ in sand varies a lot. As shown, in the literature different empirical studies have found different relationships between soil moisture and soil thermal properties.

This study focuses on the soil temperature in urban areas during the summer. In urban areas, the upper soil level has been modified. Typically, in the Netherlands sand is used to improve urban soils, and this layer is often compacted, which affects thermal properties of the soil. In this study, we selected Rotterdam as case study, and sandy soils are assumed. At a latter stage, this assumption is confirmed with measurements (Figure 33). Since we focus on the upper meter and given the large uncertainty of the spatial variation of the soil profile, an average soil profile with average soil moisture is assumed to model the soil temperature in the summer. Thermal properties are based on literature values.

3 Soil temperature

3.1 Introduction

Variations on land surface temperature affect subsurface temperature. Daily and seasonal ground temperature cycles are common. The ground temperature distribution is affected by structure and physical properties of the ground, ground surface cover, e.g. bare ground, lawn, snow, climate interaction, i.e. boundary conditions, determined by air temperature, wind, solar radiation, air humidity and rainfall.

From the point of view of the temperature distribution, three zones can be identified (Popiel, Wojtkowiak et al. 2001):

1. Surface zone reaching a depth of about 1m, in which the ground temperature is very sensitive to short time changes of weather conditions.
2. Shallow zone extending from the depth of about 1–8m, for dry light soils, or 20m, for moist heavy sandy soils, where the ground temperature is almost constant and close to the average annual air temperature; in this zone the ground temperature distributions depend mainly on the seasonal cycle weather conditions.
3. Deep zone, below about 8–20 m, where the ground temperature is practically constant (and very slowly rising with depth according to the geothermal gradient).

In the Netherlands, most water distribution pipes are located in urban areas at 1 meter depth, which means that they are located in the boundary between the surface and shallow zone.

3.2 Measured soil temperature

Jacobs, Heusinkveld et al. (2011) analysed 27 year soil temperature records in a peri-urban location in a grassland in the Netherlands at five depths. Figure 8 shows the annual mean distribution per month of the five soil temperatures and the annual mean air temperature at 0.10m height. The standard deviations have been plotted in Figure 8. It is interesting to note that the deeper the soil temperature measurement, the smoother the soil temperature distribution. Accordingly, the standard deviations decrease with depth, which is clearly seen in Figure 8. An interesting feature, particularly in the lower soil regions, is that the standard deviation around February is much larger than for January or March. This is because in February The Netherlands can have either a cold month with a high chance of snow cover or a relatively warm month. Such large standard deviations also occur for November/December. Jacobs, Heusinkveld et al. (2011) reported as well the annual mean soil temperatures together with their mean annual maximum and mean annual minimum temperatures, (Figure 9). From the centre panel of Figure 9, the annual mean soil temperature profile is more or less constant with depth, although the variances are high and decrease somewhat with depth. This implies that the inter-annual differences must be high. In Figure 9, the mean maximum temperature profile decreases with depth and the mean minimum temperature profile increases with depth and this is a function of soil thermal properties. In addition, the variances of the maximum and minimum profiles are high and decrease somewhat with depth.

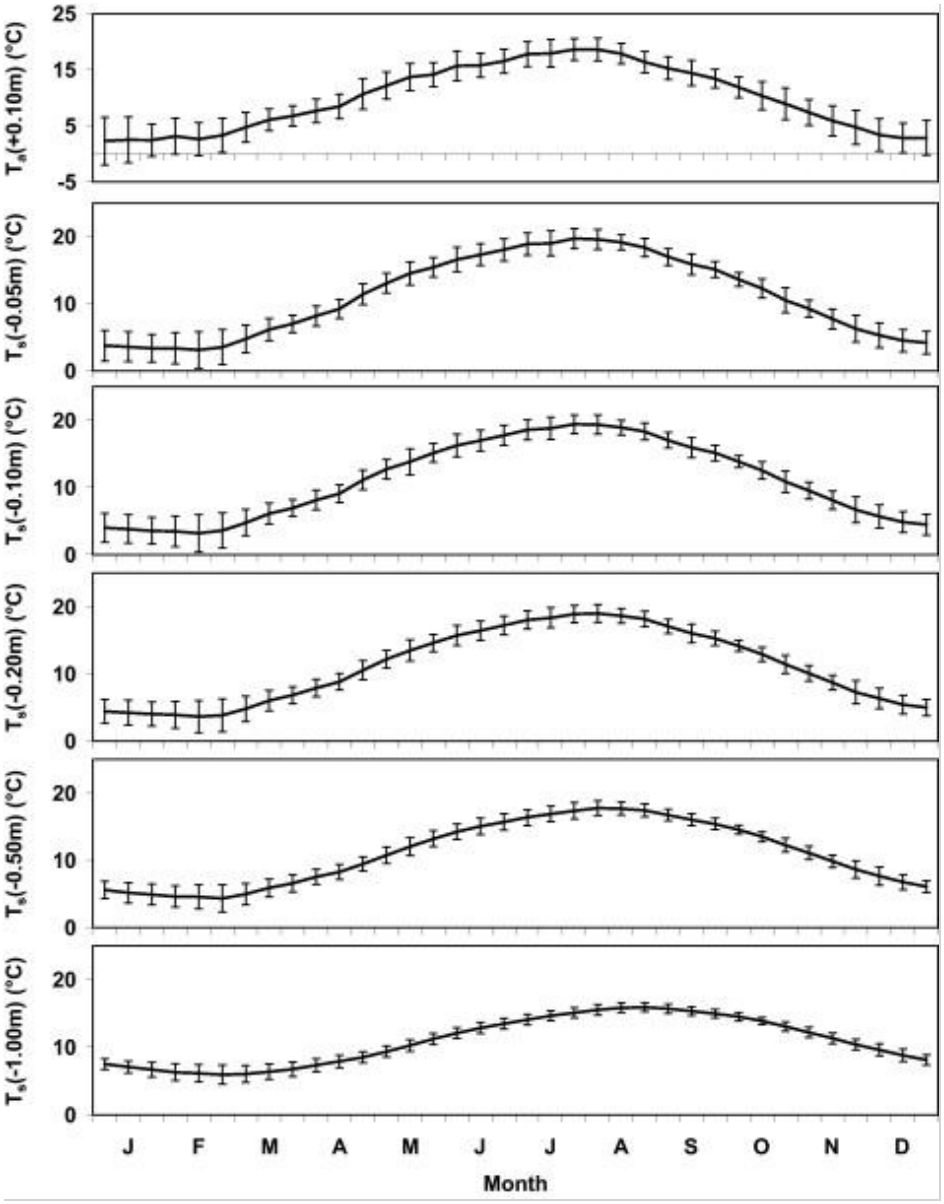

Figure 8 Annual mean distribution of the soil temperature in a grassland in the Netherlands at five depths and air temperature at 0.10 m, with standard deviations plotted (Jacobs, Heusinkveld et al. 2011).

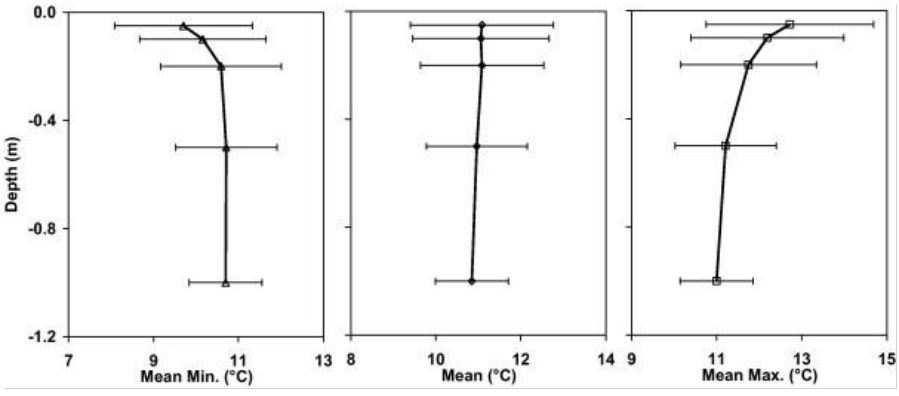

Figure 9 Annual mean soil temperature and the mean maximum and mean minimum temperatures in the surface zone in a grassland in the Netherlands (Jacobs, Heusinkveld et al. 2011).

In this study, existing soil measurements from four weather stations are used. The measurements are done by the KNMI at 5 cm, 10 cm, 20 cm, 50 cm and 100 cm depth. The stations are located in Wilhelminadorp, De Bilt, Marknesse and Nieuw Beerta, (Figure 10). The weather stations are located outside the cities. They all have grass as surface coverage and the soil is in these locations undisturbed, meaning that the original soil has not been disturbed by anthropogenic action. In this study the KNMI measurements are used as reference measurement (rural temperature). Data sets for two periods of time 1995 - 1997 and from 2008 - 2012, with a six hour interval, were used.

Figure 10 Location of the four KNMI weather stations where soil temperature is measured (in red) and the city of Rotterdam where measurements were conducted for this research (in green).

Figure 11 shows the measured soil temperature at -1.0m for the four locations. The maximum temperature recorded in the four locations was 18.5°C in Wilhelminadorp in 1995. In 1995 the maximum temperature difference at -1.0m between the four locations was 1.7°C, comparing Wilhelminadorp and Nieuw Beerta, which are the most distant locations. In the summer of 1995, daily maximum atmospheric temperature variation between locations is up to 7°C, difference in radiation is 1240 W/m² and difference in precipitation is 23 mm. Thus, although the local soil conditions and weather show considerable variations, the soil temperature at -1.0 showed a variation of less than 2°C in the summers. Soil temperature at -1.0m showed slightly higher variations in the winter, and almost no variations in spring and autumn.

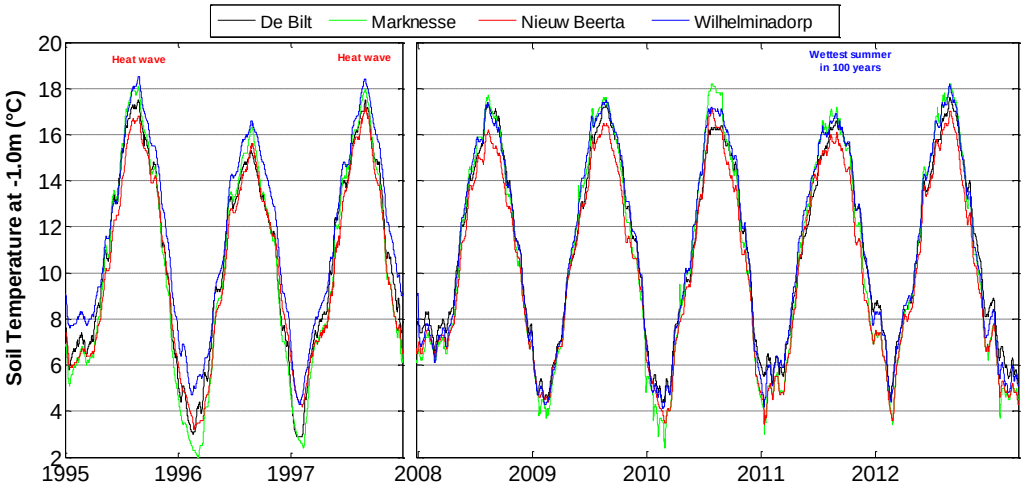

Figure 11 Soil Temperature at -1.0m depth for the four KNMI locations.

The year 2011 was reported as the wettest summer in the last century, with a precipitation of 350 mm in comparison with 225 mm, on average. Looking at the spatial distribution of the precipitation (Figure 12), we can see that there are large differences varying from 250 to 500 mm. For the summer of 2011, a maximum difference of 1°C was found between the maximum soil temperatures of the four locations. For the following comparison, the temperature of the soil at -1.0 m at weather stations is assumed to be a good approximation to the soil temperature in a rural area anywhere in the Netherlands.

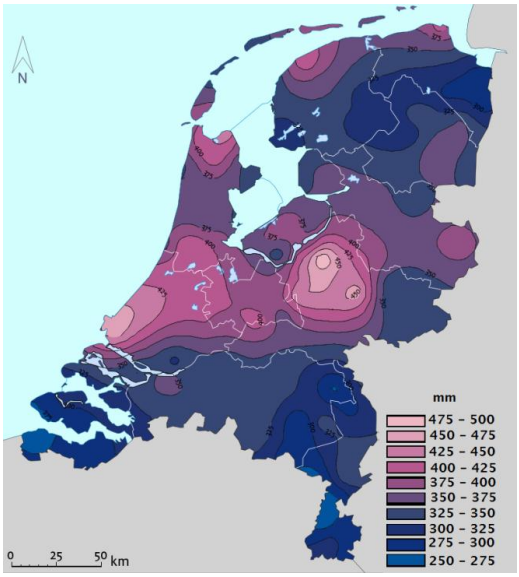

Figure 12 Distribution of the precipitation in mm during the summer 2011, spatial variations from 250 mm to 500 mm in three months (June-August).

3.3 Ground water temperature

Groundwater flow and groundwater temperature depend on climate and hydrogeology. Groundwater, especially shallow groundwater, gains or loses heat from the ground surface. The mean annual ground surface temperature is controlled by climate and land use (surface cover). If climate and land use do not vary in time, the mean annual temperature of the ground surface and the mean annual temperature of the groundwater are theoretically the same (Taylor and Stefan 2009).

The two processes of heat transfer to groundwater are: (1) heat transfer from a warm ground surface by effective thermal diffusion and (2) infiltration (unsaturated flow) of warm water from the ground surface, into the soil or seepage (saturated flow) of warm water from a stream, river, lake, pond or infiltration pond into the subsurface. Effects of urbanization and groundwater flow on the subsurface temperature in Osaka have been modelled in great detail by Taniguchi, Uemura et al. (2005)

Soil temperature also affects ground water temperature. In Canada it has been reported that in urban areas, the ground water can be up to 5°C warmer than in the surrounding rural areas (Ferguson and Woodbury 2004).

3.4 Measured drinking water temperature at the tap

Using the assumption that the drinking water temperature reaches the soil temperature, based on Blokker and Pieterse-Quirijns (2013), we assume that the temperature at the tap is a surrogate variable for the soil temperature. Thus, records of the regular random

temperature sampling at the customer's tap provide an indication of the soil temperature at approximately one meter depth. To take these samples, the water tap is opened and the reported temperature is recorded when a stable water temperature is reached.

An additional check was made, by comparing the temperature at the pumping station and the temperature at the tap. Two areas with different water sources (groundwater and surface water) were compared. Figure 13 shows the temperature at P.S. Halsteren, where the source is ground water and P.S. Berenplaat, where the source is surface water. Temperature at the tap for three areas were selected, Tholen and Halsteren which is supplied by Halsteren and Schiedam which is supplied by Berenplaat. Temperature at the P.S. Halsteren is shown in black markers, with a variation between 10.4°C and 13.4°C. However, tap samples showed similar temperatures as the ones found for Schiedam. These results confirm that the water reaches soil temperature, and that temperature at the tap is not determined by temperature at the pumping station.

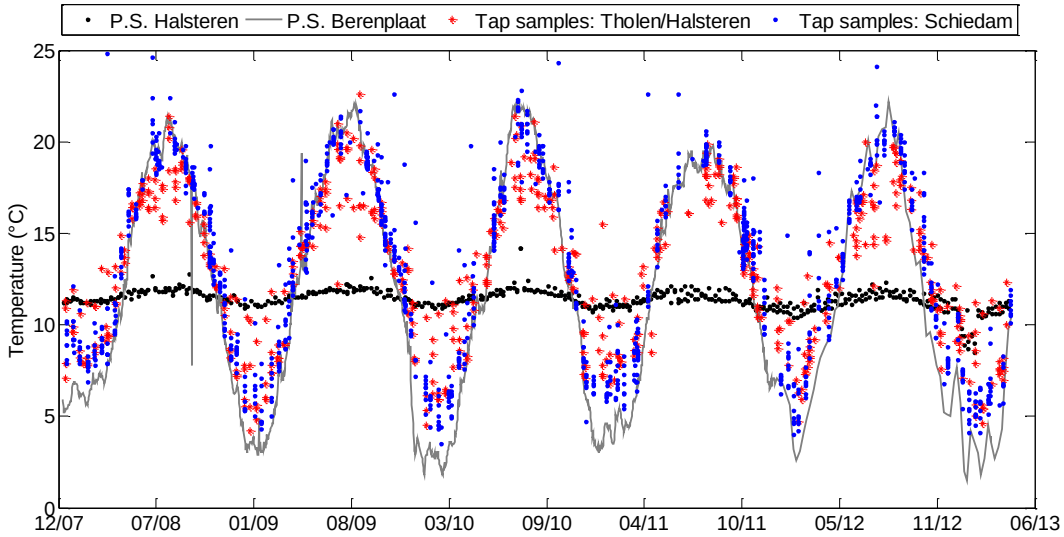

Figure 13 Comparison of the measured water temperature at the pumping stations Halsteren (ground water) and Berenplaat (Surface water) and the temperature at the tap at Tholen/Halsteren area supplied by P.S. Halsteren and Schiedam area supplied by P.S. Berenplaat.

3.5 Conclusions

Despite relative large changes in the weather conditions and different soil types, the soil temperature measurements at -1.0m of the four KNMI locations showed minor differences. The maximum soil temperature at -1.0m for the analysed period (8 years) in four peri-urban areas varied from 15.5°C to 18.5°C. In 1995 the maximum temperature difference at -1.0m between the four locations was approximately 2.0°C. This can be partly explained by similar coverage (grass) and the undisturbed condition of the soil in the peri-urban area. During a hot summer, 1997, all the KNMI locations showed temperatures above 17°C, at -1.0m depth.

Temperature at the tap showed to be independent of the temperature of the water leaving the pumping station. Specially in winter, the temperature of the samples at the tap are higher than the temperature at the pumping station. These results confirm that the water temperature in the pipes reaches soil temperature.

Comparing the soil temperature of the KNMI locations, which do not reach 19°C, and the temperature of the drinking water at the tap we can conclude that the water temperature at

the customer's tap can be higher than the soil temperature at KNMI locations. These locations are in general located outside the build area, in a field. The higher temperatures at the tap, can be caused by many factors influencing the soil temperature in a village or city: the covering layer of stone or asphalt instead of field and factors that cause urban heating, like local heat sources. The water temperature at the tap shows a large variation, which is caused by a combination of several local factors.

4 Urban Climate

4.1 Urban energy balance and urban temperature

Urbanization is characterized by, among others, land cover change, higher concentration of urban population and larger density of buildings. These characteristics influence the energy budget in various aspects leading to the development of distinct urban climates. It is known that the urban climate compared with its pre-existing landscape, presents (Stewart and Oke 2012):

- Greater absorption of solar radiation due to multiple reflection and radiation trapping by building walls and vertical surfaces in the city;
- Greater retention of infrared radiation in street canyons due to restricted view of the radiatively "cold" sky hemisphere;
- Greater uptake and delayed release of heat by buildings and paved surfaces in the city;
- Greater portion of absorbed solar radiation at the surfaces is converted to sensible, rather than latent heat forms;
- Greater release of sensible and latent heat from the combustion of fuels for urban transport, industrial processing and domestic space heating/cooling.

Although in the last two decades substantial advances have been made in understanding the scientific basis of urban climates (Grimmond, Roth et al. 2010), quantifying the urban energy fluxes at local scale remains difficult. This difficulty emerges from the heterogeneity of urban areas and the interaction of several dynamic processes. Heterogeneity in cities emerges from variations in surface morphology (i.e., urban form) and presence of impervious building materials, sparseness of vegetation, and anthropogenic heat, etc. Urban heterogeneity results in spatial variability in temperatures across urban areas, meaning that exposure to extreme heat events is variable at the sub-city scale. Such variability must be quantified in order to better understand urban temperature interactions and to identify areas with the greatest potential exposure to extreme heat events.

Traditionally, urban temperatures have been measured using terrestrial weather station networks. However, many urban areas lack a sufficient spatial distribution to characterize intra-urban temperature dynamics (Eliasson and Svensson 2003). This is a major limiting factor to improve our understanding of intra-urban heat hazards (Holderness, Barr et al. 2013). More recently data acquired using satellites give a range of valuable information but have not yet provided a comprehensive understanding of the complicated physical processes that contribute to the urban climate (Kanda 2006).

During the last decades a variety of numerical models, varying on levels of complexity and fluxes modelled, have been developed to simulate the key processes governing heat, moisture and momentum exchanges of the urban canopy. Grimmond, Blackett et al. (2010) compared 33 models in which a wide range of urban features are incorporated (Appendix IV). They concluded that some classes of models perform better for individual fluxes but no model performs best or worst for all fluxes. In general, the simpler models perform as good as the more complex models based on all statistical measures.

“Land surface temperature quantification” is gaining attention not only due to its relation with thermal comfort and heat island effect, but also for its interactions with urban infrastructure, for instance, to determine pavement durability (Diefenderfer, Al-Qadi et al. 2006). Subsurface temperatures in urban areas also experience thermal variations. The relation with surface processes is complex and not yet well described but there is a relationship between subsurface warming and urban development (Grimmond, Roth et al. 2010). The urban soil profile is often highly disturbed and there may be obstructions or anomalously warm or cool artefacts (e.g. empty, full, leaking water pipes, sewers, heat conduits), Figure 14, (Menberg, Bayer et al. 2013).

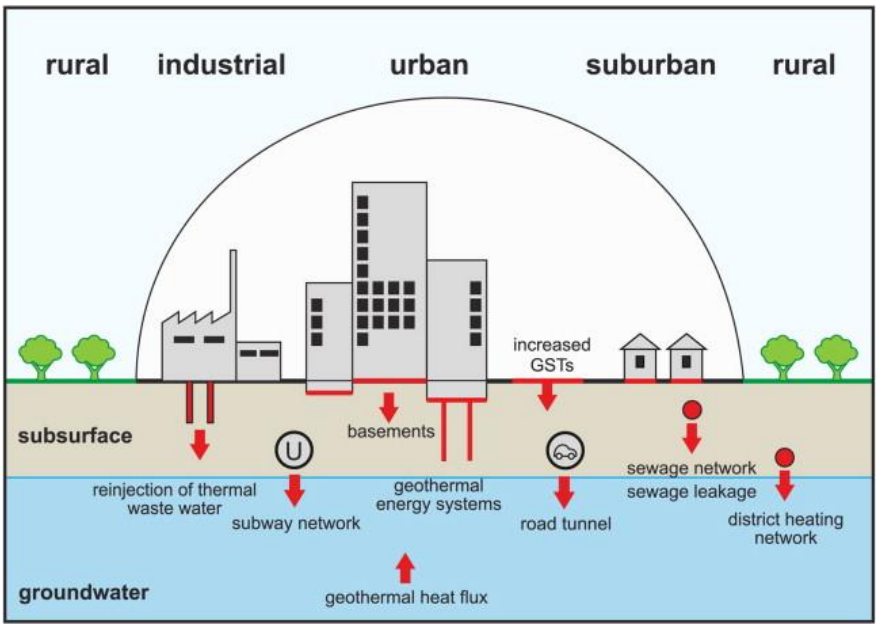

Figure 14 Potential anthropogenic and natural heat sources in urban areas (Menberg, Bayer et al. 2013).

Quantifying soil temperature is of significance to engineering design, for instance, to determine and monitor the thermal interaction of the soil with pipelines (Blokker and Pieterse-Quirijns 2013), ground heat storage and ground heat exchangers. For this purposes, modelling offers the flexibility to simulate a range of urban configurations, though generally relying on simplified expressions of the energetic processes. Study of the urban heat island has so far focused on air temperature and only recently on surface temperature (Klok, Zwart et al. 2012). Effect of soil temperature is not yet known. This is the focus of this study.

4.2 Scales and the urban energy balance

The urban climate can be described at multiple spatial scales. The spatial scale is crucial to understanding observations and modelling of urban climates. At each scale different processes are incorporated. Scale is fundamental to understand the interaction of urban areas with adjacent atmospheric layers. Cities present a distinct climate that can modify precipitation and wind patterns, air quality and atmospheric chemistry thousands of kilometres away from the source. Advances in computing power have enabled the development of Global Climate Models (Best and Grimmond 2013, Jackson, Feddema et al. 2010, Peng, Piao et al. 2012). These models describe the dynamics of the atmosphere and ocean in an explicit way in coarse spatial and temporal scales. Fundamental to the issue of scale is the distinction between the urban canopy layer (UCL) and the urban boundary layer (UBL), in (Blokker and Pieterse-Quirijns 2013) “atmosphere” and “roughness layer”.

In the UCL (roughly from ground to roof level), processes of airflow and energy exchange are controlled by micro-scale, site-specific characteristics and processes (Figure 15). The UBL, above roof level, in contrast, is that part of the planetary boundary layer whose characteristics are affected by the presence of the urban surface (or its land-use zones) below and is a local- to meso-scale phenomenon controlled by processes operating at larger spatial and temporal scales. It has a characteristic depth of the order of 1000m.

Urban climate phenomena play a role on various spatial scales, from meso-scale to human scale. Three horizontal scales and related vertical scales can be distinguished (Hove, Steeneveld et al. 2011), Figure 15:

- Micro-scale or street canyon scale: Typical scales of urban microclimates relate to the dimensions of individual buildings, trees, roads, streets, courtyards, gardens, etc. The dimensions extend from less than one meter to hundreds of meters.
- Local scale or neighbourhood scale: It includes landscape features such as topography but excludes micro-scale effects. In urban areas this translates to a mean climate of neighbourhoods with similar types of urban development (surface cover, size and spacing of buildings, activity).
- Meso-scale or city scale: The city elements in the micro-scale are affected by phenomena at the local scale. In their turn, the phenomena at the local scale or neighbourhood scale are affected by the conditions and interactions at the meso-scale.

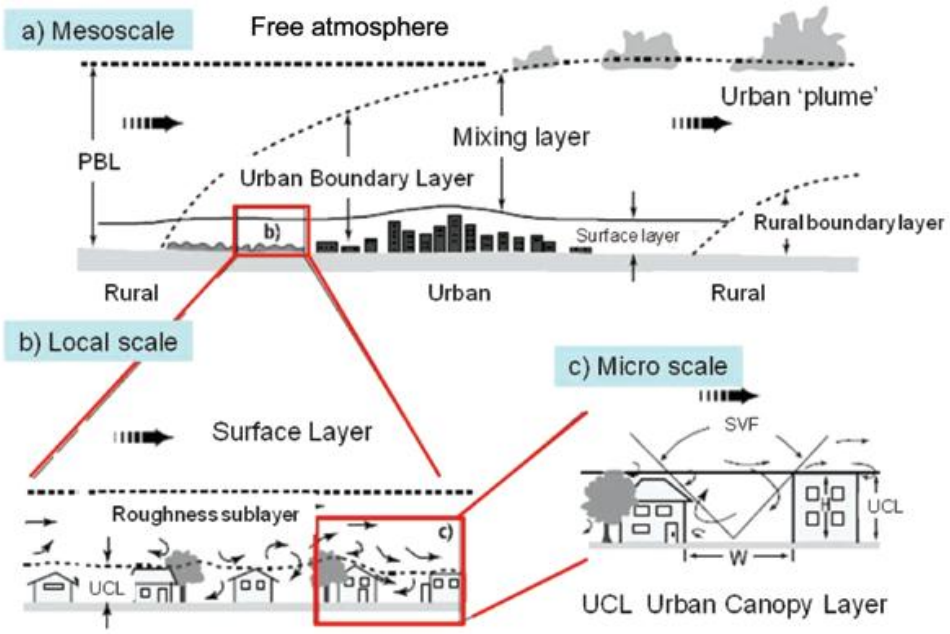

Figure 15 Urban energy balance: three scales used to distinguish atmospheric processes in urban area and the atmospheric layers which are typically identified at each scale. PBL the planetary boundary layer, UBL the urban boundary layer, UCL urban canopy layer. The bold arrow in each of the sub-figures going towards the right indicates the mean wind direction. The smaller arrows shown in (b) and (c) indicate the nature of the mean and turbulent flow (Hove, Steeneveld et al. 2011).

4.3 Urban morphology

Focusing on cities, urban climate is influenced by the city's geographical setting: latitude, proximity to water, surrounding topography, etc. These factors also influence the design of a

city (for example, building styles, urban morphology, built materials, amounts of vegetation) and the behaviours and activities of its inhabitants (amounts of heat, water, etc., released). Within a city, neighbourhoods with similar land use and land cover, generate distinct local-scale climates (10^2–10^4 m). Although several studies described urban energy balances, there has been a lack of uniformity on reporting the characteristics of the studied urban setting, which limited the comparability of the results. To solve this problem, Stewart and Oke (2012) developed a set of "Local Climate Zones" to standardize description of surface structure and cover. These zones are regions of uniform surface cover, structure, material, and human activity that span hundreds of meters to several kilometres in the horizontal plane, Figure 16. This type of classification has been already used to describe some Dutch cities, Table 5 (Hove, Steeneveld et al. 2011).

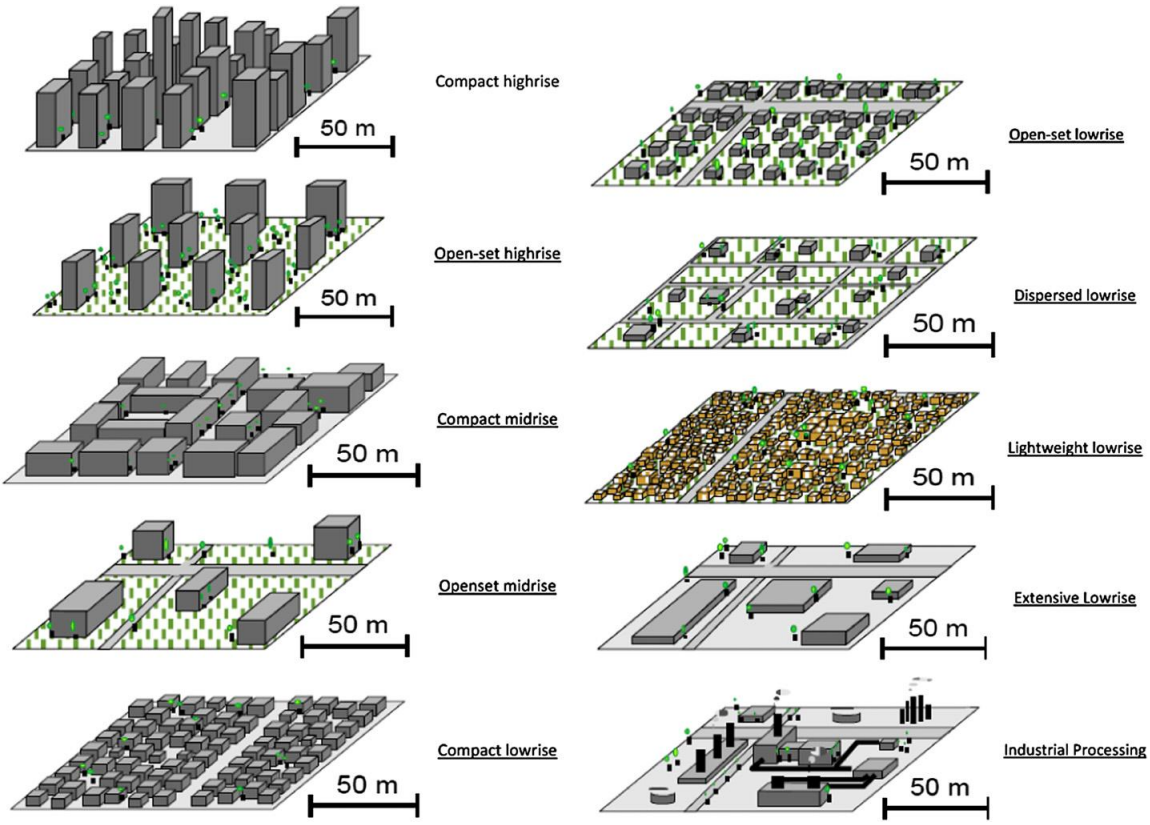

Figure 16 Local Climate Zone (LCZ) classification (Stewart and Oke 2012). Classification number and properties of each zone is given in Table 6.

4.3.1 Roughness layer (RL)

In the roughness layer, the heat flow is affected by the individual roughness elements, and is hence fully three-dimensional in nature. The upper boundary of the roughness sublayer, z_0, is the level at which the horizontal variability vanishes and the flow becomes horizontally homogeneous. The depth of the roughness layer depends on the height and distribution of the roughness elements. For most surfaces $2h < z_0 < 5h$ covers the range of estimates, where h is the average height of roughness elements. To illustrate intra-urban variability, Table 6 shows a classification proposed by (Stewart and Oke 2012).

Table 5 Classification of some Dutch cities according the LCZ (source:Hove, Steeneveld et al. 2011).

City	LCZ	City	LCZ
Apeldoorn	5	Ijsselmuiden	3
Assen	3	Leeuwarden	3-5
Damwoude	5-7	Leiden	3
Delft	2-3	Losser	3-5
Doornenburg	5	Purmerend	3
Groningen	3	Rotterdam	2-3
Haarlem	3	The Hague	3-5
Heemskerk	3	Voorburg	2
Heerhugowaard	3-5	Wageningen	3-5
Houten	3		

4.3.2 Albedo – reflectance

Global radiation comes from the sun and is reflected on surfaces. The terrestrial surface influences the partitioning of available energy between sensible and latent heat fluxes. This partitioning depends both on material characteristics and urban geometry (Arnfield 1990).

Albedo is the ratio of reflected to incident radiation at a particular surface or combination of surfaces, over all the wavelengths of solar irradiation. Lighter materials tend to have higher albedos than darker building fabrics. Building materials (paints, roofing covers, etc), which have higher albedos, have been used to reduce the radiative loading of urban areas and thus mitigate urban heat islands. The urban area has a smaller albedo than the rural surrounds due to multiple reflections between vertical and horizontal facets. Therefore, urban albedo declines with increased canyon aspect ratio. Methods to determine urban albedo vary from simple aggregation: Effective albedo = $\Sigma(A_i\ \alpha_i)/\ \Sigma A_i$, where A_i is the area of the land use (i), and α_i is its albedo (Taha, Akbari et al. 1988) to more advance three dimensional models take into account urban configurations and a change of solar positions, as well as the effects of multiple reflections and shading in an urban canopy (Chimklai, Hagishima et al. 2004).

Theoretically, albedo values will be between 0 and 1.0. However, these limits are not approached in practice. Extreme values around 0.90 are typical of whitewash and snow surfaces, while values near 0.10 are typical of dark asphalt pavements (Taha, Akbari et al. 1988). As shown in Table 6, urban albedo varies between 0.12-0.25. One-dimensional meteorological simulations estimated a maximum of 4°C reduction of localized afternoon air temperatures on summer days by changing the surface albedo from 0.25 to 0.40 in a typical mid-latitude warm climate (Taha, Akbari et al. 1988).

Table 6 Local Climate Zone (LCZ) classification based on Stewart and Oke (2012). Schematic representation of the Local Climate Zone is presented in Figure 16.

Local climate zone (LCZ)	Zone properties					
	SVF	BSF %	Z_H m	RC	albedo	Q_F W m^{-2}
Compact high-rise (1)	0.2–0.4	40-60	>25	8	0.10–0.20	50–300
Compact midrise (2)	0.3–0.6	40-70	10–25	6–7	0.10–0.20	<75
Compact low-rise (3)	0.2–0.6	40-70	3–10	6	0.10–0.20	<75
Open-set high-rise (4)	0.5–0.7	20–40	>25	7–8	0.12–0.25	<50
Open-set midrise (5)	0.5–0.8	20–40	10-25	5–6	0.12–0.25	<25
Open-set low-rise (6)	0.6–0.9	20–40	3–10	5–6	0.12–0.25	<25
Lightweight low-rise (7)	0.2–0.5	60–90	2–4	4–5	0.15–0.35	<35
Extensive low-rise (8)	>0.7	30-50	3–10	5	0.15–0.25	<50
Dispersed low-rise (9)	>0.8	10–20	3–10	5–6	0.12–0.25	<10
Industrial processing (10)	0.6–0.9	20–30	5–15	5–6	0.12–0.20	>300

SVF: Sky View Factor; BSF = building surface fraction; Z_H = height of roughness elements; RC = terrain roughness class; QF = anthropogenic heat flux.

4.3.3 Sky view factor (SVF)

SVF is defined as the fraction of the visible sky from the total possible sky hemisphere at a certain location, Figure 17. The SVF is the variable explaining most of the variation of the magnitude of the UHI. The height/width ratio of the street canyons in the city is sometimes used as an alternative for the SVF. Table 6 shows the ranges for SVF for the different local climate zones. SVF influences local climate by affecting wind directions and reflection of radiation, (Figure 18). At micro scale, it is important to consider the SVF in the energy balance. At larger scales, at neighbourhood or city level, SVF becomes less relevant due to variation of geometry of buildings, and therefore it is not considered in this study.

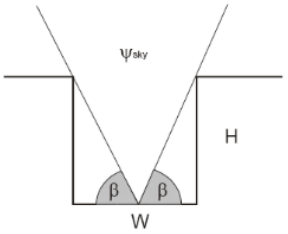

Figure 17 Sky view factor in a symmetrical street canyon, described by its width (W) and its height (H).

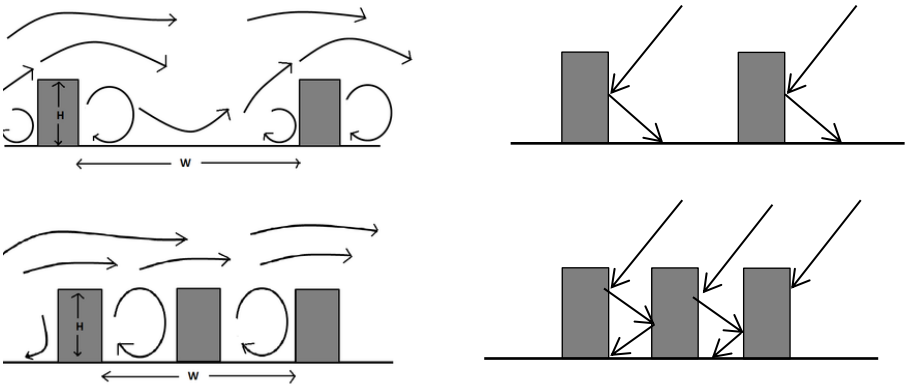

Figure 18 Influence of the Sky view on wind directions (left) and reflection of solar radiation (right).

4.3.4 Advection

Advection results from spatial differences of surface characteristics, for example in surface temperature, moisture availability or roughness. The city's setting, for example, coastal or valley, dictates the magnitude and direction of these exchanges at scales larger than the city. Within the city, the patchiness of urban surfaces, at property or neighbourhood scale, affects horizontal energy exchanges and mixing. Oke (1982) assumed that horizontal advection is negligible in urban energy balance calculations, and it is in general not included in energy balance studies. Steyn (1985) demonstrated that in a suburban site in Vancouver, where there is a sea breeze circulation, advection is small: for all hours 2.5 W m^{-2}; values are larger when individual time periods are considered, but still 16 W m^{-2} at the maximum. In the extended soil temperature model for urban areas, advection is neglected.

4.3.5 Vegetation and latent heat flux

Evapotranspiration, evaporation and transpiration, from soil-vegetation systems is another effective moderator of near-surface climates. Given the right conditions, evapotranspiration can create 'oases' that are 2-8°C cooler than their surroundings (Taha, Akbari et al. 1988).

Rural evapotranspiration has been studied for several decades. Two main methods are broadly applied: "Makkink" and "Penman Monteith". An overview of variables and equations for the Penman Monteith method are available in the web site of the FAO[1]. There is also software able to simulate the water balance in detail for rural areas. One of the models is the Dutch SWAP-model (Soil, Water, Atmosphere and Plant)[2]. SWAP simulates transport of water, solutes and heat in unsaturated/saturated soils. The model is designed to simulate flow and transport processes at field scale level, during growing seasons and for long term time series. However its applicability to urban areas is limited.

Urban evapotranspiration is a function of the level of urban development, specifically of the land cover, (*Figure 19*). The average distribution of the water balance for the different LCZ can be estimated, using *Figure 19*.

[1] http://www.fao.org/docrep/x0490e/x0490e06.htm.
[2] http://www.swap.alterra.nl/

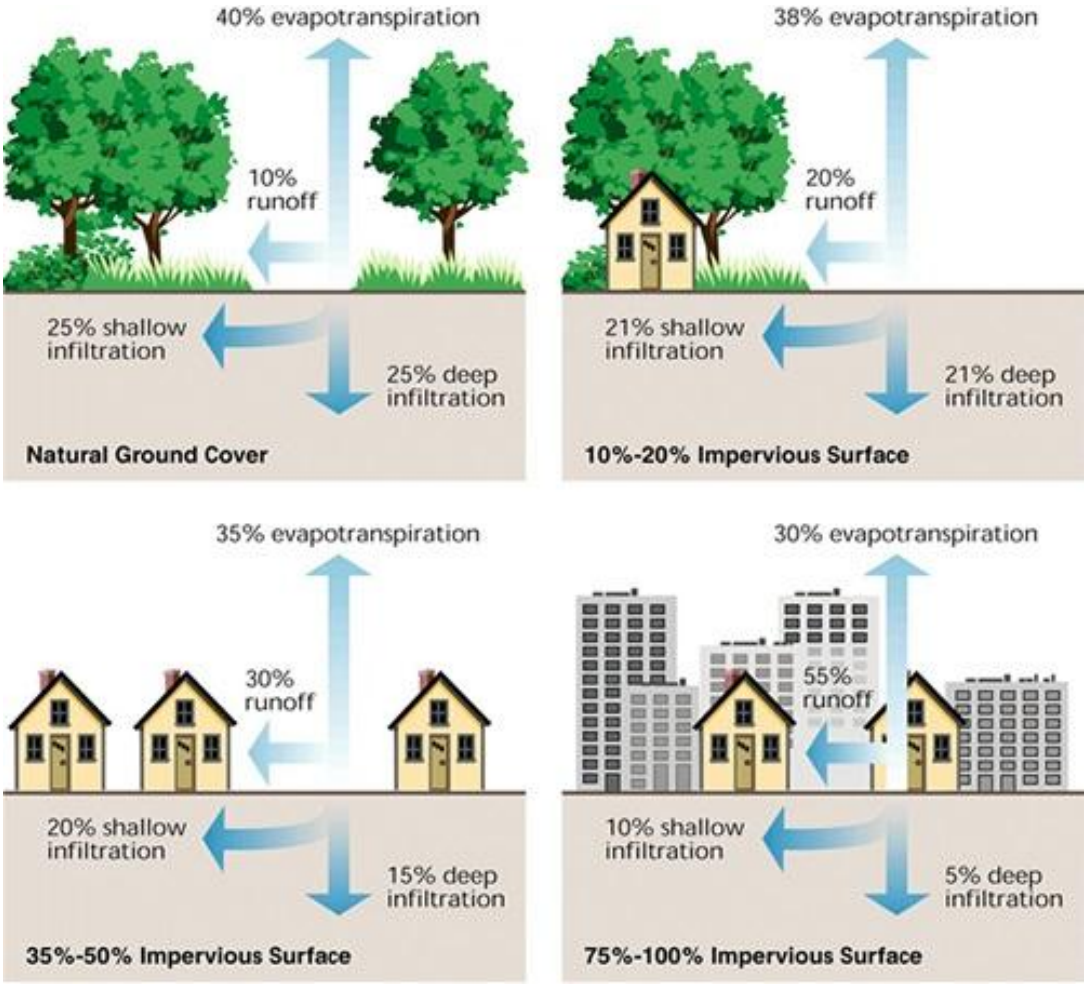

Figure 19 Water balance for different urban areas (Source: EPA).

Evaporation is the process occurring along the water-air or soil-air interface by which water transforms into water vapor escaping into the atmosphere. Transpiration is the process of vaporization of water at the surface of plant leaves after the soil water has been transported through the plant. For simplification, transpiration is combined with evaporation from water and soil surfaces into evapotranspiration (Marsalek et al., 2008). In this study, *ET* refers to evaporation from permeable and impermeable surfaces and evapotranspiration from green areas. In this study, the adapted Penman-Monteith method for urban areas was used to calculate the reference evapotranspiration. The reference evapotranspiration was assumed as potential evapotranspiration (ET_{pot}). The actual evapotranspiration (ET_{act}) is determined by the water availability on each of the surfaces and roofs (see §5.3).

Infiltration (*I*) refers to the process of water passing through the ground surface into the pores of the soil, and entering the groundwater system. *I* depends on soil type, structure and compaction, initial moisture content, surface cover and the depth of the water layer in the soil (Butler and Davies, 2000). The infiltration rate tends to be high initially, but decreases exponentially to a final quasi-steady rate when the upper soil zone becomes saturated. Some standard values used to estimate infiltration are presented in Table 7. In this study, infiltration is neglected based on the assumption that in urban areas the drainage system will collect the excess water instantly and also due to increasing compaction of the urban soil which is less permeable.

Table 7 Typical values of runoff coefficients according surface.

Surface type	Description	Runoff coefficient C
Paved	High quality paved roads with gullies < 100 m apart	1.00[a]
Paved	High quality paved roads with gullies > 100 m apart	0.90[a]
Paved	Medium quality paved roads	0.85[a]
Paved	Poor quality paved roads	0.80[a]
	Asphalt and concrete pavement	0.70-0.95[b]
	residential	0.3-0.7[b]
Roofs		0.75-0.95[b]
Permeable	High to medium density housing	0.55-0.45[a]
Permeable	Low density housing or industrial areas	0.35[a]
Permeable	Open areas	0.00-0.25[a]
Lawns		0.05-0.35[b]

[a] Loucks et al., (2005), [b] Butler and Davies, (2000)

4.3.6 Anthropogenic heat (QF)

Anthropogenic heat is related to the waste heat resulting from heating and cooling of buildings, manufacturing, transportation, and lighting. Human and animal metabolisms are also considered sources of artificial heat. Heat from these sources warms the urban atmosphere by conduction, convection, and radiation. The contribution of anthropogenic heat to the urban energy balance is largely a function of latitude and season of the year.

Anthropogenic heat flux has generally been ignored as climate forcing. Averaged globally anthropogenic waste heat is of the order of 0.03 Wm^{-2} (Flanner 2009). However, QF has been reported to range from tens to hundreds of Wm^{-2} in U.S. and European cities (Sailor and Fan 2004, Pigeon, Legain et al. 2007) and as high as 1590 Wm^{-2} for the business district of Tokyo (Ichinose, Shimodozono et al. 1999), Table 8. Therefore, anthropogenic heat can have a significant, dynamic, contribution to the surface energy budget, which changes according urban characteristics as shown in Table 6. A detailed description of the temporal, diurnal and monthly variations of anthropogenic heat for cities located on the northern hemisphere is given by Allen, Lindberg et al. (2011). Allen, Lindberg et al. (2011) described how to determine average daily or year values, they have developed a software called LUCY (Large scale Urban Consumption of energY), which can be used for more detailed analysis according to the location.

Table 8 Reported anthropogenic heat for different cities/country (Hove, Steeneveld et al. 2011).

City/country	Reported QF W/m²
Basel, Switzerland	5-20
Lodz, Poland	32
USA	60-75
Tokyo, Japan	200-1590

Stewart and Oke (2012) also defined typical values of anthropogenic heat for each LCZ, Table 5. For Rotterdam, TNO performed an assessment of the anthropogenic heat, Table 9. Although the anthropogenic heat shows a diurnal patterns, due to lack of detailed information a fixed valued was used.

Table 9 Reported average anthropogenic heat for Rotterdam during the summer.

Source	W/m²
Large sources	48
S&ME's	0.3
Traffic	3.2
Body	0.2
Cooking	0.5
Electrical appliances	0.5
Lighting	0.4
Air conditioning	0.8
Total	53.9

4.3.7 Heat storage

Typically the storage heat flux is considerably larger in an urban area than in its rural surroundings. This is due to the increase in effective thermal mass per unit urban surface area. In rural areas, it is only the top 20-50 cm of the soil which plays an active role in the diurnal energy balance. In urban areas, because of the increased roughness of the city and larger heat transfer surface area resulting from building's geometry, the effective mass contributing to the diurnal thermal storage is higher than in rural areas. This increased thermal storage moderates the diurnal fluctuation in urban temperature and delays the time of the peak temperature. The differential in cooling rates and their different timing result in the largest urban-rural temperature difference in the evening.

This flux is the net uptake or release of energy, per unit area and time, by sensible heat changes in the urban canopy air layer, buildings, vegetation and the ground. Key characteristics that influence the size of the storage heat flux are the surface materials, the urban structure and the resulting thermal mass. In general, urban surface materials have good ability to accept, conduct and diffuse heat into, and out of, the urban fabric. The flux is therefore significant because there is a large mass to heat up and cool down, plus there is a large surface area when vertical faces are included.

Although different approaches have been developed, this term remains a source of imprecision in urban energy balance measurement and modelling due to the lack of a standard for quantifying heat storage (Roberts, Oke et al. 2006). The complexity of the urban surface makes the storage heat flux difficult to observe. Two approaches have primarily been used: (a) calculation as a residual of the energy balance, and (b) intensive sampling of the temperatures of all surface, using heat conduction equations. The storage heat flux ΔQ_s [W m^{-2}] has been parameterized by Grimmond and Oke (1999):

$$\Delta Q_s = a_1 R_{net} + a_2 \frac{\partial R_{net}}{\partial t} + a_3 \qquad (3)$$

Where a_1.[-], a_2 [s] and a_3 [W/m²] are empirical coefficients for different surface type. Values for these coefficients for grass are given in Grimmond and Oke (1999) and Roberts, Oke et al. (2006).

Both approaches have the possibility to contain errors but comparisons of the two methods show consistency in their results (Grimmond and Oke 1999). The storage heat flux, determined as the residual of energy balance observations, is a significant component of the energy balance at all of the urban sites studied. It accounts for 17%–58% of the daytime net radiation (Grimmond and Oke 1999).

Similarly to the calculation of effective albedo, the effect of increased urban thermal storage can be simulated through the combined effects of modified soil properties, building materials characteristics, and roughness. That is: effective thermal mass = $\Sigma\ (\rho_i C_i A_i)/\Sigma A_i$, where $\rho_i C_i$ is the thermal mass of the participating material in a component land use (i), and A_i is the area of the component land use (Taha, Akbari et al. 1988)

4.4 Typical Dutch cities

The term urban "heat island" describes built up areas that are hotter than nearby rural areas. The heat island is often determined using the atmospheric temperature. Figure 20 shows the urban heat island (UHI) effect in the Netherlands, measured with thermal infrared satellite images, left during the day and right during the night.

The atmospheric heat island effect can be as high as 8°C during the day and during the night in summer. The spatial distribution shows clear differences. During the day, clearly the city of The Hague has the strongest UHI effect, in the night Rotterdam has the strongest UHI effect.

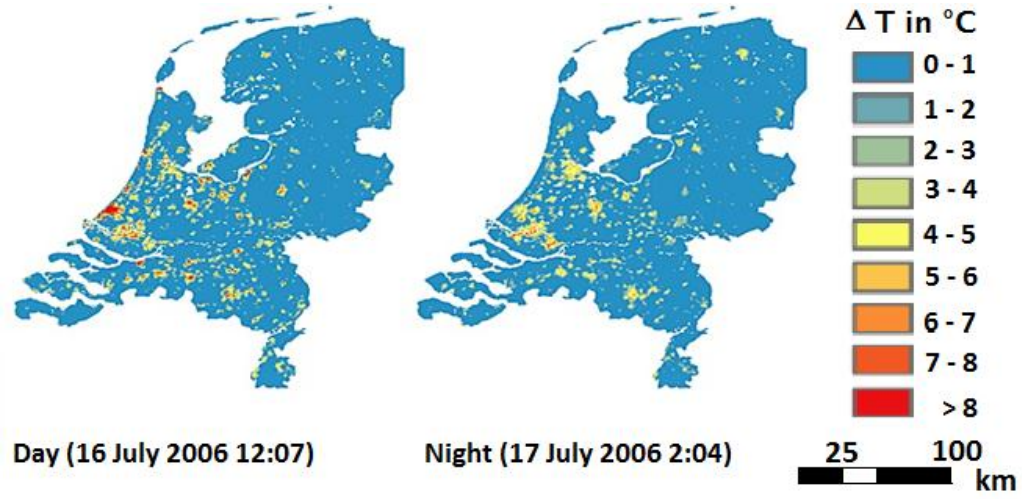

Figure 20 Average Heat Island effect in the Netherlands, left: during the day (16 July 2006) and right: during the night (17 July 2004), source: (Klok, Schaminee et al. 2012).

4.4.1 Urban climate in Rotterdam

For Rotterdam, not only UHI has been monitored, but also the Surface Urban Heat Island Effect (SUHI), (Klok, Broeke et al. 2010; Klok, Schaminee et al. 2012; Klok, Zwart et al. 2012). The SUHI is the difference between the surface temperature in the rural area and the surface temperature in the city. Figure 21 shows the spatial variation of the surface temperature in Rotterdam, based on 15 Landsat images taken between 1984 and 2007, with a resolution of 60m x 60m. The peri-urban area has an average temperature of 295K (~23°C), while the

urban area shows a temperature between 305K and 308K (~33°C – 36°C). Therefore, the average SUHI in Rotterdam is circa 10°C. However, "hot spots" within the urban area are identified. These spots have a temperature > 311K (~39°C) and a ΔT=16°C. The gradient of the urban heat island refers to the spatial rate of variation, which is given by presence of green areas and water bodies, by the urban density and urban materials. Water surface temperatures are lowest, followed by grassland north and east of the city. A striking result is that not just the centre of Rotterdam, but also its industrial areas and harbours in the west of Rotterdam show high surface temperatures. This is related to the numerous dark rooftops and the large areas of paved and impervious surfaces (Klok, Zwart et al. 2012). Also the

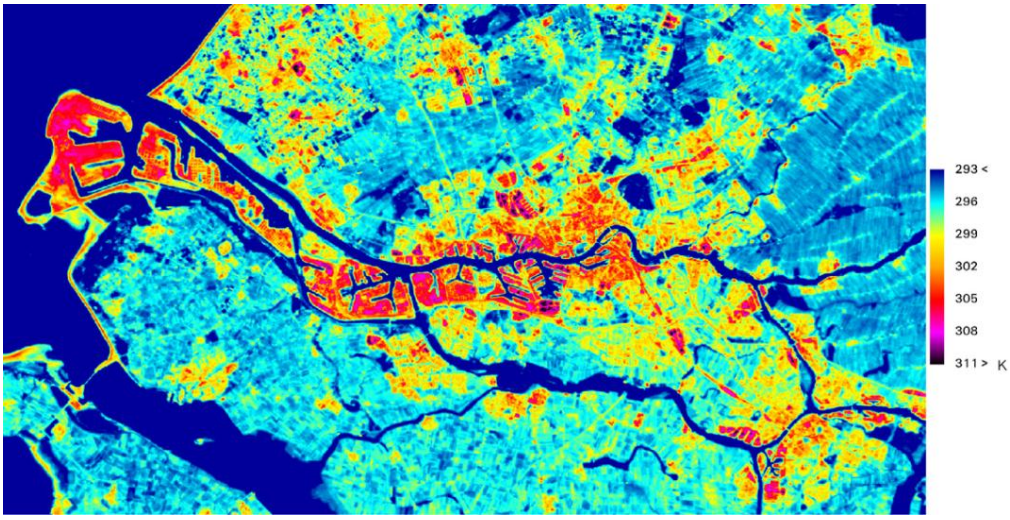

Figure 21 Average surface temperature distribution (K) of Rotterdam based on 15 Landsat images (Klok, Zwart et al. 2012).

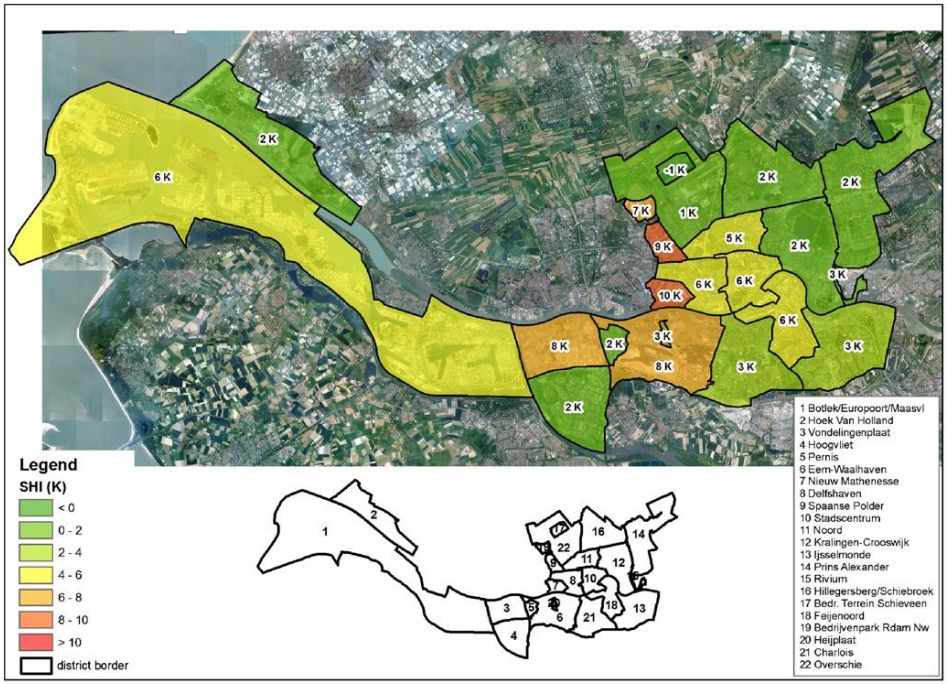

Figure 22 Average surface heat island (SUHI) in Rotterdam during the summer per neighbourhood, (Klok, Zwart et al. 2012).

higher location of the western harbour area (> 5 meters above NAP) and the heat emissions from industry may play a role. An average SUHI per neighbourhood can be reported by aggregating this information, Figure 22. The maximum SUHI per neighbourhood is 10°C.

Classification of the local zones is also sensitive to the scale. Table 5 showed that considering the complete city, Rotterdam could be described as LCZ 2-3. However looking at smaller scale, in different areas of the city, different classification can also appear, Table 10. In this case it is not recommended to use average city values but to consider different areas.

Table 10 Characteristics of the different monitored sites by (Hove, Steeneveld et al. 2011) in the city of Rotterdam and its peri-urban area.

Location	Description	Roughness class	Aspect ratio	% built	UCZ
City centre	Intensely developed urban area with detached close-set high-rise buildings	8	>2	>90	1
South	Intensely developed high density urban area with 2-5 story, attached or very close-set buildings often of brick or stone	7	1.0–2.5	>85	2
East	Highly developed, low or medium density urban with row or detached but close-set houses, stores and apartments	7	0.5–1.5	70-85	3
Rural site	Scattered houses in agricultural area	4	>0.05	<10	7

4.5 Subsurface thermal interactions

Soil models are coupled with water models to simulate evaporation flows. Previous studies of heat and moisture transport in soil have shown that transport of both liquid water and water vapour can be important processes in a soil heat budget (Herb, Janke et al. 2008).

4.6 Conclusions

Urban areas have their own micro-climate. However different parameters are involved in the urban energy balance, which are not easy to determine with precision. To solve this problem, recently a typology of urban zones has been defined. Ten categories describe urban areas and provide ranges for different variables involved in the energy balance, based on previous studies. The soil temperature model allows to estimate the temperature at different depths for specific areas. The urban typologies described in the LCZ are used to further define the input variables for the soil temperature model.

5 Extending the existing soil temperature model

5.1 Introduction

Blokker and Pieterse-Quirijns (2013) developed a model to calculate the heat transfer between atmosphere and soil. Four layers are considered for the description of the soil temperature under certain weather and environmental conditions: the atmosphere, the roughness layer (RL), the soil surface (SS) and the soil, see Figure 23. The heat transfer is described by two energy balances: the energy balance in the roughness layer and the heat balance in the soil surface. Appendix V contains the description of the variables of the model.

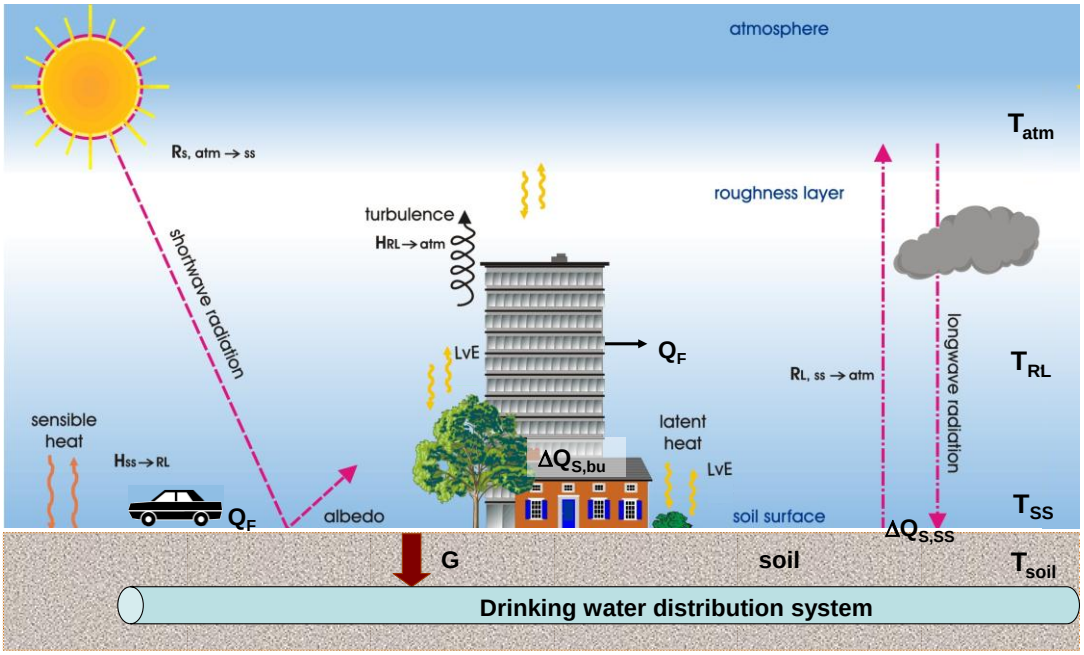

Figure 23 Schematic heat transfer in a urban setting (after Blokker and Pieterse-Quirijns, 2013).

As described by Blokker and Pieterse-Quirijns (2013) , the heat transfer in the RL is driven by the sensible heat fluxes between the atmosphere and the RL (HRL→atm) and between the SS and RL (HSS→RL). The total heat transfer between SS and the atmosphere is described by:

$$\rho C_p h_{RL} \frac{\partial T_{RL}}{\partial t} = H_{SS \rightarrow RL} - H_{RL \rightarrow atm} = \rho C_p \left(T_{SS} - T_{RL}\right) / R_g + \rho C_p u^* T^* \quad (4)$$

in which ρ [kg m-3] and C_p [J kg-1K-1] are density and specific heat capacity of air and hRL [m] is the height of the RL air column. T_{SS} [K] and T_{RL} [K] are the temperatures of SS and RL respectively, Rg [s m^{-1}] is a flux resistance associated with the transfer of heat and moisture from the SS to the RL. The corrected variables are given by the friction velocity u* [m s^{-1}] and friction temperature T* [K] and are described in Appendix VI.

Rewriting Eq. 4 leads to the following equation for the temperature in the RL that can be solved numerically:

$$h_{RL}\frac{\partial T_{RL}}{\partial t} = \left(T_{SS} - T_{RL}\right)/R_g + C_D u\left(T_{atm} - T_{RL}\right) f_h \quad (5)$$

Where, C_D [-] is the friction drag coefficient, u is the wind velocity [m s^{-1}], T_{atm} [K] is the atmospheric temperature and f_h is a stability factor.

In an urban area, the heat transfer at the SS is driven by the net irradiation from the sun (R_{net}) and the anthropogenic heat emissions (Q_F), the sensible heat flux between SS and RL ($H_{SS\rightarrow RL}$), the storage heat in the surface (ΔQ_s), the latent heat flux due to evaporation ($L_v E$) and the heat flux into the subsurface (G)

$$\rho_{soil} C_{p,soil}\frac{\partial T_{soil}}{\partial t} = \frac{\partial}{\partial z_{soil}}\left(R_{net} + Q_F - H_{SS\rightarrow RL} - \Delta Q_s - L_v E\right)\Big|_{z=0} + \frac{\partial}{\partial z_{soil}} G \quad (6)$$

ρ_{soil} and $C_{p,\,soil}$ are soil parameters, ΔQ_s is the heat storage in the surface and urban elements [W m^{-2}]. The net radiation R_{net} [W m^{-2}] is the sum of the incoming short wave radiation ($R_{s,\,atm\rightarrow SS}$, the direct radiation from the sun minus the reflected radiation) and the incoming and outgoing long wave radiation ($R_{l,\,in}$ and $R_{l,\,SS\rightarrow atm}$, the temperature related radiation). The albedo (a_i) is a property of the land cover i, therefore for a given area with n number of surface types, R_{net} can be expressed as:

$$R_{net} = \sum_{i=1}^{n} \left(1 - a_i\right) R_{global} + \varepsilon_{eff}\sigma T_{atm}^4 - \sigma T_{SS,i}^4 \quad (7)$$

With a_i [-] the albedo for each of the i land cover types in a given area, R_{global} [J m^{-2} s^{-1}] is the global radiation, σ the Stefan-Boltzmann constant (5.67 10^{-8} W m^{-2}K^{-4}), and ε_{eff} [-] the effective or apparent sky emissivity.

5.2 Extending the model for urban areas

The latent heat flux due to evaporation [W m-²] from each surface is calculated with the modified version for urban areas of the Penman-Monteith equation (Grimmond and Oke 1991).

$$L_v E = \frac{s(R_{net} + Q_F - \Delta Q_S) + C_p \rho V / r_a}{s + \gamma(1 + r_{ss}/r_a)} \quad (8)$$

Where s is the slope of the saturation vapour pressure curve in [hPa K^{-1}], V [hPa] the air vapour pressure deficit of the air and γ the psychrometric constant [hPa K^{-1}]. The formulas are described in the appendix A. r_{ss} [s m^{-1}] is a redefined surface resistance which includes dry and wet conditions.

$$r_{ss} = \left[\frac{W}{r_b(s/\gamma + 1)} + \frac{(1 - W)}{r_s + r_b(s/\gamma + 1)}\right]^{-1} - r_b(s/\gamma + 1) \quad (9)$$

Where W is a function of the amount of water on the individual surfaces (C_i) relative to the surface water storage capacity (S_i), both in mm. W=1 if the amount of water in the surface is equal to the storage capacity of the surface, and then r_{ss} is equal to zero.

$$W = \begin{cases} W = 1 & C_i = S_i \\ W = \dfrac{(K-1)}{K - S_i / C_i} & C_i < S_i \end{cases} \quad (10)$$

K [-] relates to the aerodynamic (r_a) and surface (r_s) resistances [s m^{-1}] (Berthier, Dupont et al. 2006) and are defined as:

$$K = \frac{(r_s / r_a)/(r_a - r_b)}{r_s + r_b(s/\gamma + 1)} \qquad \begin{cases} r_a = 1/(0.007 + 0.0056 * u) \\ r_b = 1.1 u^{* -1} + 5.6 u^{* 1/3} \end{cases} \quad (11)$$

Where r_b [s m^{-1}] is the mean boundary layer resistance and a single integrated surface resistance r_s [s m^{-1}], which is the inverse to the surface conductance (g_s), for an area with different surface type can be described as,

$$r_s^{-1} = g_s = G_1 \sum_{i=1}^{n} \left(f_i g_{i,\max} \frac{LAI}{LAI_{\max}} \right) \quad (12)$$

Järvi, Grimmond et al. (2011) included additional parameters due to the daily time step. In our case, the time step is one minute, therefore these parameters are not needed.
G_1 [mm s^{-1}] is a parameter related to the maximum surface conductance. The maximum conductance values vary between 5 and 20 mm s^{-1} (Järvi, Grimmond et al. 2011). f_i is the fraction cover of vegetation [-] and $g_{i,max}$ [m s^{-1}] is the maximum conductance values for the surface type *i*. *LAI* is the leaf area index [-]. *LAI* is calculated based as the ratio of leaf to ground area. *LAI* varies per vegetation type.

5.3 Evapotranspiration (E)

In the model, potential evapotranspiration (E_{pot}) is calculated with equation 13. Then, the water availability in the surface for evapotranspiration is determined with a water balance. Each surface (*i*) has a storage capacity of S_i (mm). Since we focus on the urban area, we assume that excess of water in the surface is quickly discharged into the drainage system and thus infiltration is neglected. Available water at the surface is calculated for each time step (t), based on the storage level of the previous time step and the precipitation of the current time step, P_t [mm]. Then the actual evapotranspiration, E_{act} [mm], is determined by

$$E_{act,t} = \begin{cases} E_{pot,t} < C_{i,t-1} + P_t & \Rightarrow E_{act,t} = E_{pot} & \Rightarrow C_{i,t} = C_{i,t-1} + P_t - E_{pot} \\ E_{pot,t} > C_{i,t-1} + P_t & \Rightarrow E_{act,t} = C_{i,t-1} + P_t & \Rightarrow C_{i,t} = 0 \end{cases} \quad (13)$$

Finally, based on the actual evapotranspiration, *LvE* is recalculated as well as the total energy balance for each time step.

With Δz being the thickness of the top soil layer and assuming the soil's thermal conductivity coefficient λ_{soil} to be independent of z, Eq. 6 becomes:

$$\rho_{soil} C_{p,soil} \frac{\partial T_{soil}}{\partial t} =$$
$$\lambda_{soil} \frac{\partial^2 T_{soil}}{\partial z_{soil}^2} + \frac{1}{\Delta z}\left(R_{net} + Q_F - \Delta Q_s - L_v E - \rho C_p \left(T_{SS} - T_{RL}\right)/ R_g\right) \quad (14)$$

5.4 Heat storage (ΔQS)

The heat storage flux is the net uptake or release of energy from an urban system. All surfaces and objects in an area absorb or release energy. The storage heat flux ΔQ_s [W m^{-2}] has been parameterized by Grimmond and Oke (1999):

$$\Delta Q_s = a_1 R_{net} + a_2 \frac{\partial R_{net}}{\partial t} + a_3 \quad (15)$$

Where a_1.[-], a_2 [s] and a_3 [W/m²] are empirical coefficients for different surface type, Table 11. Values for these coefficients for grass are given in (Grimmond and Oke 1999) and (Roberts, Oke et al. 2006).

Table 11 Literature values of the coefficients to determine heat storage.

Surface cover	a_1	a_2 (h)	- a_3 (W m^{-2})
Grass	0.32	0.54	27.4
Rooftop	0.17-0.82	0.10-0.57	17.0-55.7
Concrete	0.81-0.85	0.32-0.48	28.5-79.9
Asphalt	0.36–0.82	0.23–0.68	19.3–150.0

5.5 Anthropogenic heat (QF)

For the peri-urban area, QF is set to zero. Although anthropogenic heat shows daily and seasonal patterns, due to the lack of information for Rotterdam, anthropogenic heat is added as a fixed value in the model, using the reference values and the specific estimation for Rotterdam described in 4.3.6.

5.6 Conclusions

The extended model includes urban evapotranspiration, heat storage and anthropogenic heat. Advection is neglected and SVF is not specifically included because this is included in the ΔQs coefficients. Although literature values are found to use as input model, different studies have shown that heat storage calibration provides different coefficients for different areas.

Table 12 Overview of the variables used in this study for summer condition.

Variable	Unit	Peri-urban areas (De Bilt - Rotterdam)	Rotterdam
λ_{soil}	W/m.K	0.7	0.7 – 1.2 - 2.6
ρ_{soil} x Cp	J/m³.K	2 x 10^6	2 x 10^6
G1	mm/s	14.97	11.54
Zo	m	0.15	0.15
h_{RL}	m	10	10 - 25
QF	W/m²	0	50 - 100 - 150
a_1	[-]	0.3	0.8
a_2	[s]	6[a]	30 - 42[a]
$-a_3$	W/m²	10	90 - 100 -120

[a] Value is fitted using data. Values differ from values given in Table 11, due to the difference in the time step of simulation.

6 Model validation in a peri-urban area

6.1 Available data and assumptions for the soil temperature model

To calibrate the soil temperature model, one peri-urban location was selected: de Bilt. This allows to analyse the heat flows due to evapotranspiration and to avoid interference with urban related heat flows, such as heat emissions from traffic or heating losses from buildings, therefore, Q_F=0. De Bilt is the main weather station of the Dutch Royal meteorological institute (KNMI). For this location, historic hourly T_{atm}, R_{global}, u and P records are publicly available from the KNMI website (KNMI 2013). De Bilt is located on sand. To validate and calibrate the model, soil temperature measurements for this location were used. Soil temperature measurements were provided by the KNMI at 5cm, 10cm, 50cm and 100cm from 1st January 2008 until 31st December 2012. The soil temperature was logged every 6 hours. As an additional parameter to test the model, the simulated potential evapotranspiration was compared with the daily values reported by the KNMI, using Makkink equations (KNMI 2013).

The ratio LAI/LAImax was assumed to be 0.9, albedo for vegetation equal to 0.19 was used. The roughness length z_0 [m] equals 0.15 m for grass, Rg was estimated at 30 s m^{-1} and ε_{eff} was determined with a beta probability density function, α = 14.8616, β = 1.6411, and the condition that ε_{eff} > 0.7, as described in (Blokker and Pieterse-Quirijns 2013). The height of the RL air column h_{RL} [m] was set to be 10m (van der Molen 2002). G_1 is an empirical variable, assumed to be 14.97 mm s^{-1} (Järvi, Grimmond et al. 2011).

De Bilt evaporates normally about 540 mm for a whole year through the reference crop. Over the entire month of January it is about 8 mm against about 90 mm during the entire month of July. From year to year this quantity varies little; during the period 1961 – 1990, the highest and the lowest yearly evapotranspiration were 629 mm and 497 mm respectively. At the beginning of the growing season (early April), daily evaporation is on average about 1.5 mm. As the growing season progresses, the daily evaporation is up to about 3 mm in early July. Thereafter, the evaporation decreases (KNMI, 2013).

The soil temperature at -1.0 m for De Bilt was simulated using the original model (SM: simplified model) (Blokker and Pieterse-Quirijns 2013) and the extended model (EM) described in Chapter 5, including evapotranspiration and heat storage in the surface, for a warm summer, with a heat wave. Soil thermal properties for De Bilt are not available; therefore, literature values were used. The saturation level of the soil was assumed to be 50%. For this saturation value a ρ_{soil}=1.83x10³ kg/m³ and $C_{p,soil}$=1.11 J/Kg K. Thus, $\rho_{soil}c_{p,soil}$=2.03 x 10^6 J/m³ K.

Figure 24 shows that by considering the evapotranspiration the simulated soil temperature, for given soil thermal properties, cools down by ca. 0.4°C, in comparison with the original soil temperature model (SM), (Figure 24). However, the simulated evapotranspiration shows an error of 33%. This overestimation of the evapotranspiration is the result of neglecting the storage in the surface.

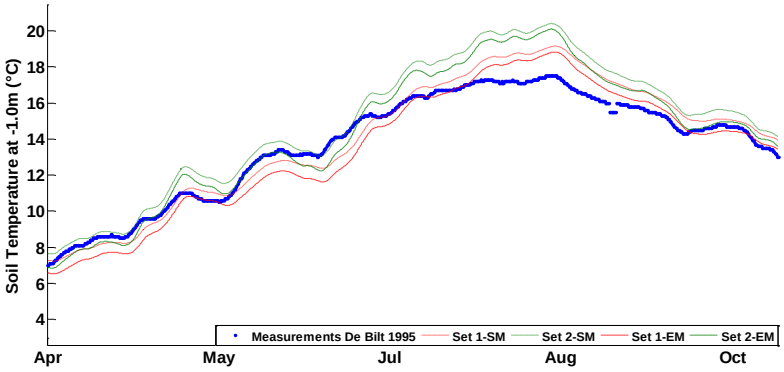

Figure 24 Calibration of the model for De Bilt, for a warm summer (heat wave). SM: simplified model and EM: extended model, ET: Evapotranspiration, without considering heat storage in the surface.

Table 13 Overview of the results for the extended model.

	KNMI	Set 1	Set 2
Daily ET (mm)	3.3	4.3	4.57
Total ET summer (mm)	300.0	395.4	410.8
Absolute Error total (mm)		95.6	111.0

Using the daily evapotranspiration calculated by the KNMI, the soil parameters and the parameters for the heat storage were calculated. The comparison of measured and simulated temperature at -0.5m and -1m are shown for the whole year in Figure 25 and for the summer in Figure 26. At -0.5m the error is larger than at -1.0m, this can be explained by the assumptions of an homogeneous soil profile and an average moisture in the soil.

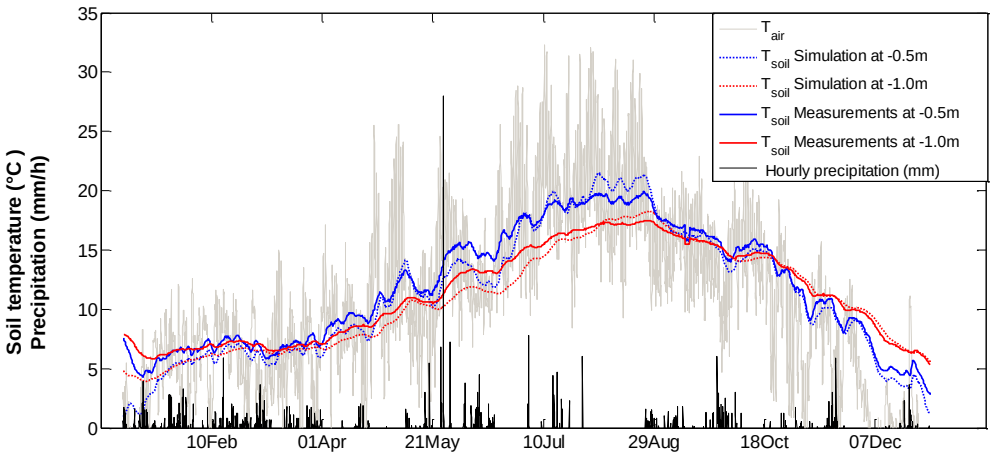

Figure 25 Calibration of the model for De Bilt, for a warm summer in 1995 (with a heat wave) with the EM: extended model, considering heat storage in the surface.

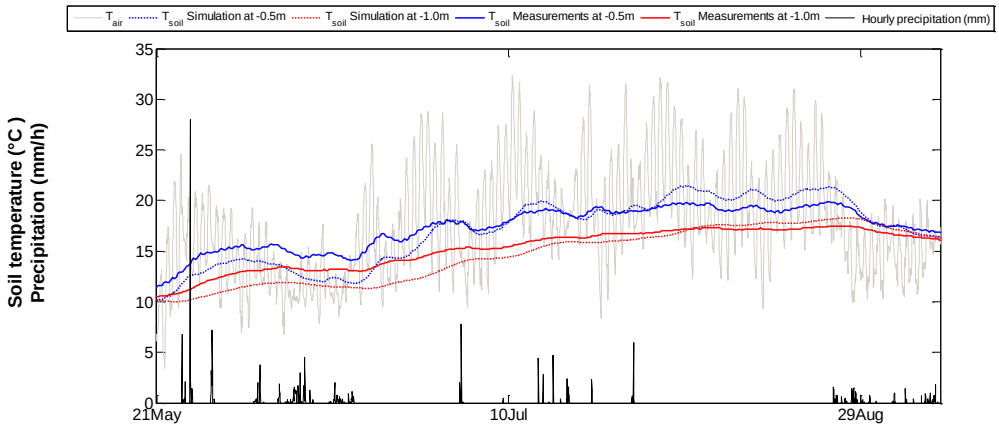

Figure 26 Calibration of the model for De Bilt, for a warm summer in 1995 (with a heat wave) with the EM: extended model, considering heat storage in the surface.

6.2 Sensitivity analysis

For peri-urban areas, a sensitivity analysis was conducted by varying the values of all variables +/-25% and +/- 50%. Figure 27 shows the variation of the mean average error (MAE) for De Bilt. These results confirm that the thermal soil characteristics are crucial to determine the soil temperature in peri-urban areas.

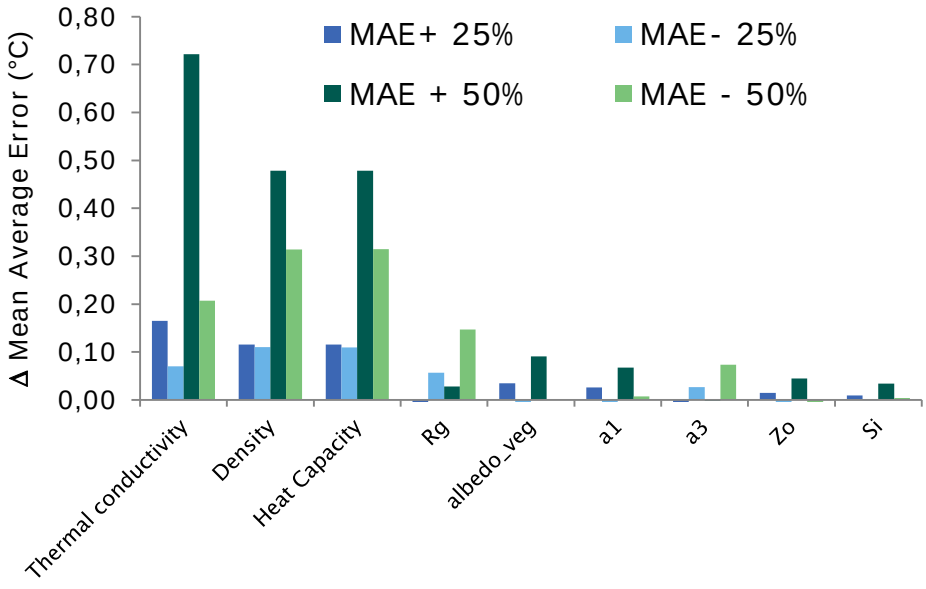

Figure 27 Sensitivity analysis of the different variables for a peri-urban area, varying each of the variables +/-25% and +/-50%.

6.3 Conclusions

The model meets the expectation of predicting the soil temperature for peri-urban locations. Although the parameters are not easy to determine, literature values can be used for a good approximation in the summer. Defining a fixed value for the soil properties (soil type and moisture) for the complete profile, for the complete analysed period, provided a good approximation.

By modelling the evapotranspiration and heat storage a better simulation of the soil temperature was achieved.

It is confirmed that soil thermal properties play a large role in the calibration of the model for peri-urban areas. However, a fixed value can be used to simulate the soil temperature for a specific season. The model analyses the effect of different soil thermal properties, to gain insight in the potential variation range of temperatures. The sensitivity analysis showed a comparable importance of the density and heat capacity, as described in Chapter 2. Both vary with the moisture content of the soil, given the uncertainty of both, ρ_{soil} $c_{p,soil}$. The product of the two will be used for further analysis.

7 Model validation in an urban area

7.1 Available data and assumptions for the soil temperature model

To calibrate the soil temperature model, Rotterdam was selected. For this location, historic hourly T_{atm}, R_{global}, u and P records are publicly available from the KNMI website (KNMI 2013) for a meteorological station, which is located approximately 0.5 km from the city. The soil temperature at -1.0 m for Rotterdam was simulated using the extended model, including evapotranspiration and heat storage in the surface, for a warm summer, with a heat wave. Soil thermal properties for Rotterdam are not available. Therefore, literature values were used. Based on the ground water levels interpolation, ground water levels vary from -1.0 m to -2.0 m from surface level in the summer of 2013. The moisture level is expected to be between 100% (for the water table at -1m) and 50% for water table at 2m depth (average water content of 0.20, with reference to a maximum water content of 0.40, an average sandy soil using Figure 4). Therefore, from Table 4, $\rho_{soil}\, c_{p,soil}$ is assumed to vary from 2.0 – 2.5 x 10^6 J $m^{-3}K^{-1}$.

7.2 Model validation for Rotterdam

For Rotterdam, the results of the regular random temperature sampling at the customer's tap were used to validate the model. To take these samples, the water tap is opened and the reported temperature is recorded when a stable water temperature is reached. Evides reported tap water temperature for two areas: Rotterdam North and Rotterdam South. Both areas are supplied with treated surface water. Figure 28 shows the comparison of the two areas. The north area shows higher temperatures at the customer's tap, especially in the winter. The north area has a stronger level of urbanization than the south. Moreover, North Rotterdam has a district heating network, that can cause a higher temperature during winter. In general, the difference at -1.0m depth between rural and urban soil is ca. 4°C based on the simulations for urban soils (continuous black line). However, looking at the measurements, water at customer's tap can show a difference of up to about 8°C taking as reference the "rural" soil temperature. The urban soil temperature is calibrated for "compact" urban soil.

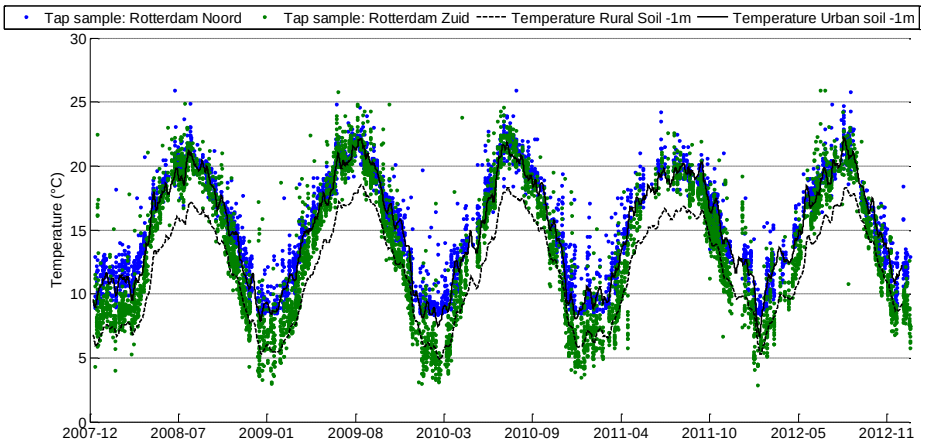

Figure 28 Comparison of the measured water temperature and the simulated soil temperature in the rural and urban area in Rotterdam at -1 m depth.

This means that the thermic properties are different than for the rural soil. Additionally a 50 W/m² anthropogenic heat was used, based on data from TNO.

Figure 29 shows the simulated rural temperature for Rotterdam using the parameters for De Bilt. These temperatures are compared with the water temperature at the pumping stations Berenplaat and Kralingen. In the summer the rural soil temperature at -1 m is close to 4°C colder, while in the winter soil temperature is 3°C warmer.

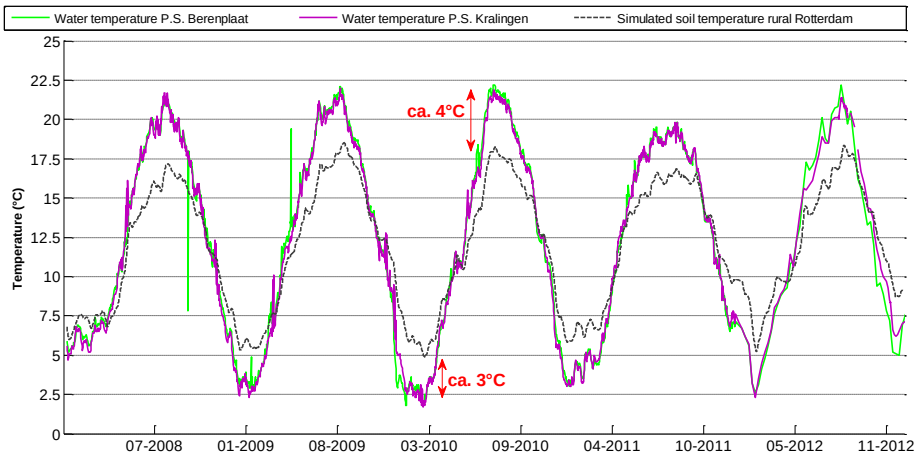

Figure 29 Comparison of the measured water temperature at the pumping stations Berenplaat and Kralingen and the simulated soil temperature in the rural area in Rotterdam at -1 m depth.

Figure 30 shows the overview of the rural and urban soil at -1.0m, simulation of the average soil temperature in Rotterdam shows seasonal variations between 10°C and 20°C. It can be seen that in the winter, urban soil temperatures coincide with temperature at the tap, while temperature at the pumping station is approximately at least 5°C cooler. In the winter, the temperature in the pumping station is also lower than the soil temperature. Therefore, after leaving the pumping station water warms up, first to the rural soil temperature, after that to the urban soil temperature, and finally water can be heated by local variation given by local heat sources.

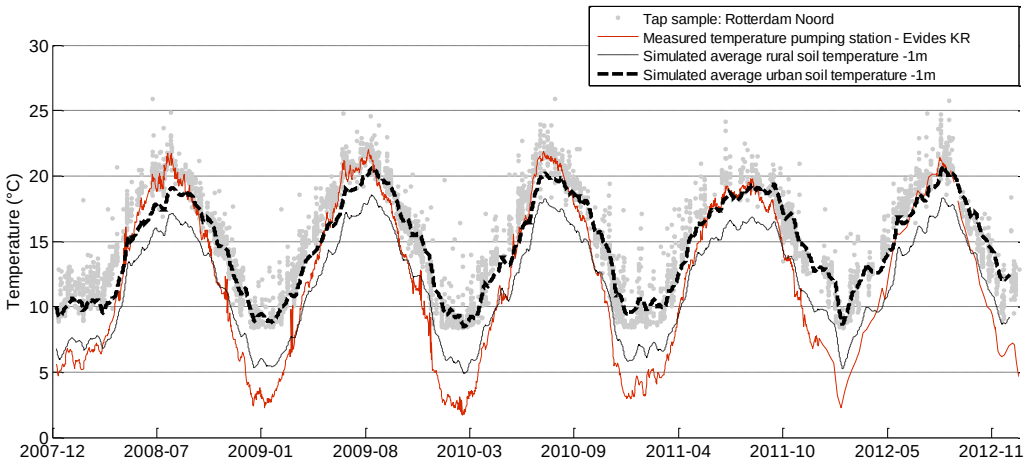

Figure 30 Temperature of the rural and urban soil at -1.0m compared with the TAP results and pumping station water temperature.

In the summer, for the five studied years, temperatures at the pumping station are similar to urban soil temperatures. In some years water temperature is slightly higher than soil temperature. Therefore, in some cases the rural soil may cool down the drinking water in the pipe and after that the urban soil may warm up the drinking water in the pipe.

Figure 31a shows the temperature measurements at the tap for Rotterdam North for the summer 2012 and the simulated soil temperature for the average city. These measurements show a large spreading. This spreading can be explained by the heterogeneity of the urban environment, in which, due to different land cover of building density, two locations can have a difference of up to 7°C. To test the difference in temperature in a given location on the same day, three urban types were defined: average city, hot-spots and peri-urban neighbourhoods, Figure 31b. Hot spots are places with high UHI, therefore large heat storage in the buildings and high anthropogenic heat emissions. For each of these types, the soil temperature was modelled using literature values. To describe these variations different values for heat storage and anthropogenic heat were used.

a)

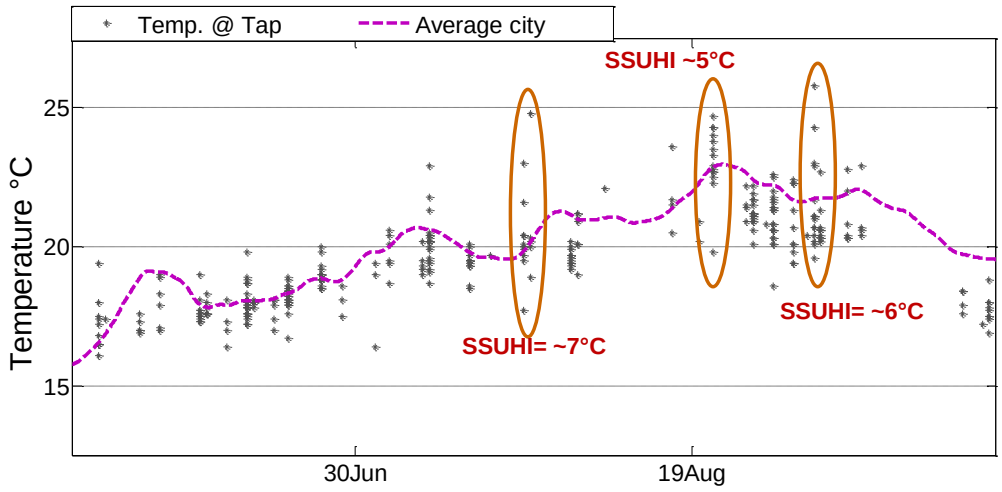

b)

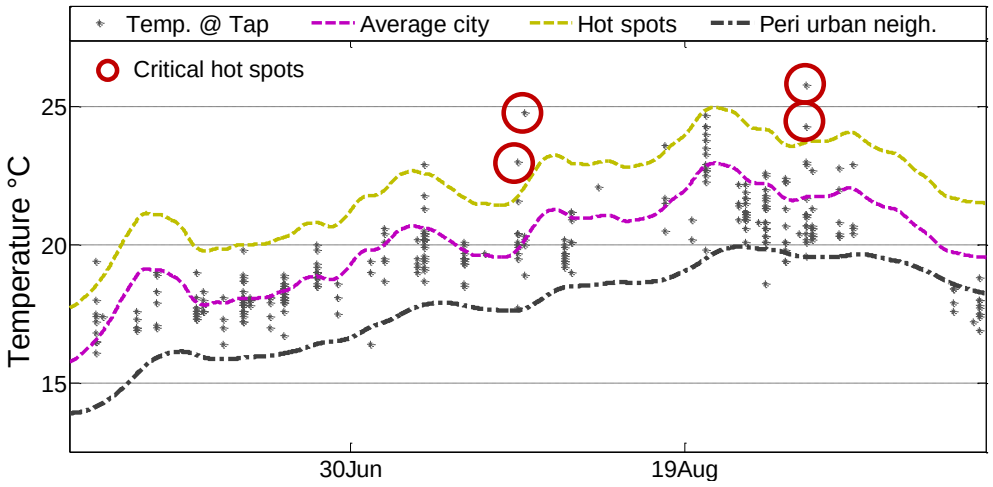

Figure 31 a) Simulation of soil temperature for the city of Rotterdam (average). b) Simulation of soil temperature for three areas within the city of Rotterdam North: Average city, peri-urban neighbourhoods and hot-spots in 2012.

The simulations, considering differences in QF and heat storage, seem to describe the upper and lower values of the temperatures in Rotterdam North. The simulations showed that the model can predict the range of temperature for different areas in the city. Figure 31b also shows a few critical hot-spots, which are above the simulated soil temperature, probably these locations have a large local anthropogenic sources of heat.

To compare the results of the temperature at the tap in other urban areas, the soil temperature of De Bilt was used as reference. Figure 32 shows the comparison for seven cities in the Netherlands. It can be observed that the temperature at the tap is almost always higher than the rural soil temperature. Amsterdam and Eindhoven showed higher temperature than the other cities. However, the available data is too limited to draw conclusions.

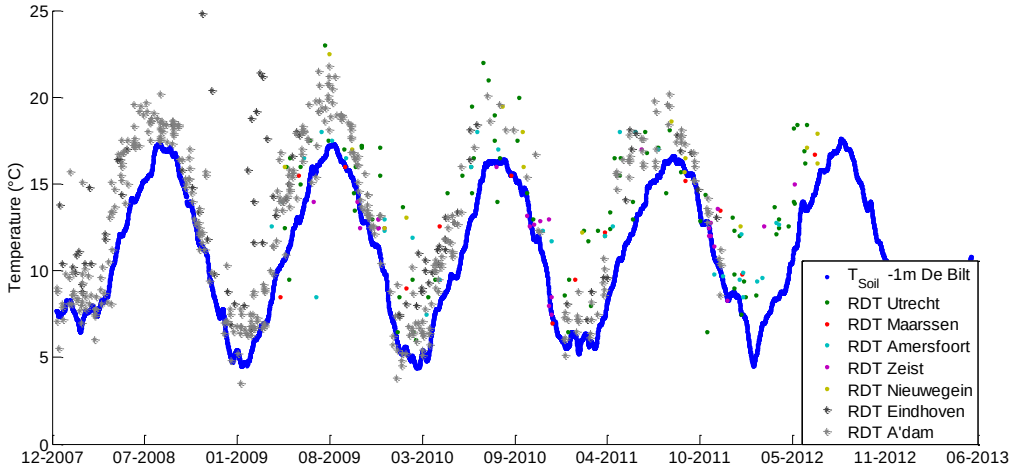

Figure 32 Comparison of temperature at the customer's tap for different cities, taking as reference soil temperature of de Bilt.

7.3 Soil temperature measurements in Rotterdam – September – October 2013

Two locations in Rotterdam were selected to measure the soil temperature in an urban area and to investigate the spatial variations of soil temperature within the urban area, (Figure 33). The soil temperature was measured at seven depths 1, 5, 10, 25, 50, 100 and 150 cm, from 3 September 2013 until 7 October 2013. The two locations had similar surface cover, namely tiles.

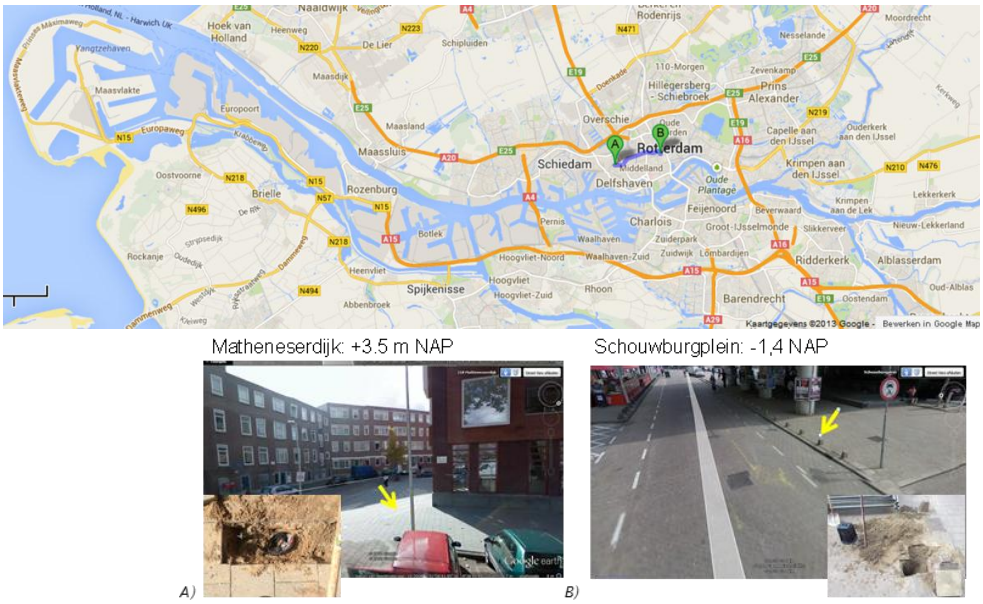

Figure 33 Location of the soil temperature measurement is Rotterdam, A) Mathenesserdijk and B) Schouwburgplein.

To determine the influence of the urban environment in the measurement location, the height of the building around the locations were plotted with the help of GIS, Figure 34. Location A is surrounded by buildings with a height of 7.4 - 10.5m, while location B is surrounded by building with a height of 19.1 – 31.8m. GIS analysis also allows the dynamic identification of shade for a specific location at a specific time, Figure 35.

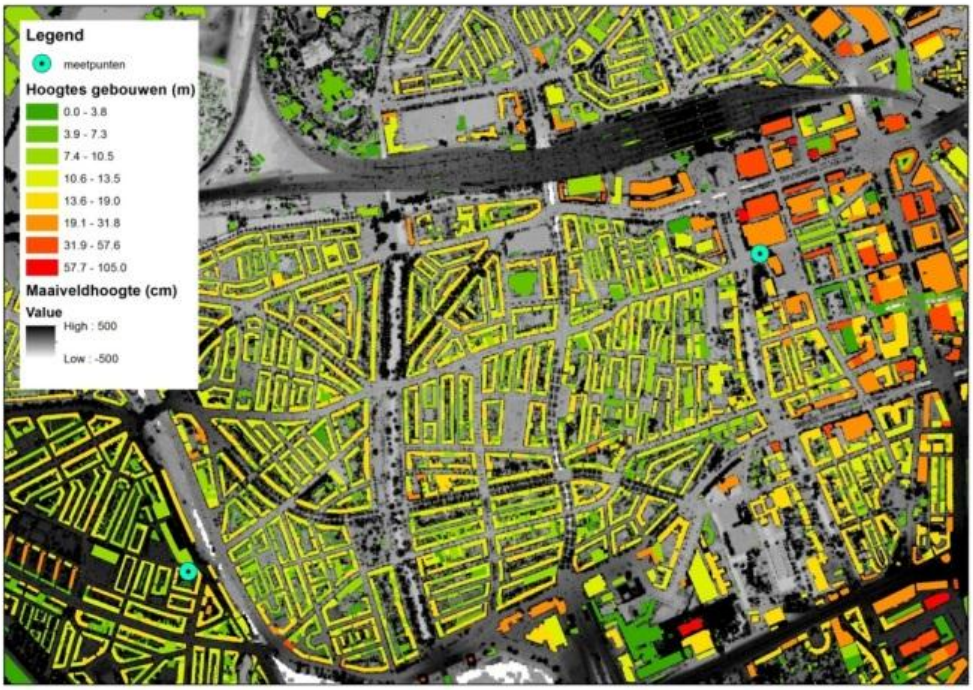

Figure 34 Overview of the height of the buildings around the two measurement locations in Rotterdam (Source: GIS service - Rotterdam Municipality).

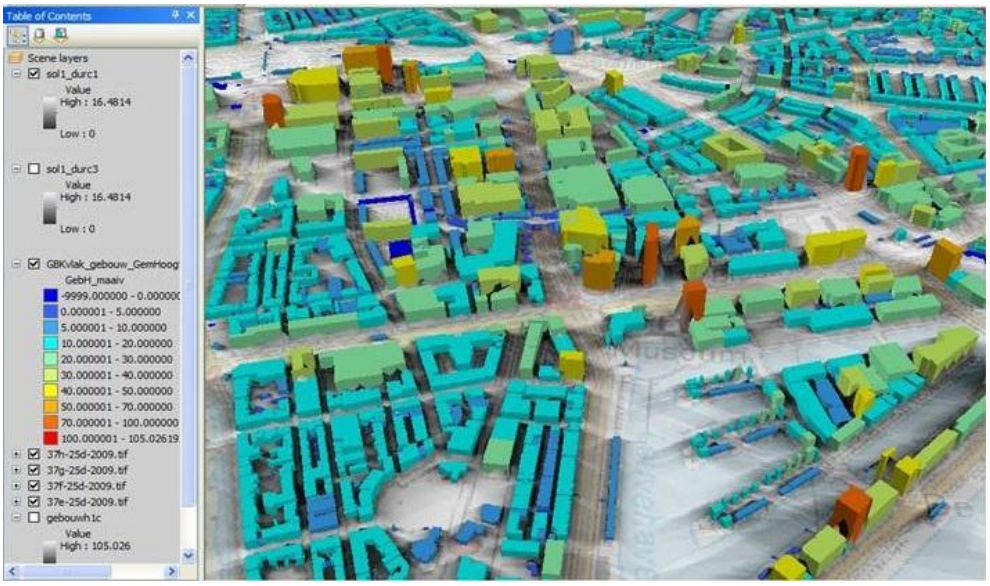

Figure 35 Detailed view of the shade due to buildings in Rotterdam.

Using the parameters from Table 12, the average soil temperature 2013 was simulated and compared with the measured soil temperatures, Figure 36. The measurements in Mathenesserdijk shows 1°-2°C higher temperatures than the simulated average, while Schouwburgplein shows approximately 1°C lower. The soil temperature measurements in two locations showed a difference of 4°C, being the temperature in the city centre lower than in the residential neighbourhood. This can be explained by: *i*) the fact that in the location *B*, there was shade from the buildings a few hours a day during the measured period and *ii*) measurements in an urban area are limited by the locations available. In this study, the measurement devices were set in a location where construction works were taking place. Therefore no traffic was possible in the area, which influenced the anthropogenic heat.

As shown in Figure 36, 5 September was a warm day, registering 31°C air temperature. This peak is clearly visible in the measurements and in the simulations. On 9 September, it shows a change of temperature in Schouwburgplein, this can be explained by the precipitation. In this location building activities were taking place. Probably water is infiltrated in the soil, and possibly drained, which may cause cold water to quickly reach -1.0m depth and cool the soil, or maybe only the sensor.

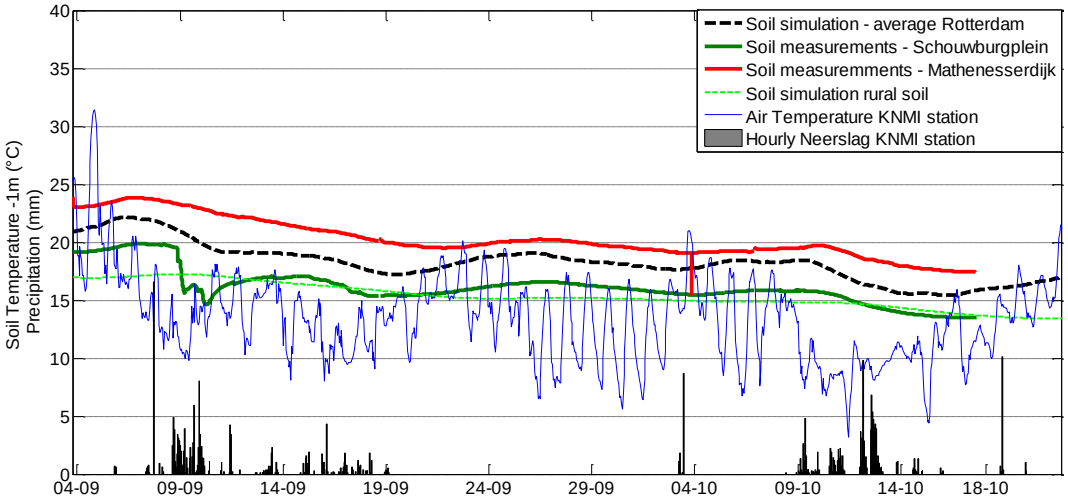

Figure 36 Comparison of simulated average soil temperature for Rotterdam and soil measurements and overview of air temperature and precipitation during the measurement period.

7.4 Overview of the results for Rotterdam

The heat island effect can be determined at different spatial scales (city – one measurement location), over different periods of time (specific time, during the day, in the summer, etc.) and at different levels (atmosphere, surface or subsurface). Table 14 shows an overview of the heat island for Rotterdam. Although these results show that surface heat island effect (SHI) is larger than the atmospheric UHI, this large temperature can occur on an urban roof. Measurement in the subsurface (-1 m) at two locations showed a lower SSHI than the atmospheric. These measurements took place in September, which is a relative cooler period than July.

Table 14 Overview of the heat island for Rotterdam in the summer.

	Difference in temperature in relationship with the rural surrounding area in °C		Time	Method	Spatial scale	Source
	Average	Maximum				
UHI (atmospheric)	3 - 4	8	16 July 2006 - noon	1 Landsat images	City	Figure 20
SUHI (Surface)		16*	July (1984 – 2007)	15 Landsat images	60 m x 60 m	Figure 21
	~ 4	10			Neighbourhood	Figure 22
SSHI (Sub-surface)	2 - 3	5	Sept – Oct 2013	Soil temperature measurements	Average of two measurements	Figure 36
		7	Summer 2012	Temperature at the tap		Figure 31

* This high temperature can occur at a roof.

7.5 Sensitivity analysis

The sensitivity analysis of the evapotranspiration shows that the evapotranspiration in urban areas is limited. By using the daily evapotranspiration reported by the KNMI similar results are obtained as when using equation 8 to calculate potential evapotranspiration. This can simplify the model, by reducing the number of unknowns.

The sensitivity analysis shows that for the urban area simulation the most relevant parameters, again, are the thermal properties of the soil (λ, ρ, C_p). The model is also sensitive to QF and a_3. Due to lack of precise information for the urban area and soil properties, to calibrate the model, different combinations of these factors provide a fit with the measurements, Figure 37. Although the differences are around 5°C, once the model is validated, data 5 and data 12 are the extreme values in the sensitivity analysis. Comparing data 4 vs. data 13 results in only a difference of 2.5°C. However the following pair of combination produces similar results: 2&3, 10&11, 14&15 and 6&7. These results show that QF and a_3 can compensate for each other, Table 15.

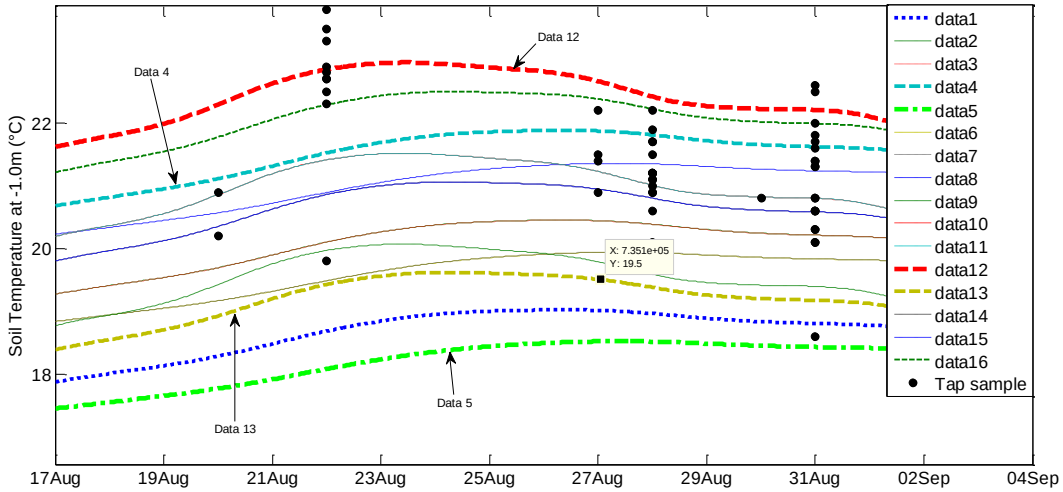

Figure 37 Overview of the sensitivity of the model to soil properties, QF and a_3.

Table 15 Overview of the changes in temperature and precipitation for the four future climate scenarios in summer time.

	λ (W/m/K)	ρ Cp (10^6 J/m³K¹)	QF (W/m²)	a_3 (W/m²)		λ (W/m/K)	ρ Cp (10^6 J/m³K¹)	QF (W/m²)	a_3 (W/m²)
data 1	0.7	2.0	50	-50	**data 9**	1.2	2.0	50	-50
data 2	0.7	2.0	50	-100	**data 10**	1.2	2.0	50	-100
data 3	0.7	2.0	100	-50	**data 11**	1.2	2.0	100	-50
data 4	**0.7**	**2.0**	**100**	**-100**	**data 12**	**1.2**	**2.0**	**100**	**-100**
data 5	**0.7**	**2.5**	**50**	**-50**	**data 13**	**1.2**	**2.5**	**50**	**-50**
data 6	0.7	2.5	50	-100	**data 14**	1.2	2.5	50	-100
data 7	0.7	2.5	100	-50	data 15	1.2	2.5	100	-50
data 8	0.7	2.5	100	-100	data 16	1.2	2.5	100	-100

7.6 Conclusions

Assuming that urban soil temperature at -1.0m is equal to the water temperature at the tap, a difference of up to 5°C in the winter and up to 2°C in the summer was found between two areas, north and south, in Rotterdam. These results suggest a gradient of temperatures within the urban area, which can be due to higher urbanization level, differences in land cover or higher traffic heat emissions.

The temperature measurements at the tap provided a clear overview due to the large number of samples. In this study we use the meteorological data from the closest meteorological station to the urban area. This seems to be useful as reference temperature.

Measurements of soil temperature at two locations in the urban area showed a difference of 4°C. Local factors such as shade, traffic, among others, can have a large influence on local temperatures. Scatter soil temperature measurements provided limited information about an urban area and are subject to local variations which have to be filtered before extrapolating the results.

8 Future urban climate and adaptation measures

8.1 Future climate

According to current knowledge, climate change is expected to continue in the coming centuries, although the extent and rate of change remain uncertain. In 2006, four future climate scenarios for the Netherlands were defined by the KNMI.

http://www.knmi.nl/bibliotheek/knmipubWR/WR2006-01.pdf

http://climexp.knmi.nl/Scenarios_monthly/

Table 16 Overview of the changes in temperature and precipitation for the four future climate scenarios.

Scenario	Global temperature increase in 2050	Change of atmospheric circulation
G	+1°C	Weak
G+	+1°C	Strong
W	+2°C	Weak
W+	+2°C	Strong

Table 17 Overview of the changes in temperature and precipitation for the four future climate scenarios in summer time.

Variable	G	G+	W	W+
Mean temperature (°C)	+0.9	+1.4	+1.7	+2.8
Mean precipitation (%)	+2.8	-9.5	+5.5	-19.0

Based on these scenarios, the KNMI has developed a tool to estimate the future temperature and precipitation. In this case, we use the year 2012 as base year which was projected forward onto 2030 and 2050. *Figure* 38 shows the overview of number of days exceeding a given temperature at a depth of 1 meter in 2012, 2030 and 2050 for three locations in the city: peri-urban neighbourhoods, average urban and hot spots for the W+ scenario. Table 18 shows the comparison between the scenarios G and W+ for 2050 for the three different years and locations.

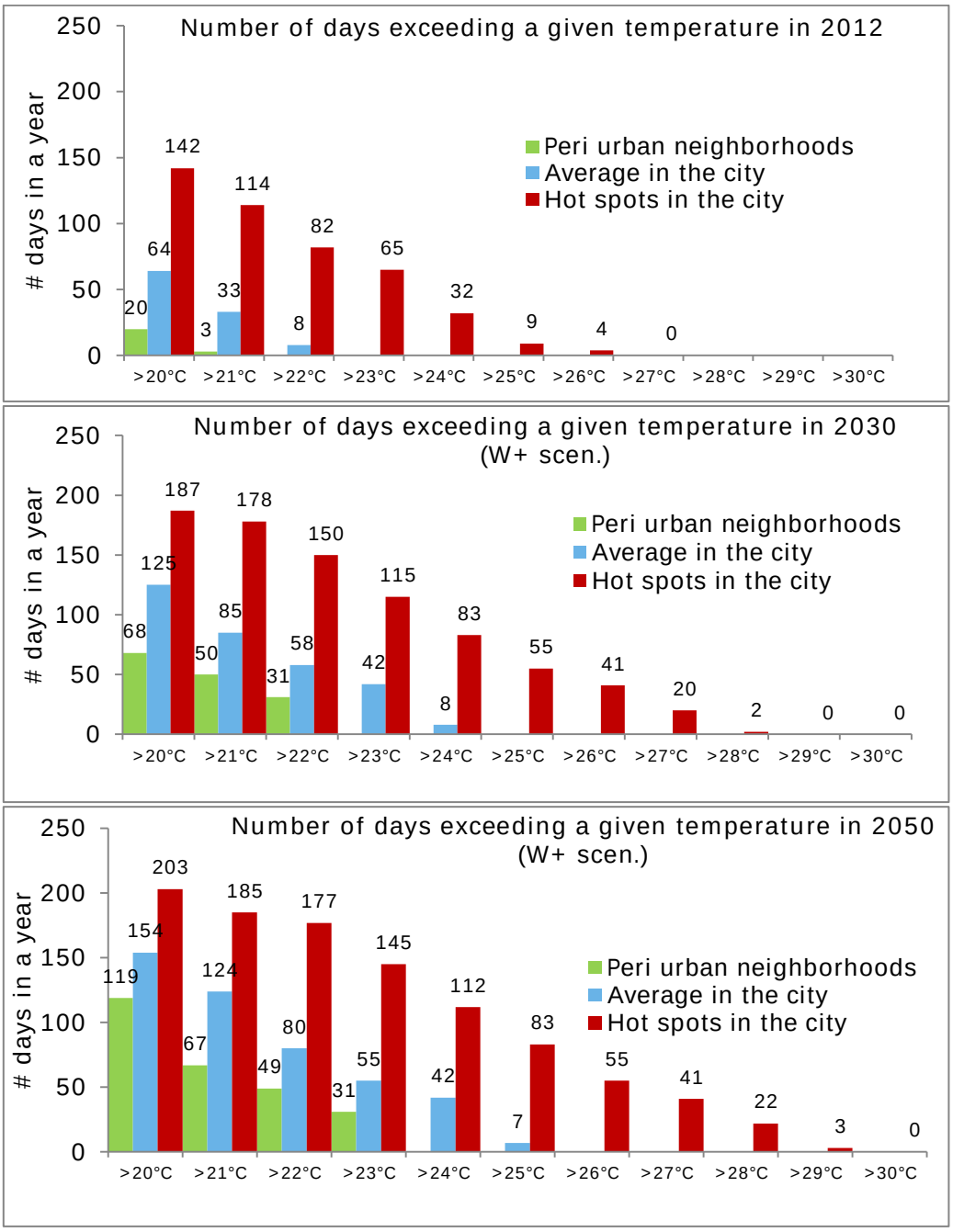

Figure 38 Overview of number of days exceeding a given temperature at a depth of 1 meter in 2012, 2030 and 2050 for three locations in the city: peri-urban neighbourhoods, average urban and hot spots for the W+ scenario.

Table 18 Comparison of the number days in 2050 year in which drinking water temperature will exceed 25˚ and 28˚C for scenarios G and W(+).

	Number of days per year with drinking water temperature >25°		Number of days per year with drinking water temperature >28°C	
	2050 (G)	2050 (W+)	2050 (G)	2050 (W+)
Peri-urban neighbourhoods	0	0	0	0
Average city	0	7	0	0
Hot-spots	11	83	0	22

8.2 Adaptation measures

A recent literature review, Bowler, Buyung-Ali et al. (2010), reported that green roofs are able to cool down the air temperature in an urban area by approximately 1-2°C, (Figure 39). Despite the impact on reducing urban soil temperature at -1.0m, indirectly green roofs cool down the building, which in the summer is translated into less cooling demand and therefore less anthropogenic emissions.

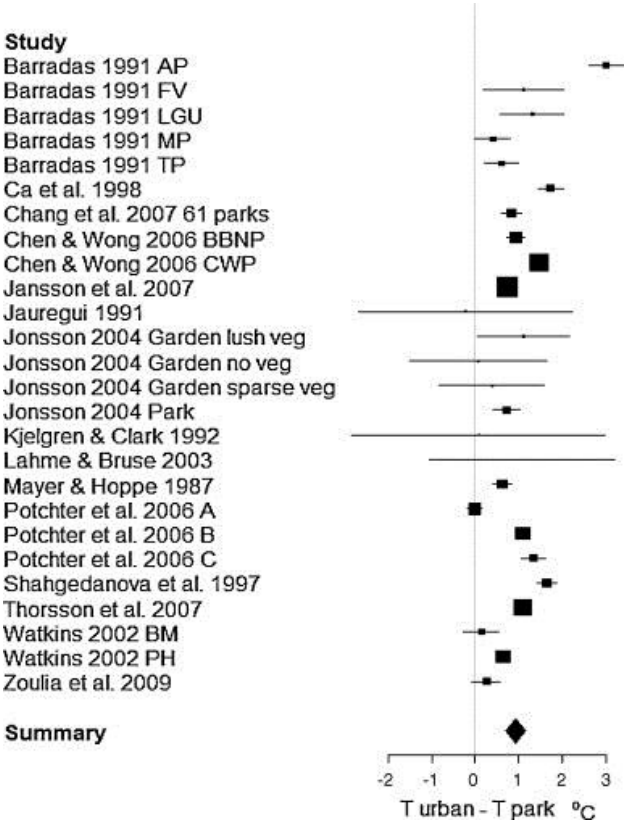

Figure 39 Black squares represent the average temperature difference between a built-up area and a park or green area in the day (the effect size; Turban − Tpark ° C), Source: *Bowler et al. (2010).*

Blokker and Pieterse-Quirijns (2012) studied a series of measures that can be considered to reduce the temperature, *Figure 19*. They concluded that these measures have only a limited impact on water temperature in the distribution network.

Table 19 Overview of measurement to reduce temperature on the distribution network based on (Blokker and Pieterse-Quirijns 2012).

Phase	Measurement	Effect on temperature at the tap
Design	self cleaning networks (small diameters, branched network) PVC (insulating material);	+/0
Construction	place mains deeper or under vegetation	+
Operation	cooling at PS, use energy gain	0
Maintenance	close valves or flush over hydrants to shorten residence time	0
Replacement	take water quality into consideration with replacement decisions, choose smaller pipe diameter, or lay pipe deeper	+/0

Scenarios to determine the measures to reduce the warming up of the water in the distribution network have been analysed by means of business cases in a parallel project (Blokker, Horst et al. 2014). Here the temperature in the distribution network was simulated, and three scenarios were tested: increasing water use, laying water pipes deeper and using an ATES (Artificial Thermal Energy Storage) to cool down the end of the transport, Table 20 .

Table 20 Scenarios studied in a parallel research (Blokker, Horst et al. 2014).

Scenarios	Effect reducing temperature at the tap during consumption
Increasing water use	No effect
Increase depth of the pipes	Effective in combination with other measures, such as use of vegetation as land cover.
Use of ATES	Although this was the best option (out the three scenarios), the benefits are limited

This study contributes by quantifying the effect of different parameters, however, further research is needed to better calibrate the model parameters. Remaining research questions are i) what is the optimal size of the area to apply the soil temperature model; ii) what is the influence of other warm sources in the urban environment, e.g. sewers, heat district, electricity cables, of buildings such as swimming pools, etc.

In the case of Rotterdam, assuming a reduction of 2°C (optimal green roofs), this reduction does not compensate the 10°C of UHI. Therefore, and integral approach is needed to reduce drivers, such as increasing urbanization, and pressures, such as limited evapotranspiration, or reduction of anthropogenic sources.

8.3 Discussion

Measures can have different objectives:

- Reduce soil temperature: by reducing anthropogenic heat sources and increasing vegetation;
- Reduce drinking water temperature: increase depth of pipes;
- Accepting the temperature increase and addressing drinking water quality by additional treatment;

As reported in other studies and literature, single mitigation measures have a limited effect in reducing the air and soil temperature in urban areas. Not a single solution will drastically reduce the temperature in the distribution network. Therefore, a combination of measures adapted for each type of location in the city is needed to reduce the risk of exceeding the threshold temperature. An overview of measures at different levels is shown in Figure 40, using the DPSIR approach (Drivers-Pressures-State-Impact and Responses), where different adaptation and mitigation measures at different levels are identified.

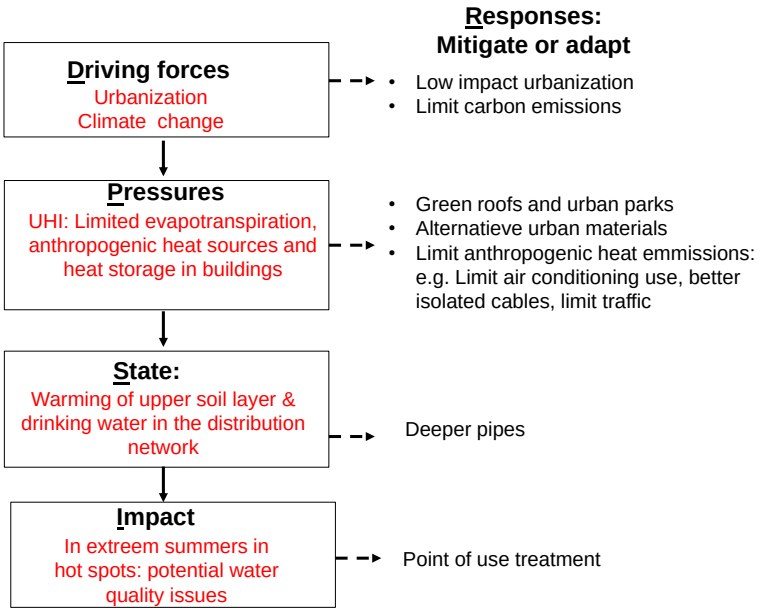

Figure 40 Integral approach to reduce temperature in the distribution network.

9 Risk of pathogen regrowth in drinking water under future urban climate

9.1 Introduction

Conditions like nutrient concentration, temperature and pH determine the regrowth level and the composition of the microbial community in the drinking water distribution system. Consequently, a temperature increase of the drinking water in the distribution system has an effect on: the composition of the microbial community in the distribution system, bacterial regrowth parameters that have to be determined according to legislation and pathogenic microorganisms that can multiply in the drinking water environment (van der Kooij, Wullings et al. 2009). A change in the species composition of the microbial community caused by a temperature increase will, in general, not result in problems, because most microorganisms in drinking water do not play a role in public health, legislation or aesthetic complaints. A temperature increase of drinking water can, however, influence microbiological parameters for which maximum values (quality demands) are mentioned in 'het Drinkwaterbesluit' (colony count at 22°C, *Aeromonas*, bacteria of the coligroup and *Legionella*) and, more importantly, can affect the growth of microorganisms which are undesirable because of their possible role in disease (van der Kooij, Wullings et al. 2009). In this chapter, the effect of the future urban climate on growth of opportunistic pathogens in the drinking water distribution system is being discussed. The main focus will be on *Legionella pneumophila*, but other opportunistic pathogens that are capable to multiply in the drinking water environment are discussed as well.

9.2 Future urban climate and growth of opportunistic pathogens

9.2.1 Legionella pneumophila

Legionella pneumophila can cause a life-threatening pneumonia, which is called 'Legionnaires' disease. *L. pneumophila* causes mainly disease in humans with a less active immune system, like elderly, persons with an immune disease, patients that are treated with medicines that decreases the activity of the immune system (e.g. cancer therapy, organ transplantation) or heavy smokers. Most humans with a normal functioning immune system will not get ill by *L. pneumophila*. 'Legionnaires' disease is obligatory for doctors to report to the authorities in the Netherlands and around 300 to 350 cases are reported every year, but this number can increase to 450 cases in the 'peak' years, such as 2006 and 2010 (Figure 41).

L. pneumophila is a bacterium that mainly grows is an aquatic environment and which has a complex live style. The organism can, in general, not grow outside certain protozoa (unicellular organism of animal origin). These protozoa graze on biofilms (a layer of microorganisms that has developed on a fixed surface) and can also take up *L. pneumophila* during these grazing activities. Subsequently, *L. pneumophila* will start mutliplying inside the cells of some protozoan species (e.g. *Hartmanella vermiformis*, *Acanthamoeba* spp.), until the cells get so filled with *L. pneumophila* cells that the protozoan cell will burst open (*Figure* 42). These free *L. pneumophila* cells can be taken up again by other protozoan cells and the cycle will be repeated. This life style means that biofilm and protozoa have to be present in

the (drinking) water system before *L. pneumophila* is able to grow. Biofilms develop on surfaces that are in contact with drinking water. Nutrients for biofilm growth can come from the drinking water or from pipe material that is in contact with drinking water. The minimal amount of easily assimilable organic carbon (AOC) necessary to provide biofilm concentrations suitable for growth of *L. pneumophila* is extremely low (~ 1 µg degradable C l^{-1}). In addition, research has demonstrated that materials like PVC-P, rubber and PE releases enough nutrients that the biofilm concentration on the surface gets high enough for growth of *L. pneumophila*.

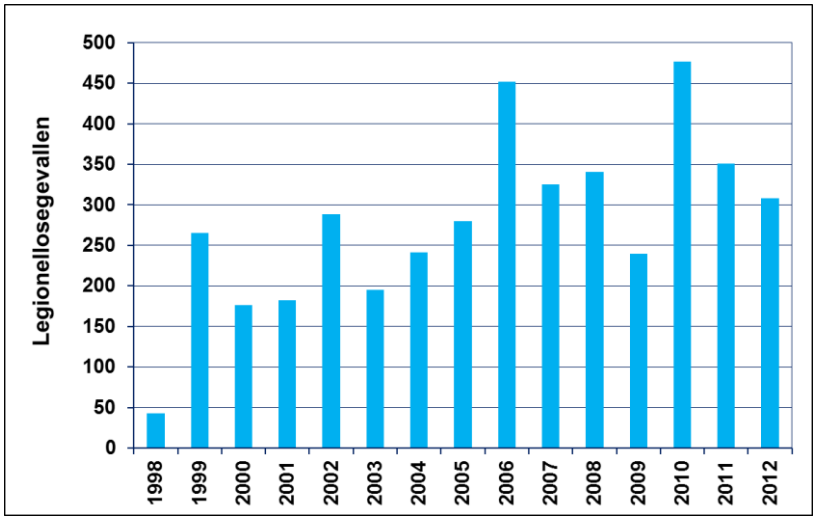

Figure 41 Number of reported cases of Legionnaires' disease in the Netherlands over the period 1998 till 2010. A big outbreak occurred in 1999 at the Westfriese flora (information from RIVM).

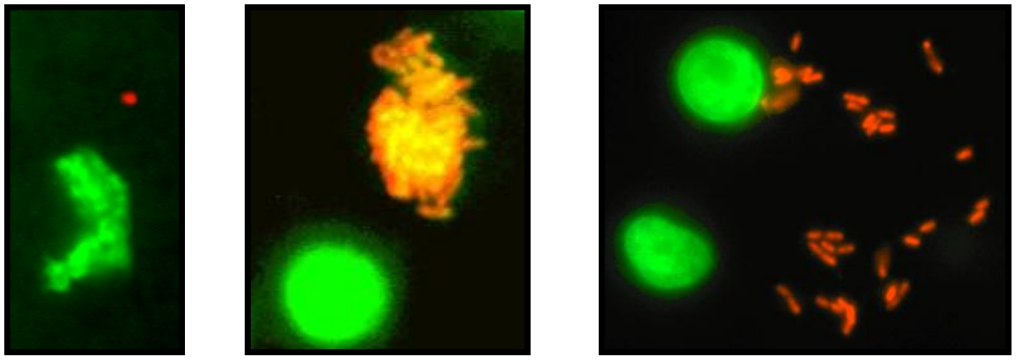

Figure 42 Growth of L. pneumophila in the protozoan H. vermiformis. Red/orange: L. pneumophila; Green: H. vermiformis cells. Left: cell of L. pneumophila and a non-infected cel of H. vermiformis; Middle: Non-infected cell of H. vermiformis (lower cell) and a H. vermiformis cell filled with cells of L. pneumophila (upper cell); Right: Free cells of L. pneumopihila after protozoan cell has bursted open and two (not) yet infected H. vermiformis cells (taken from (Kuiper, Wullings et al. 2004)).

The temperature of the (drinking) water is another important factor that can influence the growth of *L. pneumophila*. In 2009, KWR performed a research project for the Ministry of Housing, Spatial Planning and the Environment (VROM) to determine the effect of water temperature on the growth of *L. pneumophila* and *Legionella anisa* in the biofilm (van der Kooij, Wullings et al. 2009). *L. anisa* also belongs to the genus *Legionella*, but is less virulent than *L. pneumophila* and causes only disease in patients that have a very weak immune

system. Therefore, the presence of *L. anisa* in drinking water is normally not considered to pose a significant risk for public health. In that VROM research project, biofilm monitors filled with PVC-P rings were used through which drinking water was continuously flowing at different temperatures. These biofilm monitors were inoculated with *L. pneumophila* and *L. anisa* after biofilm formation had occurred on the PVC-P rings and subsequently biofilm samples were taken from the PVC-rings and the colony forming units of *L. pneumophila* and *L. anisa* were determined. The results demonstrated that *L. pneumophila* was unable to remain or grow in the biofilm when the drinking water temperature was below 30°C, whereas *L. anisa* were present in relative high numbers (10^6 t/m 10^7 cfu cm^{-2}) in the biofilm when temperatures were above 25°C. When these temperatures were further increased to 34°C – 38.5°C (highest temperature investigated), *L. pneumophila* was capable to grow and after 7 to 10 days numbers had increased to relatively high numbers (10^6 till 10^7 cfu cm^{-2}) in the biofilm on the PVC-P surface. These numbers remained at these high levels after 10 days until the experiments were stopped. *L. anisa* was observed besides *L. pneumophila* in the biofilm at similar numbers when the temperature was 34 till 37°C. At 38.5°C, *L. anisa* was no longer observed in the biofilm. It is concluded from these results that *L. pneumophila* is able to grow in the biofilm inside protozoan hosts, when drinking water temperatures are above 30°C.

It was investigated in a follow-up study when *L. pneumophila* and *L. anisa* are able to multiply in the biofilm when the drinking water temperature is constant at 25, 27, 30, 33 and 35° for a longer period (160 days) (van der Kooij, in preparation). The results from that study demonstrated that *L. pneumophila* numbers are relatively low at 25 and 27°C (~10^3 cfu cm^{-2}). *L. pneumophila* numbers were higher at 30, 33 and 35°C (10^4 cfu cm^{-2}, 10^5 cfu cm^{-2} and 10^7 cfu cm^{-2}, respectively). These *L. pneumophila* numbers were in general reached after 10 to 20 days of inoculation. The numbers of *L. anisa* in the biofilm were for all temperatures between 10^6 and 10^7 cfu cm^{-2}. These *L. anisa* numbers were reached after 10 to 20 days at the three highest temperatures, whereas maximum *L. anisa* numbers were reached after approximately 50 days at the two lowest temperatures. These results, thus, again demonstrates that *L. pneumophila* numbers increase at temperatures of 30°C and higher, although relatively low numbers are also observed at 25 and 27°C.

Overall, it is concluded from these two studies that the water temperature is an important factor in growth of *L. pneumophila* in the drinking water environment. When temperatures remain below 30°, it is expected that growth of *L. pneumophila* will not occur or at a low level, whereas at temperatures above 30°C it is likely that growth of *L. pneumophila* occurs at significant levels, provided that the biofilm concentration in the drinking water distribution system is high enough. In addition, the results from these two studies showed that another prerequisite for growth of *L. pneumophila* is that the temperature has to be higher than 30°C for more than 7 days.

Based on the results from these studies, it can thus be concluded that an increased risk for growth of *L. pneumophila* occurs when future climate change results in drinking water temperatures that are above 30°C for more than seven days. However, these experiments were performed with one strain of *L. pneumophila* and it might be possible that other strains of *L. pneumophila* have a slightly different temperature range of growth. It is, therefore, advisable to include a safety margin of 2°C, meaning that if future drinking water temperatures increase above 28°C for more than seven days, there is an increased risk for growth of *L. pneumophila* in the drinking water distribution system.

The model to calculate the drinking water temperature was used to predict the number of days that the drinking water temperature increases above a certain value in the peri-urban

neighbourhoods, average city and hot spot locations in the city in 2012 and in 2030 under the W+ climate scenario and in 2050 under the W+ climate scenario (*Figure* 38). The number of days that the drinking water temperature exceeds 28°C is below seven, even for the hot spot locations in the city in 2012 and 2030. This indicates that, based on the model predictions, there is no increased risk for growth of *L. pneumophila* in drinking water distribution systems in 2012 and in 2030 under the W+ climate scenario. Model predictions for 2050 under the W+ climate scenario indicate that the temperature will not increase above 28°C for more than seven days in the peri-urban neighbourhoods and in the average city. However, the model predicts that the temperature will be above 28°C for more than 22 days at hot spot locations in the city in 2050 under the W+ climate scenario. Thus, in that specific situation there might be an increased risk for growth of *L. pneumophila* in the drinking water distribution system.

9.2.2 Other opportunistic pathogens

There are other opportunistic pathogens, besides *L. pneumophila*, that are capable to grow in the drinking water distribution system. A literature review has indicated that pathogenic species of the nontuberculous mycobacteria, *Pseudomonas aeruginosa*, *Stenotrophomonas maltophilia*, *Aspergillus fumigatus* and *Acanthamoeba* spp. might be capable to grow in the drinking water distribution systems in the Netherlands and might pose a threat to public health (van der Wielen and van der Kooij 2009). Therefore, molecular detection methods were developed for the specific detection of these microorganisms in drinking water (van der Wielen, Italiaander et al. 2011), and these detection methods were used to analyse whether these microorganisms were present in drinking water sampled from the distribution system of several production locations in the Netherlands (van der Wielen and van der Kooij 2011; van der Wielen 2014). The results demonstrated that DNA from *P. aeruginosa*, *S. maltophilia* and *A. fumigatus* is present in approximately 5 to 10% of the samples, whereas pathogenic species of the nontuberculous mycobacteria and *Acanthamoeba* spp. were never observed in the drinking water samples.

The influence of temperature on the growth of *P. aeruginosa*, *A. fumigatus* and *S. maltophilia* was investigated in a subsequent study. Different strains of these species were incubated as a pure culture at different temperatures (10 to 50°C) and the amount of growth was monitored (van der Wielen, in preparation). *P. aeruginosa* has a broad temperature range for growth, since growth was observed at 10 till 45 °C. *A. fumigatus* had a broad temperature growth range as well (15 till 50°C) as did *S. maltophilia* (15 till 45°C). These results indicate that these three species are capable to grow at a relatively low temperature. In contrast, a pure culture of *L. pneumophila* is capable to grow between 20 and 40°C (van der Kooij, Wullings et al. 2009). It was also investigated at which temperatures *A. fumigatus* and *P. aeruginosa* were capable to grow in natural drinking water biofilms by using biofilm monitors that were continuously fed with drinking water of different temperatures (van der Wielen, in preparation). However, the results from that study were less clear, because it was difficult to establish a stable *P. aeruginosa* or *A. fumigatus* community in the natural drinking water biofilm. Still, several biofilm samples were positive for *P. aeruginosa* or *A. fumigatus* and these positive samples were observed at most investigated temperatures, including the lowest temperatures tested (17 till 20°C). It seems that growth of these two microbial species are less influenced by higher temperatures than *L. pneumophila*. This would mean that higher drinking water temperatures that are predicted with the W+ climate scenario do not affect the growth of these organisms in drinking water distribution systems and that other factors (e.g. AOC-concentration, substrate composition, biofilm composition and disturbance) may be more important drivers for the establishment of these opportunistic pathogens in the drinking water distribution system.

Furthermore, it is currently impossible to indicate whether the presence of *P. aeruginosa*, *A. fumigatus* and *S. maltophilia* in drinking water poses a threat to public health. The strains of these species that are present in drinking water might be environmental strains that do not cause disease, as has been observed in the past for *Aeromonas*. A BTO research project has, therefore, been started in 2014 to compare the genotype of drinking water strains with patient strains to address the question whether the presence of these microorganisms may pose a threat to public health.

10 Discussion and recommendations

10.1 Soil temperature model

The soil type and soil moisture are important to determine thermal soil properties, especially in peri-urban areas. However, there is still large uncertainty about these parameters. Moreover, there are limited reliable and affordable instruments to measure soil temperature and soil moisture on site. By using theoretical values, assuming a constant value for the summer and using soil temperature measurements, the model can be validated for a specific area.

The model is a tool to estimate the soil temperature of a given area at different depths, within determined ranges of uncertainty. Higher precision would require more detailed information per location, which is currently not available. Increasing the level of detail of the model (e.g. dynamic moisture content) can significantly increase the required simulation time. However, it would not improve the results given the uncertainty and variability of λ, ρ and c_p. Although in this study, the model was calibrated only for the summer condition, the model can be used for other periods of the year.

Large data sets, such as the temperature at the tap can be used to validate the model for a specific location in a coarse spatial scale, e.g. for Rotterdam. The optimal size of the area to apply the model has to be further investigated, but this is limited by the calibration possibilities. To overcome this limitation, local soil temperature measurements can be used to validate the model. However, several locations should be simultaneously monitored, and further research is needed to determine the number of required measurement locations. Two locations (this study) provide only an indication of the urban variability. Protocols to select measurement locations are needed, for instance in relationship with shade of buildings, traffic, or other sources of heat that can affect the measurements. It can be difficult to find an appropriate location in the city centres of highly dense areas . For future research, we recommend using GIS and additional information regarding heating networks, traffic intensity, etc. for the selection of measurement locations.

In this study, the measured period was September, which does not correspond with the summer period. However, planning of the measurements in urban areas required longer than initially expected due to permits needed.

In this study, we used meteorological information as input for the model, from stations close by the urban area. Although, ideally, measurements of the meteorological variables in the city would provide a better fit, measuring these variables in the city remains a challenge. Current studies investigate where to place sensors in the city, (Kotthaus and Grimmond, in press). The use of data coming from sensors located in the city won't increase the reliability of the results. Therefore the measurements from the meteorological station are, at this moment, the best option as input information for the model.

10.2 Results simulations

The results for urban areas suggested a large influence of anthropogenic sources on the soil temperature. There is a need to quantify the "anthropogenic" underground sources and their

influence on the soil temperature. In this study we have focused on a city scale (Rotterdam) and in two large areas (North and South). However, research is needed to identify the optimal size to model soil temperature in the city. Incorporating additional information, such as building height and average distance between buildings, smaller spatial scales could be identified based on the local climate zones. The results of the temperatures at the tap, suggest that the sub-surface heat island effect varies within the city. Therefore, different areas have a different risk of exceeding the threshold temperature. The average city and the peri-urban neighbourhoods show a low risk of exceeding the temperature limit. However, hot-spots show higher risks in the current situation and in the future. The measures have to be addressed to these specific locations. Therefore, identifying the location of the hot-spots and quantifying their intensity is crucial to limit the risk of exceeding the temperature limit.

11 Conclusions

The model validation for peri-urban areas showed that soil thermal properties govern the energy balance in the soil. Measurements of soil temperature in the Netherlands at four meteorological stations showed that in peri-urban areas temperature at -1m depth does not exceed 20°C even in warm years (with a heat wave). Although determining thermal soil properties remains a practical challenge, modelling offers the possibilities of testing different scenarios and determining ranges of variation. Our results suggest that average soil moisture for the summer is appropriate to determine the soil temperature at -1m.

Comparison of the soil temperature in the peri-urban area vs. the validated urban soil temperature, based on samples at the tap, showed clearly a different soil type in the urban area. In urban areas, the upper soil level has been modified by adding sand and by increasing soil compaction, which clearly affects thermal properties of the soil. Assuming sandy soils in urban areas limits the uncertainty in the thermal properties.

By validating the model for the urban areas, distinctive areas can be identified. This can be due to different urban typologies (LCZ) or due to local anthropogenic sources, such as traffic, industries, etc. Based on this study, anthropogenic sources play a role as important as soil properties.

To further validate the model, soil temperatures in two locations were measured during six weeks. A good correlation between the simulated soil temperature and the measured soil temperature was found. This study demonstrates that it is possible to predict urban soil temperature and tap temperature using meteorological information.

The soil temperature model can be used to analyse the risk of exceeding the temperature limit, particularly during warm summers and in highly urbanized areas. Measurements of the temperature at the tap in Rotterdam North and South proved the hypothesis. Based on the analysis of the soil temperature, and other studies, we can assess the implications for water temperature and water quality which is delivered at the customers' tap.

Given the lack of information of soil temperature in urban areas and the difficulties to perform measurements in cities, modelling the soil temperature provided a good estimation of the daily and seasonal variations and complement measuring campaigns. Modelling also allows determining the soil gradients of the underground urban heat island effect.

As stated in the introduction the main questions addressed in this study were:

11.1 How often will the drinking water temperature exceed 25°C in the future, in urban areas?

The analysis of the drinking water temperature in future urban areas showed that areas in the peri-urban area do not have a risk to exceed the 25°C temperature threshold now or in the future, (Table 21). Considering the most extreme KNMI scenario, an average city may have 7 days above 25°C in the W+ scenario. Hot-spots are areas of concern. Currently in a warm summer the temperature threshold will be exceeded about 9 days. This number is expected to increase to 55 days in 2030 and up to 83 days in 2050. In 2050 temperatures above 28°C could be frequently reached, which can lead to water quality deterioration.

Table 21 Overview of the number days in a year in which drinking water temperature will exceed 25˚ and 28˚C for 2012 (warm summer) and for a warm summer in the future climate scenario W+ for 2030 and 2050.

	Number of days per year with drinking water temperature >25°			Number of days per year with drinking water temperature >28°		
	2012	2030 (W+)	2050 (W+)	2012	2030 (W+)	2050 (W+)
Peri-urban neighbourhoods	0	0	0	0	0	0
Average city	0	0	7	0	0	0
Hot-spots	9	55	83	0	2	22

Table 22 Comparison of the number days in 2050 year in which drinking water temperature will exceed 25˚ and 28˚C for scenarios G and W(+).

	Number of days per year with drinking water temperature >25°		Number of days per year with drinking water temperature >28°C	
	2050 (G)	2050 (W+)	2050 (G)	2050 (W+)
Peri-urban neighbourhoods	0	0	0	0
Average city	0	7	0	0
Hot-spots	11	83	0	22

Therefore it becomes crucial to identity these hot-spots in urban areas. Based on our analysis, hot spots are caused by anthropogenic sources but little is known about their location and impact.

11.2 What is the effect of these temperatures on the water quality?

Exceeding 25°C seems not to be the largest water quality problem. As described in Chapter 9, there is a large microbiological risk when exceeding the temperature of 28°C for more than 7 days. This will be the case in 2050 for the hot-spots areas. However a temperature above 25°C, although there is not yet a microbiological risk, does not comply with current regulations.

11.3 Which measures are feasible to reduce the risk of exceeding the temperature?

With the extended model, it is possible to evaluate the effect of measures directed to reduce the pressures, such as reduction of the anthropogenic heat, increasing actual urban evapotranspiration, etc. This was not done yet due to little available information. It is estimated that single measures only have a limited effect. A review of studies showed that there is not a single measure that can reduce considerably the soil temperature during the summers. Different measures were presented in Chapter 8, and the best way to tackle the problem is by combining measurements. Addressing these measures is outside the scope of

the drinking water companies. Therefore, key partnerships in the city are crucial, for instance with urban planners and developers, when defining new urban areas, or with municipal representatives to limit for instance, traffic in certain areas.

The simulations show that in the peri-urban area the risk of exceeding the 25°C is minimum, while hot-spots now and in the future show temperatures higher than 25°C. This analysis shows the importance to identify in which locations measures are needed. Future research should focus on the identification of the conditions that cause the hot-spots. Then, the cause of the occurrence of the hotspot is known: is it because the pipe is close to a tall building, is the pipe close to other infrastructure like a central city heating system, etc. By the identification of causes, appropriate measures can be taken, like a green rooftop in a building to reduce the temperature increase, or shadow or vegetation for pipes that are located in sunshine, etc.

Appendix I Soil thermal conductivity λ (W m^{-1} K^{-1})

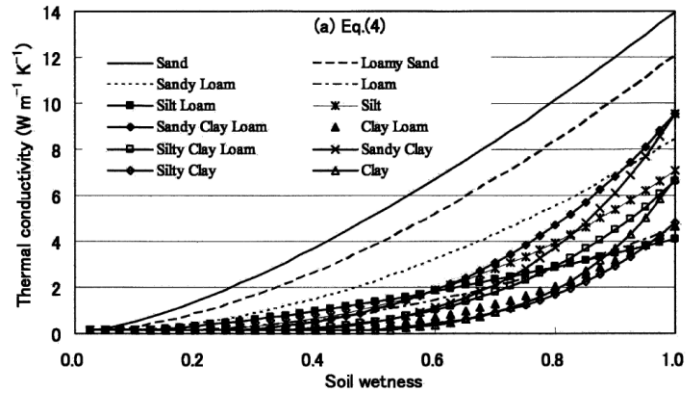

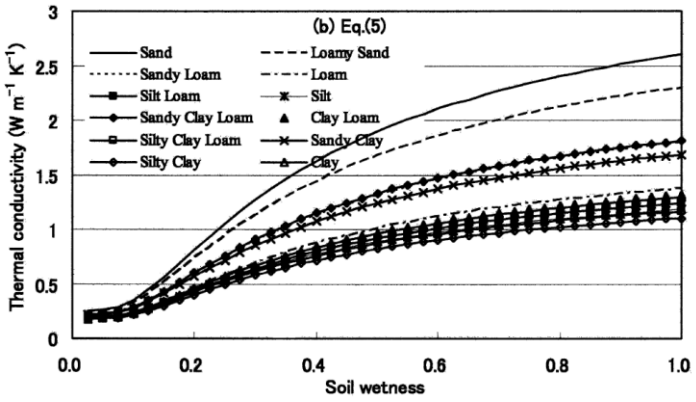

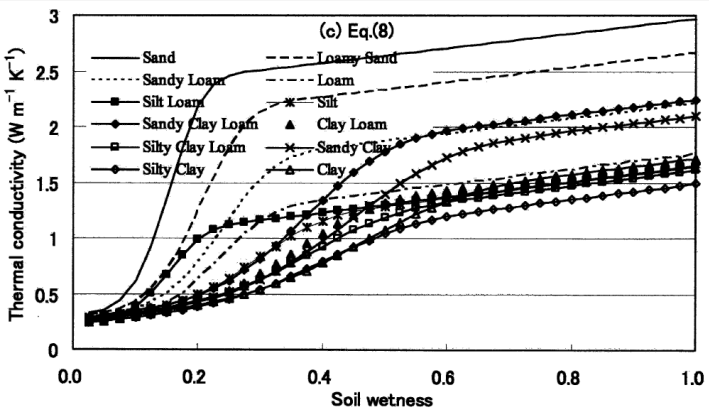

Yang, K. and T. Koike (2005).

Appendix II Soil thermal diffusivity ($m^2 s^{-1}$)

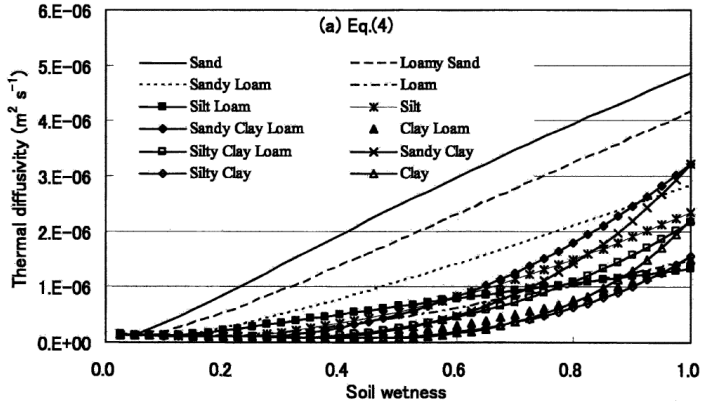

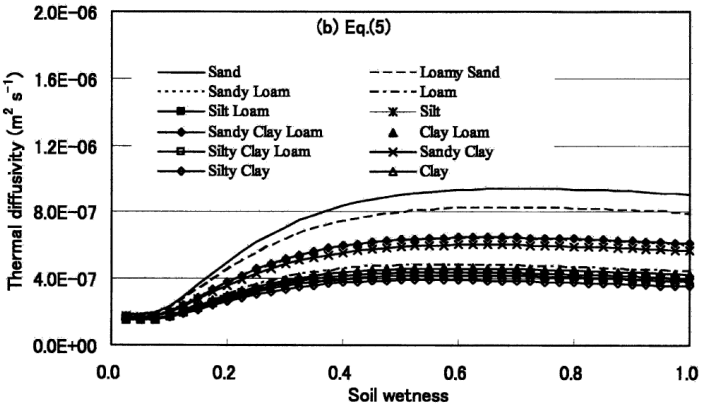

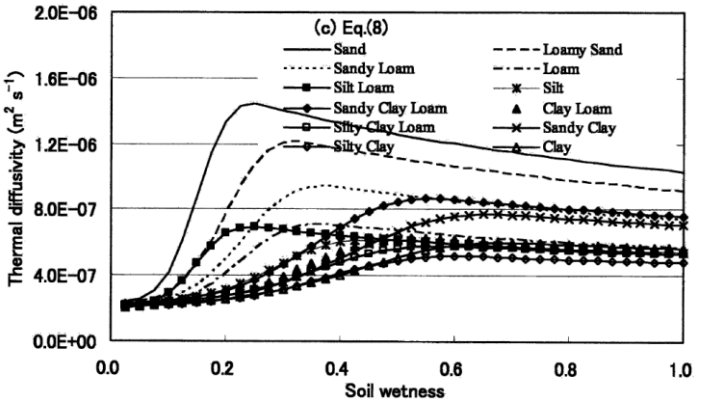

Yang, K. and T. Koike (2005).

Appendix III Additional soil moisture info

Table 1 Theta at pipe depth (100 cm-surf.lev.) for different groundwater levels and different (sandy) soil types. Sandy soil types (see table 4 for description).

GWL cm-surf.lev.	O1	O2	O3	O4	O5	B1	B2	B3	B4	B5	B6
100	0.36	0.38	0.34	0.35	0.32	0.43	0.42	0.46	0.46	0.36	0.38
125	0.28	0.31	0.29	0.31	0.20	0.35	0.36	0.42	0.42	0.25	0.35
150	0.24	0.27	0.27	0.29	0.16	0.31	0.32	0.38	0.39	0.21	0.33
175	0.21	0.25	0.24	0.27	0.13	0.28	0.30	0.36	0.37	0.18	0.32
200	0.19	0.23	0.23	0.26	0.12	0.26	0.28	0.34	0.36	0.16	0.31
225	0.18	0.21	0.22	0.24	0.11	0.24	0.26	0.33	0.34	0.15	0.30
250	0.16	0.20	0.20	0.23	0.10	0.23	0.25	0.31	0.33	0.14	0.29

Table 2 Theta at 50 cm-surf.lev. for different groundwater levels and different (sandy) soil types.

GWL cm-surf.lev.	O1	O2	O3	O4	O5	B1	B2	B3	B4	B5	B6
100	0.24	0.27	0.27	0.29	0.16	0.31	0.32	0.38	0.39	0.21	0.33
125	0.21	0.25	0.24	0.27	0.13	0.28	0.30	0.36	0.37	0.18	0.32
150	0.19	0.23	0.23	0.26	0.12	0.26	0.28	0.34	0.36	0.16	0.31
175	0.18	0.21	0.22	0.24	0.11	0.24	0.26	0.33	0.34	0.15	0.30
200	0.16	0.20	0.20	0.23	0.10	0.23	0.25	0.31	0.33	0.14	0.29
225	0.15	0.19	0.20	0.23	0.09	0.22	0.24	0.30	0.32	0.13	0.28
250	0.14	0.18	0.19	0.22	0.09	0.21	0.24	0.29	0.31	0.12	0.28

Table 3 Theta at 10 cm-surf.lev.) for different groundwater levels and different (sandy) soil types.

GWL cm-surf.lev.	O1	O2	O3	O4	O5	B1	B2	B3	B4	B5	B6
100	0.20	0.23	0.23	0.26	0.12	0.27	0.29	0.35	0.36	0.17	0.31
125	0.18	0.22	0.22	0.25	0.11	0.25	0.27	0.33	0.35	0.16	0.30
150	0.17	0.20	0.21	0.24	0.10	0.23	0.26	0.32	0.33	0.14	0.29
175	0.16	0.19	0.20	0.23	0.09	0.22	0.25	0.31	0.32	0.13	0.29
200	0.15	0.18	0.19	0.22	0.09	0.21	0.24	0.30	0.32	0.13	0.28
225	0.14	0.18	0.18	0.22	0.08	0.20	0.23	0.29	0.31	0.12	0.27
250	0.13	0.17	0.18	0.21	0.08	0.20	0.22	0.28	0.30	0.12	0.27

Appendix IV Overview of variables included in urban energy models

		Cap	VL92	
	Fluxes included (F)			
	All fluxes (a)	13	8	
	No Q_E (e)	2	2	
	No Q_F (f)	10	14	
	Neither Q_E nor Q_F (g)	2	3	
1	**Vegetation (V)**			
	Not included (n)	7	12	
	Separate tile (s)	16	11	
	Integrated (i)	4	4	
2	**Q_F (AN)**			
	Negligible or ignored (n)	11	21	
	Prescribed (p)*	5	1	
	Internal Temp. (i)*	3	3	
	Modelled (m)*	6	1	
	i,p*	2	1	
3	**Temporal Q_F variation (T)**			
	None (n)	11	21	
	Fixed (f)	3	2	
	Variable (v)	13	4	
4	**Urban Morphology (L)**			
	Slab(s)	9	9	
	Single layer(1)	11	11	
	Multiple layer (m)	7	7	
5	**Facets & orientation (FO)**			
	Whole (w)	4	4	
	No orientation (n)	14	14	
	Orientation (o) no intersections	5	5	
	Orientation (w) with intersections	4	4	
6	**Reflection (R)**			
	Single (s)	8	9	
	Multiple (m)	12	11	
	Infinite (i)	7	7	
7	**Albedo, Emissisivity (AE)**			
	Bulk (b)	4	5	
	Two facets (2)	4	4	
	Three or more facets (f)	19	18	
8	**ΔQ_S (S)**			
	Residual (r)*	5	6	
	Conduction (c)	20	19	
	Net radiation based (n)*	2	2	

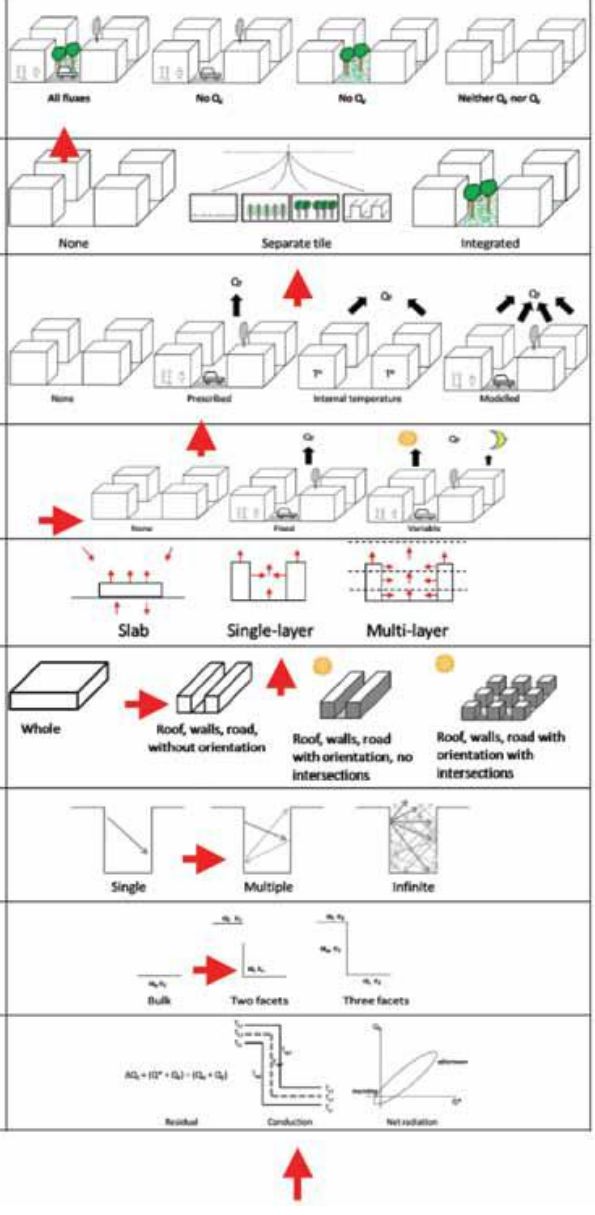

Appendix V List of symbols of the variables included in the soil temperature model

a_1	=	empirical value to estimate heat storage [-]
a_2	=	empirical value to estimate heat storage [s]
a_3	=	empirical value to estimate heat storage [W m^{-2}]
a_i	=	albedo of surface type i [-]
C_D	=	drag coefficient in relations for friction velocity and friction temperature [-]
C_i	=	interception state of the canopy of the i^{th} surface [mm]
C_p	=	heat capacity of air [J kg^{-1} K^{-1}]
$C_{p,soil}$	=	heat capacity of soil [J kg^{-1} K^{-1}]
e_a	=	vapour pressure of the air [Pa]
e_s	=	saturation vapour pressure [Pa]
E_{act}	=	Actual Evapotranspiration [mm]
E_{pot}	=	Potential Evapotranspiration [mm]
f_h	=	factor, that incorporates the surface roughness and atmospheric stability [-]
f_i	=	fraction cover [ ]
f_m	=	stability factor [-]
G	=	heat flux into the ground [W m^{-2}]
G_1	=	parameter related to the maximum surface conductance [mm s^{-1}]
g	=	gravitational constant [m.s^{-2}]
$g_{i,max}$	=	maximum conductance values for the surface type i [m s^{-1}]
g_s	=	surface conductance [m s^{-1}]
H	=	sensible heat flux [W m^{-2}]
h_{RL}	=	height of the air column representing roughness layer [m]
k	=	overall heat transfer coefficient [W m^{-2} K^{-1}]
K	=	relates r_a and r_s [-]

LAI	=	leaf area index [-]
L_v	=	latent heat of vaporization [J kg^{-1}]
L_vE	=	latent heat flux due to evaporation [W m^{-2}]
M_w	=	molecular weight of water [g/mol]
m	=	number of layer in ground [-]
P	=	Precipitation [mm]
p	=	pressure [hPa]
ΔQ_s	=	heat storage [W m^{-2}]
Q_F	=	anthropogenic heat [W m^{-2}]
R	=	molar gas constant [8.314 J mol^{-1} K^{-1}]
r_a	=	aerodynamic resistance [s m^{-1}]
r_b	=	mean boundary layer resistance [s m^{-1}]
r_s	=	surface resistance [s m^{-1}]
r_{ss}	=	Redefined surface resistance [s m^{-1}]
R_g	=	flux resistance, associated with heat transfer from SS to RL [s m^{-1}]
R_{global}	=	global radiation [J m^{-2} s^{-1}]
$R_{l,in}$	=	incoming long wave radiation [J m^{-2} s^{-1}]
$R_{l,\ SS\rightarrow atm}$	=	outgoing long wave radiation [J m^{-2} s^{-1}]
R_{net}	=	net radiation [W m^{-2}]
$R_{s,\ atm\rightarrow SS}$	=	incoming short wave radiation [J $m^{-2}s^{-1}$]
Ri_b	=	Richardson's bulk number [-]
RL	=	roughness layer
s	=	slope of saturation vapour [hPa K^{-1}]
S_i	=	Maximum storage capacity of the surface *i* [mm]
SS	=	soil surface
T_{atm}	=	atmospheric temperature [K]
T_{RL}	=	temperature in the roughness layer [K]
T_{soil}	=	temperature of soil [K]
T_{SS}	=	temperature of soil surface [K]
T^*	=	friction temperature [K]

t	=	time [s]
u	=	wind velocity [m s^{-1}]
u^*	=	friction velocity of wind [m s^{-1}]
V	=	air vapour pressure deficit of the air [hPa]
W	=	function of the amount of water on the canopy of the individual surfaces (C_i) relative to the canopy surface water storage capacity (S_i) [-].
z	=	height at which the wind speed is determined [m]
z_0	=	roughness length [m]
z_{soil}	=	depth in ground [m]
α	=	constant in beta probability density function for ε_{eff}
β	=	constant in beta probability density function for ε_{eff}
ε_{eff}	=	effective or apparent emissivity [-]
γ	=	psychrometric constant [hPa K^{-1}]
κ	=	von Kármán's constant (0.4) [-]
λ_{soil}	=	thermal conductivity of soil [W m^{-1} K^{-1}]
ρ	=	density of air [kg m^{-3}]
ρ_{soil}	=	density of soil [kg m^{-3}]
σ	=	Stefan-Boltzmann constant (5.67 10^{-8}) [W $m^{-2}K^{-4}$]

Appendix VI Additional equations of the soil temperature model

$$\gamma = \frac{Cp(p/1000)}{e\ Lv} = \frac{1004.67\frac{J}{Kg\ K} * \frac{101.3*10^3 Pa}{1000}}{0.622*2.45x10^6\frac{J}{kg}}$$

s can be calculated according to (Monteith and Unsworth, 1990) and it is valid for values of air temperature up to 313 K (40 °C).

$$s = \frac{L_v}{1000}\frac{M_w 0.6108\ e^{\frac{17.27(T_{atm}-273.15)}{T_{atm}-35.8}}*10}{R\cdot T_{atm}^{\ 2}}$$

Where M_w is the molecular weight of water (18 g/mol); and R is the molar gas constant (8.314 J/mol/K); V [hPa] can be calculated as (Berthier et al., 2006)

$$V = (610.7*10^{7.5(T_{atm}-273.16)/(T_{atm}-35.86)} - e_a)/100$$

The vapour pressure of the air e_a [Pa] can be assumed equal to the saturation vapour pressure e_s [Pa] is defined as, :

$$e_s = 0.6108\ e^{\frac{17.27(T_{atm}-273.15)}{T_{atm}-35.8}}*1000$$

$$C_D = \left(\frac{\kappa}{\ln\left(z/z_0\right)}\right)^2$$

Stability factors f_h and f_m

$$f_h = \begin{cases} \dfrac{1}{1+15Ri_b\sqrt{1+5Ri_b}} & Ri_b > 0 \\ 1-\dfrac{15Ri_b}{1+75C_D\sqrt{z/z_0}\sqrt{|Ri_b|}} & Ri_b < 0 \end{cases}$$

$$f_m = \begin{cases} \dfrac{1}{1+10Ri_b/\sqrt{1+5Ri_b}} & Ri_b > 0 \\ 1-\dfrac{10Ri_b}{1+75C_D\sqrt{z/z_0}\sqrt{|Ri_b|}} & Ri_b < 0 \end{cases}$$

Richardson's bulk number $$Ri_b = \frac{g \cdot z}{\frac{1}{2}(T_{atm}+T_{RL})}\frac{T_{atm}-T_{RL}}{u^2}$$

friction temperature [K] $$T^* = \frac{C_D u(T_{atm}-T_{RL})}{u^*} f_h$$

friction velocity of wind [m.s^{-1}] $$u^* = u \cdot \sqrt{C_D f_m}$$

12 References

Agudelo-Vera, C., M. Blokker, and I. Pieterse-Quirijns. (2014) "Early Warning Systems to Predict Temperature in the Drinking Water Distribution Network." Procedia Engineering 70, no. 0: 23-30.

Allen, L., F. Lindberg, et al. (2011). "Global to city scale urban anthropogenic heat flux: Model and variability." International Journal of Climatology 31(13): 1990-2005.

Baker, J. and D. Baker (2002). "Long-Term Ground Heat Flux and Heat Storage at a Mid-Latitude Site." Climatic Change 54(3): 295-303.

Berthier, E., S. Dupont, et al. (2006). "Comparison of two evapotranspiration schemes on a sub-urban site." Journal of Hydrology 328(3-4): 635-646.

Best, M. J. and C. S. B. Grimmond (2013). "Analysis of the Seasonal Cycle Within the First International Urban Land-Surface Model Comparison." Boundary-Layer Meteorology 146(3): 421-446.

Blokker, E. J. M., P. Horst, et al. (2014). Haalbaarheid van maatregelen tegen ongewenste opwarming van drinkwater in het ledingnet. Nieuwegein, KWR Watercycle Research Institute.

Blokker, E. J. M. and E. J. Pieterse-Quirijns (2012). Scenariostudies voor beperken invloed klimaatveranderingen op temperatuur en kwaliteit drinkwater in het net. Nieuwegein, KWR Watercycle Research Institute.

Blokker, E. J. M. and I. Pieterse-Quirijns (2013). "Modeling temperature in the drinking water dristribution system." AWWA 105: E19-E28.

Bowler, D. E., L. Buyung-Ali, et al. (2010). "Urban greening to cool towns and cities: A systematic review of the empirical evidence." Landscape and Urban Planning 97(3): 147-155.

Chimklai, P., A. Hagishima, et al. (2004). "A computer system to support Albedo Calculation in urban areas." Building and Environment 39(10): 1213-1221.

Diefenderfer, B. K., I. L. Al-Qadi, et al. (2006). "Model to predict pavement temperature profile: Development and validation." Journal of Transportation Engineering 132(2): 162-167.

Dinoloket (2014). "www.Dinoloket.nl." Last access March 2014.

Drink Water Directive (2011). "Drinkwaterbesluit." 2013, from http://wetten.overheid.nl/BWBR0030111/geldigheidsdatum_25-02-2013.

Eliasson, I. and M. K. Svensson (2003). "Spatial air temperature variations and urban land use - A statistical approach." Meteorological Applications 10(2): 135-149.

Ferguson, G. and A. D. Woodbury (2004). "Subsurface heat flow in an urban environment." Journal of Geophysical Research: Solid Earth 109(B2): B02402.

Flanner, M. G. (2009). "Integrating anthropogenic heat flux with global climate models." Geophysical Research Letters 36(2).

Garcia Gonzalez, R., A. Verhoef, et al. (2012). "Interactions between the physical soil environment and a horizontal ground coupled heat pump, for a domestic site in the UK." Renewable Energy 44: 141-153.

Gentine, P., D. Entekhabi, et al. (2012). "Systematic errors in ground heat flux estimation and their correction." Water Resources Research 48(9).

Grimmond, C. S. B., M. Blackett, et al. (2010). "The international urban energy balance models comparison project: First results from phase 1." Journal of Applied Meteorology and Climatology 49(6): 1268-1292.

Grimmond, C. S. B. and T. R. Oke (1991). "An evapotranspiration-interception model for urban areas." Water Resources Research 27(7): 1739-1755.

Grimmond, C. S. B. and T. R. Oke (1999). "Heat storage in urban areas: Local-scale observations and evaluation of a simple model." Journal of Applied Meteorology 38(7): 922-940.

Grimmond, C. S. B., M. Roth, et al. (2010). Climate and more sustainable cities: Climate information for improved planning and management of cities (Producers/Capabilities Perspective).

Hartemink, A. E. and M. P. W. Sonneveld (2013). "Soil maps of The Netherlands." Geoderma 204–205(0): 1-9.

Herb, W. R., B. Janke, et al. (2008). "Ground surface temperature simulation for different land covers." Journal of Hydrology 356(3–4): 327-343.

Holderness, T., S. Barr, et al. (2013). "An evaluation of thermal Earth observation for characterizing urban heatwave event dynamics using the urban heat island intensity metric." International Journal of Remote Sensing 34(3): 864-884.

Hove, B. v., G.-J. Steeneveld, et al. (2011). Exploring the urban heat island intensity of Dutch cities, Alterra.

Hove, B. v., G.-J. Steeneveld, et al. (2011). Modelling and observing urban climate in the Netherlands, Wageningen University.

Ichinose, T., K. Shimodozono, et al. (1999). "Impact of anthropogenic heat on urban climate in Tokyo." Atmospheric Environment 33(24-25): 3897-3909.

Jackson, T. L., J. J. Feddema, et al. (2010). "Parameterization of urban characteristics for global climate modeling." Annals of the Association of American Geographers 100(4): 848-865.

Jacobs, A. F. G., B. G. Heusinkveld, et al. (2011). "Long-term record and analysis of soil temperatures and soil heat fluxes in a grassland area, The Netherlands." Agricultural and Forest Meteorology 151(7): 774-780.

Järvi, L., C. S. B. Grimmond, et al. (2011). "The Surface Urban Energy and Water Balance Scheme (SUEWS): Evaluation in Los Angeles and Vancouver." Journal of Hydrology 411(3-4): 219-237.

Kanda, M. (2006). "Progress in the scale modeling of urban climate: Review." Theoretical and Applied Climatology 84(1-3): 23-33.

Klok, L., H. t. Broeke, et al. (2010). Ruimtelijke verdeling en mogelijke oorzaken van het hitte-eiland effect, TNO.

Klok, L., S. Schaminee, et al. (2012). De stedelijke hitte-eilanden van Nederland in kaart gebracht met satellietbeelden, TNO.

Klok, L., S. Zwart, et al. (2012). "The surface heat island of Rotterdam and its relationship with urban surface characteristics." Resources, Conservation and Recycling 64: 23-29.

KNMI (2013). Koninklijk Nederlands Meteorologisch Instituut - Hourly information from KNMI stations

Kotthaus, S. and C. S. B. Grimmond, (in press) "Energy exchange in a dense urban environment – Part II: Impact of spatial heterogeneity of the surface." Urban Climate(0).

Kuiper, M. W., B. A. Wullings, et al. (2004). "Intracellular proliferation of Legionella pneumophila in Hartmanella vermiformis in aquatic biofilms grown on plasticized polyvinyl chloride." Applied and Environmental Microbiology 70(11): 6826–6833.

Menberg, K., P. Bayer, et al. (2013). "Subsurface urban heat islands in German cities." Science of the Total Environment 442: 123-133.

Mihalakakou, G. (2002). "On estimating soil surface temperature profiles." Energy and Buildings 34(3): 251-259.

Moerman, A. (2013). Drinking water temperature modeling in domestic systems, Delft University of Technology, Delft. MSc.

Müller, N., W. Kuttler, et al. (2014). "Analysis of the subsurface urban heat island in Oberhausen, Germany " Climate research 58: 247-256.

Peng, S., S. Piao, et al. (2012). "Surface urban heat island across 419 global big cities." Environmental Science and Technology 46(2): 696-703.

Peters-Lidard, C. D., E. Blackburn, et al. (1998). "The Effect of Soil Thermal Conductivity Parameterization on Surface Energy Fluxes and Temperatures." Journal of the Atmospheric Sciences 55(7): 1209-1224.

Pigeon, G., D. Legain, et al. (2007). "Anthropogenic heat release in an old European agglomeration (Toulouse, France)." International Journal of Climatology 27(14): 1969-1981.

Popiel, C. O., J. Wojtkowiak, et al. (2001). "Measurements of temperature distribution in ground." Experimental Thermal and Fluid Science 25(5): 301-309.

Roberts, S. M., T. R. Oke, et al. (2006). "Comparison of four methods to estimate urban heat storage." Journal of Applied Meteorology and Climatology 45(12): 1766-1781.

Sailor, D. J. and H. Fan (2004). "The importance of including anthropogenic heating in mesoscale modeling of the urban heat island." Bulletin of the American Meteorological Society: 397-403.

Scharenbroch, B. C., J. E. Lloyd, et al. (2005). "Distinguishing urban soils with physical, chemical, and biological properties." Pedobiologia 49(4): 283-296.

Stewart, I. D. and T. R. Oke (2012). "Local climate zones for urban temperature studies." Bulletin of the American Meteorological Society 93(12): 1879-1900.

Taha, H., H. Akbari, et al. (1988). "Residential cooling loads and the urban heat island-the effects of albedo." Building and Environment 23(4): 271-283.

Taniguchi, M., T. Uemura, et al. (2005). "Effects of urbanization and groundwater flow on subsurface temperature in three megacities in Japan." Journal of Geophysics and Engineering 2(4): 320-325.

Taylor, C. A. and H. G. Stefan (2009). "Shallow groundwater temperature response to climate change and urbanization." Journal of Hydrology 375(3–4): 601-612.

van der Kooij, D., B. A. Wullings, et al. (2009). Invloed van temperatuurstijging op nagroei van micro-organismen in het leidingnet. Nieuwegein, KWR Watercycle Research Institute.

van der Molen, M. (2002). Meteorological impacts of land use change in the maritime tropics, Vrije Universiteit, Amsterdam.

van der Wielen, P. W. J. J. (2014). Effect van waterkwaliteit, seizoen, drinkwaterinstallatie en verblijftijd/afstand op opportunistische pathogenen in drinkwater Nieuwegein, KWR Watercycle Research Institute.

van der Wielen, P. W. J. J., R. Italiaander, et al. (2011). Kwantitatieve detectiemethoden voor opportunistisch ziekteverwekkende micro-organismen in drinkwater. Nieuwegein, KWR Watercycle Research Institute.

van der Wielen, P. W. J. J. and D. van der Kooij (2009). Literatuurstudie naar opportunistisch ziekteverwekkende micro-organismen die zich in drinkwater kunnen vermeerderen. Eigenschappen en prioritering aanvullend onderzoek in relatie tot opwarming van het leidingwater. Nieuwegein, KWR Watercycle Research Institute.

van der Wielen, P. W. J. J. and D. van der Kooij (2011). Opportunistisch ziekteverwekkende micro-organismen in drinkwater. Nieuwegein, KWR Watercycle Research Institute.

Versteegh, J. F. M. and H. H. J. Dik (2007). The quality of drinking water in the Netherlands in 2006. (In Dutch). RIVM.

Yang, K. and T. Koike (2005). "Comments on "Estimating soil water contents from soil temperature measurements by using an adaptive Kalman filter"." Journal of Applied Meteorology 44(4): 546-552.

Websites

http://www.fao.org/docrep/x0490e/x0490e06.htm

http://www.dinoloket.nl/

http://www.dinoloket.nl/ondergrondgegevens